19

Study of Electroweak Interactions at the Energy Frontier

Conveners: A. Kotwal and D. Wackeroth

M. Baak, A. Blondel, A. Bodek, R. Caputo, T. Corbett, C. Degrande, O. Eboli, J. Erler, B. Feigl, A. Freitas, J. Gonzalez Fraile, M.C. Gonzalez-Garcia, J. Haller, J. Han, S. Heinemeyer, A. Hoecker, J. L. Holzbauer, S.-C. Hsu, B. Jäger, P. Janot, W. Kilian, R. Kogler, P. Langacker, S. Li, L. Linssen, M. Marx, O. Mattelaer, J. Metcalfe, K. Mönig, G. Moortgat-Pick, M.-A. Pleier, C. Pollard, M. Ramsey-Musolf, M. Rauch, J. Reuter, J. Rojo, M. Rominsky, W. Sakumoto, M. Schott, C. Schwinn, M. Sekulla, J. Stelzer, E. Torrence, A. Vicini, G. Weiglein, G. Wilson, L. Zeune

19.1 Introduction

Particle physics research at the energy frontier has entered an exciting era: Experiments at the CERN Large Hadron Collider (LHC) are exploring the fabric of matter at an unprecedented level of precision and are expected to provide answers to some of the most fundamental questions in science. The recent discovery of a Higgs boson with SM-like properties at the LHC marks the beginning of an exciting journey with the goal to fully reveal the nature of the mechanism responsible for the generation of mass and its messenger, the Higgs boson. Besides the study of the Higgs boson at the LHC and future collider experiments, these experiments at the energy frontier strive to discover new particles and to gain new insights in the fundamental principles that govern all dynamics and properties of matter, i.e. beyond what is described by the Standard Model (SM) of particle physics.

The SM is a thoroughly tested framework for describing electromagnetic, weak and strong interactions of the fundamental constituents of matter, based on a symmetry principle and mathematically formulated as a renormalizable Quantum Field Theory. The SM successfully describes all presently observed electroweak and strong interactions of matter particles (quarks and leptons) and of the mediators of the fundamental forces (photon, W and Z bosons, and the gluon). Despite this enormous success of the SM, it is generally accepted that the SM is merely a low-energy approximation to a more fundamental theory, which is expected to reveal itself at the LHC or at future high-energy experiments, in the form of the emergence of new, non-SM particles and interactions. A promising candidate for a theory beyond the SM, which also provides a dark matter candidate, is Supersymmetry (SUSY), an additional symmetry connecting fermions and bosons. The LHC is presently searching for signals of SUSY, and already succeeded in excluding a range of possible manifestations of SUSY. While direct signals of new particles (*i.e.*, the on-mass shell production of non-SM particles) may require collider energies not yet accessible, it is possible that new physics manifests itself first in form of small deviations between measurements and equally precise predictions of properties of SM particles. The deviations can arise due to the virtual presence of new particles in quantum loops and in new amplitudes generated by their exchange at tree-level.

This is the realm of precision electroweak physics, where well-defined electroweak precision observables (EWPO) are being measured in the interactions of W and Z bosons and are equally well predicted by

complex quantum-field theoretical calculations of these quantum loop effects of SM and beyond-the-SM (BSM) particles. The powerful concept of precision physics not only tests the SM as a full-fledged Quantum Field Theory, but also provides indirect access to currently unobserved sectors of the SM and beyond. Examples of successful applications of precision physics in the recent past include the test of the electroweak sector of the SM at the 0.1% level at LEP and the SLC [1], an indirect prediction of the mass of the top quark and the SM Higgs boson prior to their discovery respectively in $p\bar{p}$ collisions at the Tevatron and pp collisions at the LHC, and exclusion of, or severe constraints on, various extensions of the SM (e. g. Technicolor). In this report, in Sec. 19.2, we will study the potential of EWPOs measured at future high-energy colliders for revealing signals of new physics, constraining the parameter space of BSM models, or providing additional information about the underlying model once a new particle is discovered.

Apart from UV-complete theories such as SUSY, an alternate way to indirectly search for signals of BSM physics is based on Effective Field Theories (EFT). If the new physics scale is well above the energies reached in experiments, the new degrees of freedom cannot be produced directly and the new physics appears only as new interactions between the known particles. These new interactions are included in the Lagrangian as higher-dimensional operators which are invariant under the SM symmetries and suppressed by the new physics scale Λ,

$$\mathcal{L}_{\mathcal{EFT}} = \mathcal{L}_{SM} + \sum_{d>4} \sum_{i} \frac{c_i}{\Lambda^{d-4}} \mathcal{O}_i \tag{19.1}$$

where d is the dimension of the operators. In the limit $\Lambda \to \infty$, this EFT Lagrangian reduces to the SM one. Since the c_i are fixed by the complete high energy theory, any extension of the SM can be parametrized by this Lagrangian where the coefficients of the operators are kept as free parameters. Below the new physics scale, only the operators with lowest dimensions can give a large contribution and need to be kept (unless the coefficient of a higher-dimension operator is substantially larger). Once truncated, the EFT Lagrangian becomes predictive even without fixing the coefficients and parametrizes any heavy new physics scenario. However, it should be kept in mind that this truncated Lagrangian is only valid at energies below the new physics scale.

EFT operators are a useful method for parameterizing the predictions of various strongly-interacting light Higgs (SILH) models [2] which describe the Higgs boson as a pseudo-Goldstone Boson arising from the breaking of a larger symmetry. The lightness of the Higgs boson is the big question raised by the non-stability of the SM Higgs potential under the effect of quantum loops. While SUSY offers an elegant solution which is weakly-coupled and perturbative, EFT operators provide a starting point for exploring strongly-coupled solutions to this important question. Some of these operators induce deviations in EWPOs and Higgs couplings as well as multi-boson production, while others are uniquely probed by multi-boson production.

In this report, in Sec. 19.3, we will use the EFT approach to explore the potential of multi-boson processes at the LHC and other machines for providing information about the scale and the dynamics of the new physics.

19.2 Electroweak precision physics

In this section we focus on two important observables, M_W and $\sin^2\theta^{\ell}_{\text{eff}}$. We start with a discussion on the theoretical predictions, followed by discussions of their measurements at various machines.

19.2.1 Uncertainties in predictions of Z pole observables, $\sin^2\theta^{\ell}_{\mathbf{eff}}$ and M_W

At e^+e^- colliders, near the Z-peak the differential cross section for $e^+e^- \to f\bar{f}$ can be written as[1]

$$\frac{d\sigma}{d\cos\theta} = \mathcal{R}_{\rm ini}\left[\frac{9}{2}\pi\,\frac{\Gamma_{ee}\Gamma_{ff}(1-\mathcal{P}_e\mathcal{A}_e)(1+\cos^2\theta)+2(\mathcal{A}_e-\mathcal{P}_e)\mathcal{A}_f\cos\theta}{(s-M_Z^2)^2-M_Z^2\Gamma_Z^2}+\sigma_{\rm non-res}\right], \tag{19.2}$$

$$\text{where } \Gamma_{ff} = \mathcal{R}_V^f g_{Vf}^2 + \mathcal{R}_A^f g_{Af}^2, \qquad \Gamma_Z = \sum_f \Gamma_{ff}, \tag{19.3}$$

$$\mathcal{A}_f = 2\frac{g_{Vf}/g_{Af}}{1+(g_{Vf}/g_{Af})^2} = \frac{1-4|Q_f|\sin^2\theta^f_{\rm eff}}{1-4\sin^2\theta^f_{\rm eff}+8(\sin^2\theta^f_{\rm eff})^2}. \tag{19.4}$$

Here Γ_Z is the total Z decay width, Γ_{ff} is the partial width for the decay $Z \to f\bar{f}$, and g_{Vf}/g_{Af} are the effective vector/axial-vector coupling that mediate this decay. These effective couplings include higher-order loop corrections to the vertex, except for QED and QCD corrections to the external $f\bar{f}$ system, which are captured by the radiator functions $\mathcal{R}_V^f$ and $\mathcal{R}_A^f$. The factor $\mathcal{R}_{\rm ini}$, on the other hand, accounts for QED radiation in the initial-state. (Specifically, as written in Eq. 19.2, it describes these effects *relative* to the final-state radiation contribution for e^+e^-.)

Equation 19.2 explicitly spells out the leading Z-pole contribution, while additional effects from photon exchange and box corrections are included in the remainder $\sigma_{\rm non-res}$.

The ratio of the vector and axial vector couplings of fermions to the Z boson, g_{Vf} and g_{Af}, is commonly parametrized through the effective weak mixing angle $\sin^2\theta^f_{\rm eff}$. At e^+e^- colliders it can be determined from the angular distribution of fermions in $e^+e^- \to f\bar{f}$ processes with respect to the scattering angle $\cos\theta$ or from the dependence on the initial electron polarization $\mathcal{P}_e$:

$$A_{\rm FB} \equiv \frac{\sigma(\cos\theta>0)-\sigma(\cos\theta<0)}{\sigma(\cos\theta>0)+\sigma(\cos\theta<0)} = \mathcal{R}_{\rm FB}\,\tfrac{3}{4}\mathcal{A}_e\mathcal{A}_f, \tag{19.5}$$

$$A_{\rm LR} \equiv \frac{\sigma(\mathcal{P}_e>0)-\sigma(\mathcal{P}_e<0)}{\sigma(\mathcal{P}_e>0)+\sigma(\mathcal{P}_e<0)} = \mathcal{A}_e. \tag{19.6}$$

$\mathcal{R}_{\rm FB}$ accounts for QCD and QED corrections. The total cross-section, decay width Γ_Z, and branching ratios of the Z boson are measured from the rates and lineshape of the cross sections $\sigma_{e^+e^-\to f\bar{f}}(s)$ on the Z pole ($\sqrt{s}=M_Z$) and for at least one value of $\sqrt{s}$ each above and below the pole ($\sqrt{s}=M_Z\pm\Delta E$).

At hadron colliders, the effective weak mixing angle can be determined from the forward-backward asymmetry of the process $q\bar{q} \to \ell^+\ell^-$ ($\ell = e,\mu$) near the Z pole. However, one cannot determine on a event-by-event basis from which side the quark and the antiquark were coming. For a $p\bar{p}$ initial state, it is generally assumed that the (anti)quark originated from the (anti)proton, respectively, and the dilution effect from the opposite possibility is evaluated based on Monte-Carlo simulations [4]. For a pp initial state, the boost direction of the $\ell^+\ell^-$ system is defined as the quark direction [5], based on the observation that the valence quarks from the proton tend to be more energetic than the sea antiquarks. Again, dilution effects from the wrong quark-antiquark assignment are studied with Monte-Carlo generators.

Due to the high precision of the experimental measurements for these observables, much effort has gone into their theoretical calculation within the Standard Model (SM).

[1] For a review, see Ref. [3].

The effective weak mixing angle can be written as

$$\sin^2\theta^f_{\rm eff} = \frac{1}{4|Q_f|}(1+\mathcal{R}e\frac{g_{Vf}}{g_{Af}}) = (1-\frac{M_W^2}{M_Z^2})(1+\Delta\kappa), \tag{19.7}$$

where $\Delta\kappa$ denotes the contribution from radiative corrections. At tree level, $\Delta\kappa = 0$ and the effective weak mixing angle coincides with the so-called *on-shell* weak mixing angle.

For leptonic final states, the effective weak mixing angle $\sin^2\theta^\ell_{\rm eff}$ has been calculated to the complete two-loop order [6, 7], and 3- and 4-loop corrections of order $\mathcal{O}(\alpha\alpha_s^2)$ [8] and $\mathcal{O}(\alpha\alpha_s^3)$ [9] are also known. Furthermore, the leading $\mathcal{O}(\alpha^3)$ and $\mathcal{O}(\alpha^2\alpha_s)$ contributions for large values of m_t [10] or m_H [11] have been computed.

The current uncertainty from unknown higher orders is estimated to amount to about 4.5×10^{-5} [7], which mainly stems from missing $\mathcal{O}(\alpha^2\alpha_s)$ and $\mathcal{O}(N_f^2\alpha^3,\ N_f^3\alpha^3)$ contributions beyond the leading m_t^4 and m_t^6 terms, respectively. (Here N_f^n denotes diagrams with n closed fermion loops. Based on experience from lower orders, the $\mathcal{O}(\alpha^3)$ diagrams with several closed fermion loops are expected to be dominant.) The calculation of these corrections requires three-loop vertex integrals with self-energy sub-loops and general three-loop self-energy integrals, which realistically can be expected to be worked out in the foreseeable future. The remaining $\mathcal{O}(\alpha^3)$ and four-loop terms are tentatively estimated to amount to $\approx 10^{-5}$. This estimate should improve when the aforementioned calculations have been completed.

When extracting $\sin^2\theta^\ell_{\rm eff}$ from $A_{\rm FB}$ and $A_{\rm LR}$, the initial- and final-state QED radiator functions $\mathcal{R}_i$ must be taken into account. In general, the QED corrections are known to $\mathcal{O}(\alpha)$ for the differential cross section and to $\mathcal{O}(\alpha^2)$ for the integrated cross section (see Ref. [12] for a summary). However, for the LR asymmetry these corrections completely cancel up to NNLO [13], while for the FB asymmetry they cancel if hard photon contributions are excluded, i.e. they cancel up to terms of order $E_\gamma/\sqrt{s}$ [13, 14, 15]. Therefore, a sufficiently precise result for the soft-photon contribution with $E_\gamma < E_\gamma^{\rm cut}$ can be obtained using existing calculations for small enough $E_\gamma^{\rm cut}$, while the hard-photon contribution ($E_\gamma > E_\gamma^{\rm cut}$) can be evaluated with numerical Monte-Carlo methods.

Other important Z pole observables are R_b and the Z width. For the branching fraction $R_b = \Gamma_b/\Gamma_{\rm had}$, two-loop corrections of $\mathcal{O}(\alpha\alpha_s)$, $\mathcal{O}(N_f\alpha^2)$, and $\mathcal{O}(N_f^2\alpha^2)$ are known [16, 17]. Assuming geometric progression of the perturbative series, the remaining higher-order contributions are estimated to contribute at the level of $\sim 2\times10^{-4}$. As before, the contribution from electroweak two-loop diagrams without closed fermion loops is expected to be small. The dominant missing contributions are the same as for $\sin^2\theta^q_{\rm eff}$.

For the total width Γ_Z, only an approximate result for the electroweak two-loop corrections in the limit of large m_t is known [18]. The remaining $\mathcal{O}(N_f\alpha^2)$ may be relatively large. As deduced from the size of individual vertex factors in the calculation of R_b [17], and assuming that there are no relevant cancellations between them, the uncertainty of Γ_Z associated with these corrections is estimated to be a few MeV, which is by far dominant compared to missing three-loop contributions. However, the $\mathcal{O}(N_f\alpha^2)$ correction can be computed with existing methods without conceptual difficulties.

Besides Z-pole observables, the W-boson mass, M_W plays an important role for electroweak precision physics. Theoretically, it can be predicted from the muon decay rate. After subtraction of QED radiation effects [19], muon decay can be described by an effective four-fermion interaction with the Fermi coupling constant G_μ, which in the SM is given by

$$\frac{G_\mu}{\sqrt{2}} = \frac{\pi\alpha M_Z^2}{2M_W^2(M_Z^2-M_W^2)}(1+\Delta r), \tag{19.8}$$

where Δr summarizes the electroweak (non-QED) higher-order corrections. This equation can be solved numerically for M_W.

Quantity	Current theory error	Leading missing terms	Est. future theory error
$\sin^2\theta^\ell_{\rm eff}$	4.5×10^{-5}	$\mathcal{O}(\alpha^2\alpha_s)$, $\mathcal{O}(N_f^{\geq 2}\alpha^3)$	$1...1.5\times10^{-5}$
R_b	$\sim 2\times10^{-4}$	$\mathcal{O}(\alpha^2)$, $\mathcal{O}(N_f^{\geq 2}\alpha^3)$	$\sim 1\times10^{-4}$
Γ_Z	few MeV	$\mathcal{O}(\alpha^2)$, $\mathcal{O}(N_f^{\geq 2}\alpha^3)$	< 1 MeV
M_W	4 MeV	$\mathcal{O}(\alpha^2\alpha_s)$, $\mathcal{O}(N_f^{\geq 2}\alpha^3)$	$\lesssim 1$ MeV

Table 19-1. *Some of the most important precision observables for Z-boson production and decay and the W mass (first column), their present-day estimated theory error (second column), the dominant missing higher-order corrections (third column), and the estimated improvement when these corrections are available (fourth column). In many cases, the leading parts in a large-mass expansion are already known, in which case the third column refers to the remaining pieces at the given order. The numbers in the last column are rough order-of-magnitude guesses.*

Within the SM, M_W has been computed including full two-loop corrections [20, 21] and leading 3- and 4-loop corrections [8, 9, 10]. The intrinsic theoretical error is estimated to be about 4 MeV, mostly due from missing $\mathcal{O}(\alpha^2\alpha_s)$ and $\mathcal{O}(N_f^2\alpha^3,\, N_f^3\alpha^3)$ contributions beyond the leading-m_t approximation. Inclusion of these effects, which would require the computation of the 3-loop self-energies, would reduce the perturbative error to less than 1 MeV.

The current status of the theoretical calculations and prospects for the near future are summarized in Tab. 19-1. Note that $\sigma_{\rm non-res}$ in Eq. 19.2 is suppressed by Γ_Z/M_Z compared to the leading pole term, so that the known one-loop corrections are sufficient to reach NNLO precision at the Z pole.

The known corrections to the effective weak mixing angles and the partial widths are implemented in programs such as `Zfitter` [12, 22] and `Gfitter` [23]. However, these programs are based on a framework designed for NLO but not NNLO corrections. In particular, there are mismatches between the electroweak NNLO corrections to the $Zf\bar{f}$ vertices and QED/QCD corrections to the external legs due to approximations and factorization assumptions. Another problem is the separation of leading and sub-leading pole terms in Eq. 19.2 [7]. While these discrepancies may be numerically small, it would be desirable to construct a new framework that treats the radiative corrections to Z-pole physics systematically and consistently at the NNLO level and beyond. Such a framework can be established based on the pole scheme [24], where the amplitude is expanded about the complex pole $s = M_Z^2 - iM_Z\Gamma_Z$, with the power counting $\Gamma_Z/M_Z \sim \alpha$.

In addition to intrinsic theoretical error, the predictions of $\sin^2\theta^\ell_{\rm eff}$, M_W, *etc.* also depend on input parameters and their experimental uncertainties. The parametric uncertainties in the currently best SM predictions for M_W and $\sin^2\theta^l_{\rm eff}$ due to uncertainties in $m_t, \Delta\alpha^{(5)}_{had}$ and M_Z of Tables 19-2,19-3 have been determined with the help of the parametrization formulae of Ref. [21] for M_W and of Ref. [7] for $\sin^2\theta^\ell_{\rm eff}$.

Two recent determinations of the five-quark hadronic contribution to $\alpha(M_Z)$ find $\Delta\alpha^{(5)}_{\rm had}(M_Z) = (275.7 \pm 1.0)\times10^{-4}$ [25] and $\Delta\alpha^{(5)}_{\rm had}(M_Z) = (276.26 \pm 1.38)\times10^{-4}$ [26]. The residual theory uncertainties due to missing higher order corrections as listed in Table 19-2 have been taken from Refs. [21, 7]. Using the following measured values in the calculation of M_W and $\sin^2\theta^l_{\rm eff}$: $m_t = 173.2 \pm 0.9$ GeV [27], $\alpha_s(M_Z) = 0.1184\pm0.0007$ [28], $M_Z = 91.1876\pm0.0021$ GeV [3], and $M_H = 125\pm1$ GeV, one finds $M_W = 80.3603\pm0.0076$ GeV and $\sin^2\theta^l_{\rm eff} = 0.23127\pm0.00007$ for $\Delta\alpha^{(5)}_{\rm had}(M_Z) = (276.26\pm1.38)\times10^{-4}$ [26] and $M_W = 80.3614\pm0.0074$ GeV and $\sin^2\theta^l_{\rm eff} = 0.23129 \pm 0.00007$ for $\Delta\alpha^{(5)}_{\rm had}(M_Z) = (275.7 \pm 1.0)\times10^{-4}$ [25].

Table 19-3 clearly shows that measurements of M_W at the few MeV level, and $\sin^2\theta^\ell_{\rm eff}$ at the level of 10^{-5}, requires significant improvements in the parametric uncertainties from $m_t, \Delta\alpha^{(5)}_{\rm had}$ and M_Z as well as in higher order calculations. Parametric uncertainties from m_{top} and $\Delta\alpha_{had}$, if reduced by a factor of 2 compared to

	$\Delta m_t = 0.9$ GeV	$\Delta(\Delta\alpha^{(5)}_{\rm had}) = 1.38(1.0)\times 10^{-4}$	$\Delta M_Z = 2.1$ MeV	missing h.o.	total
ΔM_W [MeV]	5.4	2.5 (1.8)	2.6	4.0	7.6 (7.4)
$\Delta \sin^2\theta^\ell_{\rm eff}[10^{-5}]$	2.8	4.8 (3.5)	1.5	4.5	7.3 (6.5)

Table 19-2. *Current parametric and theory uncertainties of SM predictions of M_W and $\sin^2\theta^\ell_{\rm eff}$.*

current uncertainties, will prevent them from exceeding the anticipated total precision on M_W at the LHC. At the ILC and TLEP a factor of 5 and 10 improvement, respectively, in the parametric uncertainties is needed, which is only achievable if the precision on M_Z is considerably improved as well. TLEP can improve the M_Z precision by a factor of at least 10 (for a discussion of prospects for an improvement in ΔM_Z see Section 19.2.5). The LHC may be able to achieve $\Delta m_t \sim 0.5$ GeV but further progress at the LHC will likely be limited by theoretical uncertainties in the non-perturbative QCD effects associated with translating the kinematically-reconstructed m_t to the pole mass. We refer to the summary report of the Snowmass working group on *Fully understanding the top quark* for a detailed discussion of the prospects for future precision m_t measurements.

	$\Delta m_t = 0.5(0.1)$ GeV	$\Delta(\Delta\alpha^{(5)}_{\rm had}) = 5\times 10^{-5}$	$\Delta M_Z = 2.1$ MeV	missing h.o.	total
ΔM_W [MeV]	3.0 (0.6)	1.0	2.6	1.0	4.2 (3.0)
$\Delta \sin^2\theta^\ell_{\rm eff}[10^{-5}]$	1.6 (0.3)	1.8	1.5	1.0	3.0 (2.6)

Table 19-3. *Anticipated parametric and theory uncertainties of SM predictions of M_W and $\sin^2\theta^\ell_{\rm eff}$.*

In many new physics models, the leading contributions beyond the SM to electroweak precision observables can be described by the *oblique* parameters S, T, U [29]:

$$\Delta r \approx \Delta r^{\rm SM} + \frac{\alpha}{2s_W^2}\Delta S - \frac{\alpha c_W^2}{s_W^2}\Delta T + \frac{s_W^2 - c_W^2}{4s_W^4}\Delta U, \tag{19.9}$$

$$\sin^2\theta^\ell_{\rm eff} \approx (\sin^2\theta^\ell_{\rm eff})^{\rm SM} + \frac{\alpha}{4(c_W^2 - s_W^2)}\Delta S - \frac{\alpha s_W^2 c_W^2}{c_W^2 - s_W^2}\Delta T, \tag{19.10}$$

where $s_W^2 = 1 - c_W^2 = 1 - M_W^2/M_Z^2$, and S, T, U are given at 1-loop level in terms of the transverse parts of 1-PI gauge boson self-energies, $\Pi_{VV'}$:

$$\alpha S = 4s_W^2 c_W^2 \left[\Pi'_{ZZ}(0) - \frac{c_W^2 - s_W^2}{s_W c_W}\Pi'_{Z\gamma} - \Pi'_{\gamma\gamma}(0)\right], \tag{19.11}$$

$$\alpha T = \Delta\rho = \frac{\Pi_{WW}(0)}{M_W^2} - \frac{\Pi_{ZZ}(0)}{M_Z^2}, \tag{19.12}$$

$$\alpha U = 4s_W^2\left[\Pi'_{WW}(0) - c_W^2\Pi'_{ZZ}(0) - 2s_W c_W\Pi'_{Z\gamma} - s_W^2\Pi'_{\gamma\gamma}(0)\right]. \tag{19.13}$$

Note that $\Delta T = 0$ ($\Delta\rho = 0$) and $\Delta U = 0$ in case of exact custodial $SU(2)$ symmetry. A discussion of the current and expected precision in the determination of the oblique parameters S and T, for a fixed value of $U = 0$, can be found in Section 19.2.6.

19.2.2 Uncertainties in measurements of M_W and $\sin^2\theta^{\ell}_{\mathbf{eff}}$ at hadron colliders

In this section we discuss the theoretical inputs and the experimental aspects of measuring these EWPOs at hadron colliders.

19.2.2.1 Theory and PDF aspects: M_W

In hadronic collisions, the W boson mass can be determined from the transverse mass distribution of the lepton pair, $m_T(l\nu)$, originating from the W boson decay, $W \to \ell\nu$, and the transverse momentum distribution of the charged lepton or neutrino. Both QCD and electroweak (EW) corrections play an important role in the measurement of W boson observables at hadron colliders. For the anticipated experimental precision in the measurement of M_W at the Tevatron and the LHC, as presented in Section 19.2.2.2, it is imperative to control predictions for the relevant observables at the per-mille level. For instance, the transverse momentum distribution of the W boson is an important ingredient in the current W mass measurement at the Tevatron (see, e. g., Ref. [30] for a review). In lowest order (LO) in perturbation theory, the W boson is produced without any transverse momentum. Only when QCD corrections are taken into account does the W boson acquire a non-negligible transverse momentum, p_T^W. For a detailed understanding of the p_T^W distribution, it is necessary to resum the soft gluon emission terms, and to model non-perturbative QCD corrections. This has either be done using calculations targeted specifically for resummation and parametrizing non-perturbative effects (see, e. g., Refs. [31] and [32]), or interfacing a calculation of W boson production at next-to-leading order (NLO) in QCD with a parton-shower Monte Carlo (MC) program and tuning the parameters used to describe the non-perturbative effects. The latter approach has been pursued in Refs. [33, 34, 35]. Fixed higher-order QCD corrections to fully differential distributions in W boson production are known through next-to-next-to-leading order [36, 37, 38].

While QCD corrections only indirectly affect the W mass extracted from the $m_T(l\nu)$ distribution, QED radiative corrections can considerably distort the shape of this distribution in the region sensitive to the W mass. For instance, final-state photon radiation is known to shift M_W by $\mathcal{O}(100$ MeV) [39, 40, 41, 42, 43, 44, 45, 46]. In the last few years, significant progress in providing predictions including EW corrections to W boson production in hadronic collisions has been made. The complete $\mathcal{O}(\alpha)$ EW radiative corrections to $p\overset{(-)}{p} \to W^{\pm} \to \ell^{\pm}\nu$ ($\ell = e, \mu$) were calculated by several groups [47, 48, 49, 50, 51, 52, 53] and found to agree [54, 55]. First steps towards going beyond fixed order in QED radiative corrections in W boson production were taken in Refs. [56, 57, 58, 59, 60] by including the effects of final-state multiple photon radiation. For a review of the state-of-the-art of predictions for W and Z boson production at hadron colliders see, e. g., Refs. [54, 55, 61]. Given the anticipated accuracy of the W boson mass measurement at the Tevatron and the LHC, it is necessary to not only fully understand and control separately higher-order QCD and EW corrections, but also their combined effects. A first study of combined effects can be found in Ref. [62], where final-state photon radiation was added to a calculation of W boson production which includes NLO and resummed QCD corrections. This study showed that the difference in the effects of EW corrections in the presence of QCD corrections and of simply adding the two predictions may be not negligible in view of the anticipated precision. Moreover, in the relevant kinematic region, i.e. around the Jacobean peak, the QCD corrections tend to compensate some of the effects of the EW corrections. In Ref. [63] the full set of EW $\mathcal{O}(\alpha)$ corrections of `HORACE` [52] was combined with the NLO QCD corrections to W boson production simulated by the generator `MC@NLO` [33], which is matched with the parton-shower MC program `Herwig` [64]. The results of a combination of the EW $\mathcal{O}(\alpha)$ corrections to W and Z boson production as implemented in `SANC` [51, 65] with `Pythia` [66] and `Herwig` can be found in Ref. [67], without, however, performing a matching of NLO QCD corrections to the parton shower. Recently, the complete EW $\mathcal{O}(\alpha)$ radiative corrections to W and Z boson production became available in `POWHEG` [68, 69, 70], which allows one to study the effects of

NLO EW corrections in the presence of QCD radiation and with both `Pythia` and `Herwig`. However, this approach can only capture part of the two-loop mixed QCD-EW corrections, and only a complete 2-loop calculation of $\mathcal{O}(\alpha\alpha_s)$ corrections will provide a reliable estimate of the theoretical uncertainty due to missing higher-order corrections. In view of recent improvements in the calculation of two-loop corrections [71], it is reasonable to expect that these calculations are available at the timescale of a final LHC measurement of M_W [2].

The PDF uncertainty must be considerably reduced for a target uncertainty of $\Delta M_W = 9$ (5) MeV at the Tevatron (LHC). An analysis performed in Ref. [74] has shown that the LHC measurements of the W charge asymmetry using the 2012 data has the potential to reduce the W mass uncertainty at the Tevatron by about a factor of two (see also Section 19.2.2.2). But none of the PDF sets studied in Ref. [74] included the recent constraints from the LHC measurements of electroweak boson production, which constrain PDFs for the same flavor combinations and the same kinematic regions relevant for M_W determinations. In order to update this study taking this information into account, we have repeated the determination of ΔM_W at NLO-QCD (with `DYNNLO` for the theory modeling) using the same method as in Ref. [74] but using now the NNPDF2.3 [75]. This set is particularly suited for the determination of the W mass at the LHC since it already includes constraints from W and Z/γ^* production data from ATLAS, CMS and LHCb. In order to reduce the statistical fluctuations, a dedicated set of $N_{\rm rep} = 1000$ replicas has been produced and used to compute the theory predictions for the W transverse mass distribution at NLO-QCD [76]. All of the results shown below correspond to W^+ boson production, but we know from [74] that they should apply as well for W^- boson production.

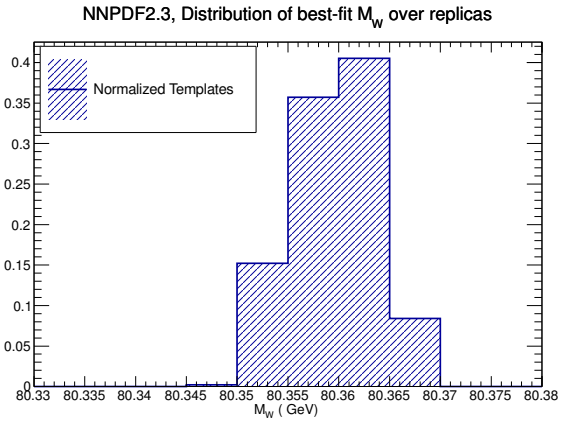

Figure 19-1. *The distribution of the best-fit M_W value obtained from the comparison of the 1000 replicas of NNPDF2.3 with the reference templates. The mean and the width value extracted from this histogram is $M_W \pm \delta_{\rm PDF} = 80.3605 \pm 0.0051$ GeV.*

For each of the $N_{\rm rep} = 1000$ PDF replicas, the fit determines which is the value of M_W which maximizes the agreement with the template distributions. The distribution of best-fit M_W over the NNPDF2.3 replicas for normalized distributions is shown in Fig. 19-1. Note that our procedure entails a methodological uncertainty due to the finite statistics used to generate the templates, which is not explicitly accounted for here. Note also that our estimate of $\delta_{\rm PDF} = 5$ MeV applies to the m_T^W distribution fits only, and to derive the final estimate we would need as well the results obtained with the MSTW [77] and CT10 [78] sets. Finally, the PDF uncertainty depends on the details of the experimental distribution being fit, and therefore the effects of the experimental resolution are also important. Resolution effects tend to increase the PDF uncertainty.

[2] See, e. g., Ref.[72] for a calculation of the two-loop virtual mixed QCD×QCD corrections to the Drell-Yan process, and Ref. [73] for a recent discussion of factorizable contributions.

In order to determine if a particular PDF combination is responsible for the bulk of the PDF uncertainties in M_W, it is useful to compute the correlations [79] between the $N_{\rm rep} = 1000$ PDF replicas of NNPDF2.3 and the 1000 determinations of M_W obtained from the template fits for each replica. The results are shown in Fig. 19-2 for the unnormalized templates (left plot) and for the normalized templates (right plot). In the case of the unnormalized templates, the correlation between PDFs and M_W is similar to the case of the inclusive W^+ cross section [80]. On the other hand, for the normalized templates the correlations are much smaller, showing that the normalization effectively decorrelates the M_W fits with respect to the PDFs. Since experimental measurements always use normalized templates, this is the result of relevance. It is clear that there is not a particular range of Bjorken-x or a particular quark flavor that dominates the M_W measurement. This implies that, in order to further reduce the PDF uncertainty in the M_W measurement from m_T^W, one needs new data constraining all quark flavors and gluons in the broadest possible x range.

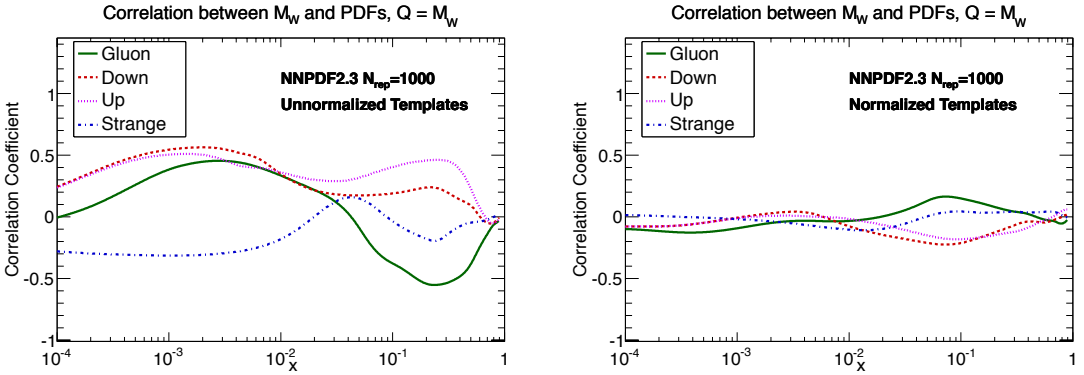

Figure 19-2. *Correlations between different PDF flavours and the M_W determination at LHC 7 TeV, as a function of Bjorken-x, for unnormalized (left plot) and normalized (right plot) templates. Note that experimental measurements always use normalized templates, and thus only the results obtained with these templates are of relevance. The predictions from the 1000 replicas of NNPDF2.3 have been used in the computation.*

The results that we have just discussed were based on the determination of M_W from the W transverse mass distribution. This distribution receives small higher-order QCD corrections, but its accurate determination at the LHC will be challenging, to achieve a competitive M_W measurement. Next we report on preliminary work towards the extension of the results of [74] to a template-fit analysis of the lepton transverse momentum distribution, which has been successfully used at the Tevatron to measure M_W.

As opposed to the transverse mass distribution, the lepton transverse momentum, p_T^l is substantially modified by higher-order QCD corrections, given its strong correlation with the W boson transverse momentum, p_T^W, which vanishes at the Born level. For this distribution the use of resummed calculations for the W boson p_T^W is required, either using analytical p_T^W resummation or NLO-QCD calculations matched to QCD parton showers, with a significant increase in the amount of CPU time needed to generate the theory templates.

The relevance of NLO-QCD corrections implies that the gluon PDF yields also a more important contribution to the PDF uncertainty on M_W than in the transverse mass case. In order to confirm this, in Fig. 19-3 we show the contribution of quark-antiquark terms to the total PDF uncertainty in the transverse mass and lepton p_T distributions, computed at NLO-QCD with `DYNNLO`. It is clear that for the lepton p_T^l distribution the contribution of the quark-gluon subprocess is substantial, in particular near the Jacobean peak. It should be stressed that the results presented in Fig. 19-3 have been obtained at fixed order, whereas a fully resummed calculation would be ideal at least in the lepton p_T^l case. Furthermore, the quark-antiquark contribution alone provides a correct estimate of its PDF uncertainty, but only the results including all the partonic subprocesses are sensible in terms of physical distributions. With these two caveats in mind, it is

clear that a dedicated analysis should be pursued in order to limit as much as possible the contribution to ΔM_W due to the gluon PDF. For example, ratios of W over Z distributions provide a significant cancellation of contributions which are common in the two cases, e.g. the quark-gluon initiated subprocesses, strongly reducing the corresponding contribution to the PDF uncertainty.

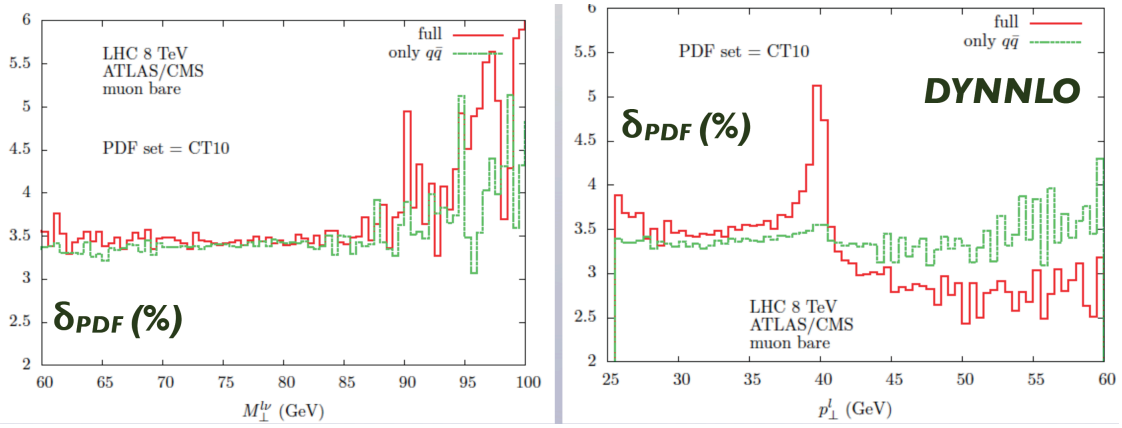

Figure 19-3. *The total relative PDF uncertainty and the separate contribution of quark-antiquark diagrams for the transverse mass (left plot) and the lepton p_T (right plot) distributions, computed at NLO with* `DYNNLO`.

As a final remark, let us mention that PDFs with QED contributions included should be taken into account to consistently assess the corrections to the M_W fits induced by QED effects. The recently released NNPDF2.3 QED set [82] is specially suitable for this purpose, since not only does it include the combined NNLO QCD with LO QED corrections, but it also includes the most recent constraints from electroweak gauge boson production data at the LHC. The implications of NNPDF2.3 QED for M_W determinations should be the topic of detailed studies in the near future.

19.2.2.2 Experimental aspects: M_W

The Tevatron experiments have made precise measurements of the W boson mass [83, 84]. The combined uncertainty on M_W using CDF and DO measurements is 16 MeV [85], significantly surpassing the combined LEP precision of 33 MeV. This is a noteworthy achievement for hadron collider experiments. Furthermore, additional statistics are available at the Tevatron (approximately a factor of 4 at CDF and a factor of 2 at DO) and very large samples are available at the LHC (which will grow further in the coming years). The Tevatron experiments have demonstrated that many systematic uncertainties related to calibrations can be reduced as the statistics of the calibration samples and other control samples increase [30]. This is a non-trivial demonstration since consistency between multiple calibration methods and channels, e.g. as shown in the CDF measurements [83, 39], is an essential component of a robust analysis.

Uncertainties due to parton distribution functions (PDFs) and electroweak radiative corrections rely on external experimental and theoretical input. Improvements in theoretical calculations have led to reductions in the latter. Collider measurements of boson distributions have provided constraints on PDFs and increased statistics in the future should continue to do so.

Table 19-4 shows the projections from CDF and DO on the M_W uncertainty they expect to achieve with their respective final datasets from the Tevatron. These projections build mostly on the 4-5 measurements that these experiments have each made over the last two decades, which show that careful analysis of data has led to the approximate scaling of many systematic uncertainties with statistics. The datasets have grown

ΔM_W [MeV]	CDF	D0	combined	final CDF	final D0	combined
$\mathcal{L}$[fb^{-1}]	2.2	4.3 (+1.1)	7.6	10	10	20
PDF	10	11	10	5	5	5
QED rad.	4	7	4	4	3	3
$p_T(W)$ model	5	2	2	2	2	2
other systematics	10	18	9	4	11	4
W statistics	12	13	9	6	8	5
Total	19	26 (23)	16	10	15	9

Table 19-4. *Current and projected uncertainties in the measurement of M_W at the Tevatron.*

ΔM_W [MeV]	LHC		
$\sqrt{s}$ [TeV]	8	14	14
$\mathcal{L}$[fb^{-1}]	20	300	3000
PDF	10	5	3
QED rad.	4	3	2
$p_T(W)$ model	2	1	1
other systematics	10	5	3
W statistics	1	0.2	0
Total	15	8	5

Table 19-5. *Current and target uncertainties in the measurement of M_W at the LHC.*

by a factor of 200-500 over this time period. The projections to the full dataset assume some improvement in the understanding of the tracking and calorimetry, modest improvement in the understanding of radiative corrections, and a factor of two improvement in the PDF uncertainty over the next few years. The analysis in Ref. [74] has shown that the LHC measurements of the W charge asymmetry using the 2012 data has the potential to reduce the W mass uncertainty at the Tevatron by about a factor of two. Thus, it is reasonable to assume that the final Tevatron measurements will achieve a combined uncertainty of 9-10 MeV, as projected.

According to Ref. [74], the PDF uncertainty at the LHC is about a factor of two larger than at the Tevatron. Thus, further improvements in the PDF uncertainty will be required to produce higher precision on the W boson mass. This will require a program of measurements of differential boson distributions such as (i) the Z boson rapidity distribution, (ii) the charged lepton rapidity distribution from W boson decays, (iii) the W charge asymmetry distribution, and (iv) the W+charm production which constrains the strange quark contribution. Combined with the increasing understanding of the LHC detectors, we suggest that a PDF uncertainty below 5 MeV is a reasonable target for the LHC (see also Sec. 19.2.2.1 for a detailed discussion). As shown in Table 19-5, we propose targets for m_W precision at the LHC, approaching 5 MeV in the long term. Note that detailed detector studies and improved analysis techniques are just as important in this endeavor as the growth of the data statistics. We consider having a 5 MeV target for the total precision as a reasonable ambition for the LHC.

19.2.2.3 Experimental aspects: $\sin^2\theta^{\ell}_{\mathbf{eff}}$

At hadron colliders, investigations around the Z resonance in single neutral-current vector-boson, $q\bar{q} \to \gamma, Z \to l^+l^-$, with charged leptons l in the final state, allow a precise measurement of the electroweak mixing angle from the forward-backward asymmetry $A_{\rm FB}$. The results of a measurement of $\sin^2\theta^l_{eff}$ at the Tevatron by the CDF and D0 collaborations and at the LHC by the ATLAS and CMS collaborations are presented in Table 19-6 and Table 19-7, respectively.

At the Tevatron, because the quark direction is better defined for $\bar{p}p$ than for pp collisions, the measurement of $\sin^2\theta^l_{\rm eff}$ is less sensitive to PDF uncertainties and higher order QCD corrections. In addition, three significant improvements have been recently introduced in the analysis at CDF. The first is the introduction of the event weighting technique [86], which to first order results in the cancellation of acceptance errors and also reduces the statistical errors by 20%. The second is the introduction of momentum scale corrections [87], which remove the bias in the determination of muon momenta, and the third is the consideration of electroweak radiative corrections using Zfitter [88]. Therefore, smaller error bars are expected for the final analysis of the full Run II Tevatron data as shown in Table 19-6. The errors in the e^+e^- channel are smaller than in the $\mu^+\mu^-$ channel, if forward electrons (i.e. large $\cos\theta$) are included in the analysis. Based on the recent improvements in the CDF analysis, we expect similar errors with the full Run II data set at D0. The recent CDF measurement [88] with an e^+e^- sample corresponding to 2.1 fb^{-1} of integrated luminosity yields (statistical and systematic errors are added linearly): $\sin^2\theta^l_{\rm eff} = 0.2328 \pm 0.0011$. D0 measures $\sin^2\theta^l_{\rm eff} = 0.2309 \pm 0.0008$ (stat) ± 0.0006 (syst) [89] using an e^+e^- sample corresponding to 5.0 fb^{-1} of integrated luminosity.

$\Delta\sin^2\theta^l_{\rm eff}$ [10^{-5}]	CDF	D0	final CDF	final CDF	final CDF
final state	e^+e^-	e^+e^-	$\mu^+\mu^-$	e^+e^-	combined
$\mathcal{L}$[fb^{-1}]	2.1	5.0	9.0	9.0	9 $\mu\mu$ + 9 e^+e^-
PDF	12	48	12	12	12
higher order corr.	13	8	13	13	13
other systematics	5	38	5	5	5
statistical	90	80	80	40	40
total $\Delta\sin^2\theta^l_{\rm eff}$	**92**	**101**	**82**	**44**	**41**

Table 19-6. *Current and target uncertainties in the measurement of* $\sin^2\theta^l_{\rm eff}$ *at the Tevatron.*

At the LHC, the measurement of the forward-backward asymmetry A_{FB} at the Z boson pole is complicated by the fact that the pp initial state dilutes the A_{FB} in the $q\bar{q}$ collision. As a result, the measurement is sensitive to the PDFs. Table 19-7 shows the uncertainties from the current LHC analyses. Systematic uncertainties due to experimental effects will very likely reduce with higher statistics as efficiencies and resolutions are better measured using control samples. In order to exploit this potential, however, a significant improvement in the understanding of PDFs will be required. We note that the PDF uncertainty will need to reduce by a factor of ~ 7 for the LHC measurement of $\sin^2\theta^l_{\rm eff}$ to have precision comparable to the LEP and SLC measurements. A factor of 2 reduction in the systematic uncertainty due to missing higher order corrections will also be required. In the following we discuss in more detail the challenges involved in reaching the target uncertainties shown in Table 19-7 based on the experience from the recent ATLAS analysis.

The main difficulty in measuring $\sin^2\theta^l_{\rm eff}$ at the LHC from the forward backward asymmetry, A_{FB}, lies in the fact that it is a pp collider. Since both beams have valence quarks (as opposed to anti-quarks), there is an ambiguity in the incoming quark direction. This ambiguity gives rise to a dilution, or reduction, in

$\Delta \sin^2\theta^l_{\text{eff}}$ $[10^{-5}]$	ATLAS	CMS	LHC/per experiment		
$\sqrt{s}$ [TeV]	7	7	8	14	14
$\mathcal{L}[\text{fb}^{-1}]$	4.8	1.1	20	300	3000
PDF	70	130	35	25	10
higher order corr.	20	110	20	15	10
other systematics	70	181	60 (35)	20	15
statistical	40	200	20	5	2
Total	108	319	75 (57)	36	21

Table 19-7. *Current and target uncertainties in the measurement of* $\sin^2\theta^l_{eff}$ *at the LHC. The target uncertainties are based on expected advancements in both theory and experiment as described in the text. A conservative and more optimistic (in parentheses) target uncertainty is provided for the measurement at 8 TeV.*

the A_{FB}. The effect of dilution can be resolved in part by using the momentum of the Z boson along the longitudinal direction (z) to determine the direction of the outgoing lepton with respect to the quark. However, for events produced in the central part of the detector, there remains about a 50% probability of misidentifying the quark direction. Therefore the best region of phase space to make this measurement is at large p_z, or equivalently rapidity, of the Z boson.

The ATLAS $\sin^2\theta^l_{\text{eff}}$ measurement [90] utilizes electrons and muons not only in the central region of the detector, which are standard for most measurements, but also electrons in the forward region ($2.5 < |\eta| < 4.9$). However, there are some difficulties in using forward electrons. The forward calorimeters are not as highly segmented and there are no tracking detectors, so reconstruction relies on less information. Also, distinguishing between photons and electrons is not possible. Finally, electrons in the forward region are more sensitive to pile-up, which not only increases the background but also makes background modeling more difficult. These difficulties can be overcome by requiring one central electron and one forward electron in the Z reconstruction.

This approach means that ATLAS has produced three search channels in total in the 2011 analysis: a muon channel with two central muons, an electron channel with two central electrons (CC electron), and an electron channel with one central electron and one forward electron (CF channel). To measure $\sin^2\theta^l_{\text{eff}}$, the A_{FB} spectra from data were compared to the asymmetry spectra from Monte Carlo (MC) predictions produced with varying initial values of the weak mixing angle. The results from the three channels are as follows

$$\text{CC electron} : \sin^2\theta^l_{\text{eff}} = 0.2288 \pm 0.0009(\text{stat.}) \pm 0.0014(\text{syst.})$$
$$\text{muon} : \sin^2\theta^l_{\text{eff}} = 0.2294 \pm 0.0009(\text{stat.}) \pm 0.0014(\text{syst.})$$
$$\text{CF electron} : \sin^2\theta^l_{\text{eff}} = 0.2304 \pm 0.0006(\text{stat.}) \pm 0.0010(\text{syst.})$$

Despite having fewer events, the CF electron has the smallest total uncertainty. This is due to the reduced effect of dilution in this channel, which allows better discrimination between the MC templates. The uncertainties in the combined ATLAS measurement of $\sin^2\theta^l_{\text{eff}} = 0.2297 \pm 0.0004(\text{stat.}) \pm 0.009(\text{syst.})$ are outlined in Table 19-7. The systematic uncertainty is dominated by the PDF uncertainty (0.0007) which is correlated and therefore did not see the reduction that the other uncertainties did. This uncertainty was estimated using the CT10 NLO PDF set. The total uncertainty for this measurement matches the precision of the most recent results from the Tevatron experiments shown in Table 19-6.

The $\sin^2\theta^l_{\rm eff}$ ATLAS measurement is limited by the PDF uncertainty in the two central channels, and by the energy scale and smearing in the CF electron channel. The future of this measurement lies in reducing the PDF uncertainty for the central channels. It is a factor of 2 larger than the next largest uncertainty. However, it is the CF electron channel that shows the most potential for being competitive with the LEP and SLC experiments. If the PDF and energy scale/smearing uncertainties were both reduced by a factor of two, ATLAS would become competitive. Although the energy scale/smearing will be increasingly difficult with increased pile-up conditions as well as higher trigger thresholds due to the increased luminosity, the increased statistics as well as better knowledge of the detector (with more use and simulation) will allow us to work toward a significant reduction.

For the 2012 projection with 8 TeV and 20 fb^{-1} of data shown in Table 19-7, the PDF and energy scale/smearing uncertainties will most likely not be reduced to the point where it will be competitive with the world's best measurements. The statistical uncertainty will be reduced by a factor of two (with the 4x increase in data). The MC statistical uncertainty can be reduced to a negligible amount which reduces the "other systematics" column to 6 instead of 7 in a conservative scenario (shown in parentheses is a more optimistic scenario where it is assumed that energy scale/smearing uncertainties can be considerably reduced). Assuming that the inclusion of LHC data in updated PDF fits yields a reduction of the PDF error by a factor of 2 (see discussion in Section 19.2.2.1), this would lead to a total uncertainty of $75(57)\times10^{-5}$.

The target uncertainties (for $\sqrt{s} = 14$ TeV and 300 fb^{-1} and 3000 fb^{-1} respectively) for a future ATLAS measurement of $\Delta\sin^2\theta^l_{\rm eff}$ shown in Table 19-7 are based on the following reasoning and expectations for advancements in both theory and experiment. We assume that with advancements in MC generators the uncertainty due to higher order corrections will decrease dramatically. Currently this is taken as a systematic uncertainty in the ATLAS and CMS measurements, however in the future, it could just be a shift or not required at all. It is difficult to reduce the energy scale/smearing uncertainty in the forward channel, but this task can be made the priority if this became the limiting systematic uncertainty. The last challenge will be triggering on CF electron events. Since there is only one central electron, ATLAS relies on the single-electron trigger. For the 2015 run, these thresholds will increase compared to the 2012 level, making it more difficult to trigger on signal events. There is currently work going on in ATLAS to overcome this challenge, so that forward-electron Z-boson events can still be used in the future.

19.2.3 Uncertainties in measurements of M_W and $\sin^2\theta^\ell_{\rm eff}$ at lepton clolliders

We now turn to the discussion of these EWPOs at lepton colliders, starting with theoretical aspects and moving to experimental issues.

19.2.3.1 Theory status of W-pair production at e^+e^- colliders

The possibilities offered by future e^+e^- colliders make it mandatory to improve the accuracy of the theoretical predictions of the $e^+e^- \to W^+W^-$ cross section beyond the level achieved for LEP2. A precise measurement of m_W with an accuracy ~ 5 MeV from a threshold scan in the GigaZ option of an ILC or at TLEP requires a cross-section calculation with a precision of a few per-mille in the threshold region $\sqrt{s} \sim 2m_W$. At high center of mass energies $\sqrt{s} \gtrsim 800$ GeV in the second phase of an ILC or at CLIC, which are particularly relevant for measurements of anomalous triple gauge couplings, electroweak radiative corrections are enhanced so that NNLO corrections can become relevant. In the following we review recent calculations that improve the theoretical predictions in these regimes and assess the remaining theoretical uncertainties.

Precise theoretical predictions for W-pair production have to take the W-boson decay into account and treat the full 4-fermion final state. The state of the art during the LEP2 run consisted of the so-called double-pole approximation (DPA) utilized in the computer programs RACOONWW [91] and YFSWW3 [92]. In the DPA the quantum corrections to four-fermion production are consistently decomposed into the corrections to on-shell W-boson production and decay (factorizable corrections), soft-photon corrections connecting W-production, propagation and decay stages (non-factorizable corrections), and into a non-resonant remainder. More recently, a complete NLO calculation of 4-fermion production was performed [93], including loop corrections to singly- and non-resonant diagrams and treating unstable particles in the complex mass scheme. As can be seen in Figure 19-4 the results of the DPA for the total cross section agree well with the full $e^+e^- \to 4f$ calculation for energies $200\,\text{GeV} \lesssim \sqrt{s} \lesssim 500\,\text{GeV}$. But the full calculation is required in the threshold region $160\,\text{GeV} \lesssim \sqrt{s} \lesssim 170\,\text{GeV}$ and at energies $\sqrt{s} > 500\,\text{GeV}$ where off-shell effects become important. The description of differential distributions for hadronic W-decays could be improved in the future since presently only QCD corrections to the inclusive W-decay width are included.

At center of mass energies $s \gg m_W^2$ as relevant for the measurement of anomalous triple gauge boson couplings, large radiative corrections to W-pair production arise due to so-called Sudakov logarithms $\log^2(s/m_W^2)$ [94]. The NNLO corrections to on-shell W-pair production at NNLL accuracy (*i.e.* corrections of the form $\alpha^2 \log^m(s/m_W^2)$ with $m = 2, 3, 4$) have been computed in [95]. They are of the order of 5% (15%) for $\sqrt{s} = 1\,\text{TeV}$ ($\sqrt{s} = 3\,\text{TeV}$) and therefore should be taken into account in the second phase of an ILC or at CLIC. The remaining uncertainty due to the uncalculated single-logarithmic NNLO terms has been estimated to be 1–2% [95]. It might also be relevant to consider NNLO Sudakov logarithms for the full 4-fermion final state instead of using the approximation of on-shell W-bosons.

Near the W-pair production threshold, Coulomb corrections of the form $(\alpha/\beta)^n$, with $\beta = \sqrt{1 - 4m_W^2/s}$, are enhanced over the remaining corrections of the same order in α. Therefore the second-order Coulomb correction $\sim (\alpha/\beta)^2$ [96] and contributions of the form α^2/β are expected to be the dominant NNLO corrections near threshold. These have been calculated in [97] using an effective-field theory (EFT) approach [98]. As can be seen in Figure 19-5, the effect of the threshold-enhanced NNLO corrections is of the order of 0.5%. The remaining uncertainty of the m_W-measurement from a threshold scan due to uncalculated NNLO corrections has been estimated to be below $\Delta m_W \approx 3$ MeV [97]. The current best prediction for the total cross section near threshold is obtained by adding the dominant NNLO corrections to the NLO_{ee4f} result [93] that includes one-loop singly and non-resonant diagrams beyond the NLO EFT calculation. For the future, a calculation of the leading NNLO corrections for differential distributions is desirable. As a caveat, further uncertainties arise since the cross section at threshold is very sensitive to initial-state radiation (ISR). In the NLO_{EFT} and $\Delta\text{NNLO}_{\text{thresh}}$ results in Figure 19-5 as well as in the DPA and ee4f results in Figure 19-4, a leading-logarithmic resummation of ISR effects [99] is performed for the Born cross section while higher-order corrections are added without ISR improvement. In the blue-dashed curve in Figure 19-5, the higher-order EFT corrections are improved by ISR resummation.[3] The numerical impact of this next-to-leading logarithmic (NLL) effect is as large as 2% directly at threshold while it soon becomes negligible at higher energies. Therefore a consistent NLL-treatment of ISR might be required for sufficient theoretical control over the cross section at threshold.

19.2.3.2 Experimental aspects: M_W

The three most promising approaches to measuring the W mass at an e^+e^- collider are:

- Polarized threshold scan of the W^+W^- cross-section as discussed in [100].

[3] Note that the IBA approximation in Figure 19-4 also contains ISR improvement of the first Coulomb correction.

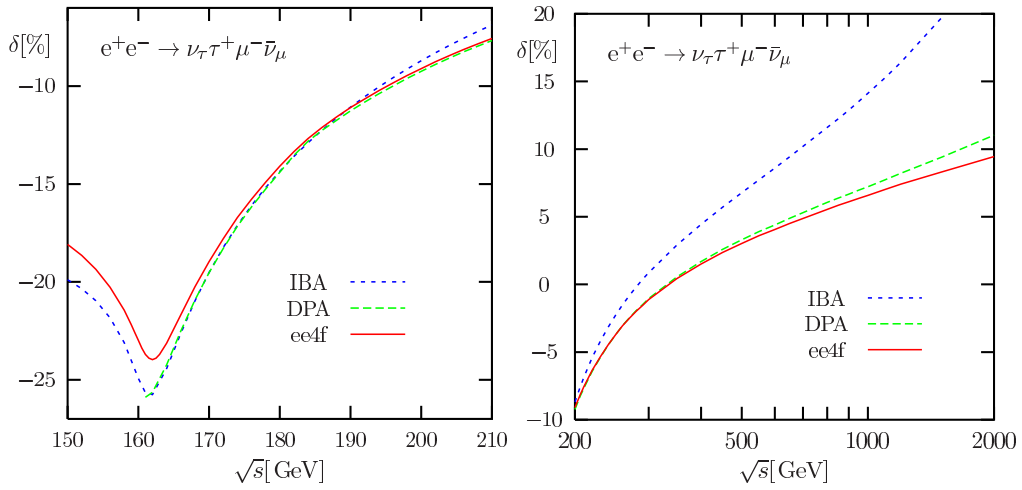

Figure 19-4. *Relative corrections to the total cross section for $e^+e^- \to \nu_\tau\tau^+\mu^-\bar{\nu}_\mu$, normalized by the Born cross section without ISR improvement: improved Born approximation (IBA, blue dashed), double-pole approximation (DPA, green short-dashed) and the NLO calculation for the 4-fermion final state (ee4f, red). Taken from Ref. [93].*

- Kinematically-constrained reconstruction of W^+W^- using constraints from four-momentum conservation and optionally mass-equality as was done at LEP2.
- Direct measurement of the hadronic mass. This can be applied particularly to single-W events decaying hadronically or to the hadronic system in semi-leptonic W^+W^- events.

The three different methods are summarized in the following tables. There is one reasonably complete study related to a polarized threshold scan at ILC [100] which has been updated for this Snowmass workshop. There is also a new, much more precise method for determining the beam energy *in situ* using di-muon events at ILC which has been developed in more depth during this workshop and was presented at [101]. This gives the potential to reduce the beam energy uncertainty on the W mass to 0.8 MeV (limited by stand-alone momentum scale uncertainties estimated at 10 ppm). This previously important systematic for the threshold method - and dominant systematic for the kinematically-constrained reconstruction method appears to be no longer such a critical issue. The reported tables should be taken as reasonable indications of the potential performance. W mass measurements were statistics limited for these methods at LEP2. It is clear that large improvements in the systematics are feasible at future machines like ILC. Exactly how much better can be done is something that can not be predicted with absolute certainty, given the orders of magnitude of improvement. In practice it is something that typically can only be pinned down once a detector is operating.

Table 19-8 has projected results for running close to the WW threshold. ILC can collide highly longitudinally polarized electrons and positrons - this is particularly advantageous for a threshold scan. In the tables it is assumed that if ILC undertakes a dedicated scan near threshold that this would be done with the highest polarization levels achievable. The estimated uncertainties assume that the beam energy scale can be established from collision data at the level of 1 part in 10^5 leading to a corresponding experimental uncertainty on M_W of 0.8 MeV. This has been shown to be statistically feasible using di-muon events provided that the momentum scale is determined to the same precision. This appears feasible using J/ψ events in Z boson decays. The ILC numbers are based on a detailed and updated study with realistic assumptions on detection efficiency, polarization determination, backgrounds, efficiency and normalization errors using

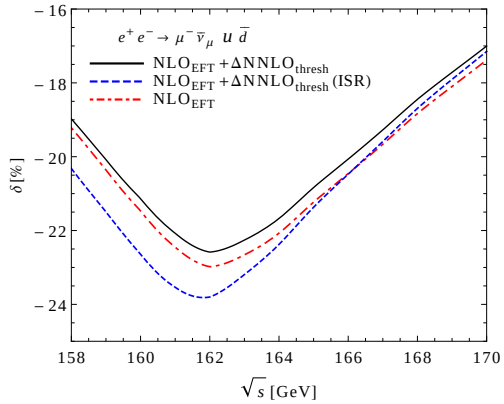

Figure 19-5. *Relative corrections to the total cross section for $e^+e^- \to \mu^-\bar{\nu}_\mu u\bar{d}$ in the EFT approach, normalized by the Born cross section without ISR improvement: NLO (red, dash-dotted), NLO with dominant NNLO corrections (black, solid). In the blue, dashed curve the higher-order corrections are convoluted with ISR structure functions. Based on Ref. [97].*

a 6-point scan with four different beam helicity combinations. The ILC numbers include the (small) effects from beamstrahlung on the cross-section and take advantage of the 150 fb cross-section of multi-hadron production for determinining the beam polarizations from the data. In addition, the table includes an indicative estimate of the anticipated theoretical uncertainty associated with interpreting cross-section measurements near threshold in terms of M_W of 1.0 MeV. A discussion of the present status of predictions for W-pair production at threshold can be found in Section 19.2.3.1. A detailed assessment of the anticipated theoretical shape and normalization uncertainties on the cross-section behavior with center-of-mass energy and including the effects of realistic experimental acceptance for all the four-fermion final states would in principle be needed to report a firm theoretical error estimate. In the table for the ILC, the systematics are essentially currently included in the overall error as the multi-parameter fit adjusts the systematics as nuisance parameters constrained within a priori uncertainties taken as 0.1% for relative efficiency and absolute integrated luminosity. The beam polarizations and backgrounds are fitted simultaneously from the data. In the context of the polarized scan this measurement is essentially *statistics* dominated.

Table 19-9 has projected results for kinematic reconstruction using the semi-leptonic channels as was used at LEP2. Details of this method are in the recently submitted LEP2 legacy paper [102] and the systematics discussed there are used as the basis for this discussion. At LEP2 the fully hadronic channel was also used. It is not expected to be competitive at the sub-10 MeV level because of final-state interaction effects and is so is neglected for these projections. There have not been dedicated studies on the semi-leptonic channel for ILC, but the measurements at LEP2 can be used to estimate/bracket some of the primary uncertainties. The beam energy uncertainty is taken again as a 10^{-5} uncertainty at 250 GeV leading to an error of 0.8 MeV. At higher energies this uncertainty is scaled linearly with center-of-mass energy reflecting in part less statistics for *in situ* checks. Systematic errors associated with knowledge of the luminosity spectrum dL/dx_1dx_2 are estimated to be at the 1 MeV level at 250 GeV and will increase with center-of-mass energy. The table assumes a linear dependence. Two of the primary systematics associated with the W boson mass measurement at LEP2, namely from hadronization and detector effects will be controlled much better with the modern ILC detectors and a more than one hundred times larger dataset. In particular for example it is reasonable to expect that the 7 MeV error associated with a 0.3% uncertainty on the muon energy scale in for example the OPAL analysis is reduced to negligible (naively 0.02 MeV). The hadronization errors which dominated the LEP2 systematic uncertainty were a result of several effects. The much larger statistics envisaged at ILC will allow the kaon and proton fractions in W boson decays to be measured at least ten

ΔM_W [MeV]	LEP2	ILC	ILC	e^+e^-	TLEP
$\sqrt{s}$ [GeV]	161	161	161	161	161
$\mathcal{L}$ [fb^{-1}]	0.040	100	480	600	3000×4
$P(e^-)$ [%]	0	90	90	0	0
$P(e^+)$ [%]	0	60	60	0	0
systematics	70			?	< 0.5
statistics	200			2.3?	0.5
experimental total	210	3.9	1.9	>2.3	< 0.7
beam energy	13	0.8-2.0	0.8-2.0	0.8-2.0	0.1
radiative corrections	-	1.0	1.0	1.0	1.0
total	210	4.1-4.5	2.3-2.9	>2.6-3.2	< 1.2

Table 19-8. *Current and preliminary target uncertainties in the measurement of M_W at e^+e^- colliders close to WW threshold, including an estimate for a future theoretical uncertainty due to missing higher-order corrections.*

times better and the particle-flow based jet reconstruction should make it more feasible to use identified particles in reconstructing jets. Given the improvements in the detector and statistics, improvements in the leading experimental systematics by a factor of 10 can be envisaged. The radiative corrections systematic can presumably be improved with further work. The growing importance of ISR at higher center-of-mass energies suggests that this systematic will degrade as the center-of-mass energy increases. The effective statistical error is not completely straightforward to estimate as it includes effects from ISR and beamstrahlung which often degrade the validity of the kinematic constraints both of which are substantially larger at higher center-of-mass energy. It has been shown that these effects can be ameliorated in the fully hadronic channel [103] by allowing for such photon radiation. It is expected that similar methods will be useful to improve the effective resolution in the semi-leptonic channel too although this is not as highly constrained given the unobserved neutrino. This method is likely to be *systematics* dominated.

Table 19-10 has projected results from the direct measurement of the hadronic mass. This measurement depends primarily on how well the hadronic mass scale can be determined. It essentially does not depend at all on measurements of the beam energy or luminosity spectrum and so is very complementary to the previous two methods. In the particle-flow approach it is in principle possible to cast this as primarily a "bottom-up" problem of determining the tracker momentum scale, the electro-magnetic calorimeter scale and the calorimeter energy scale for neutral hadrons and it is these components that affect the jet energy scale. Over the course of the envisaged ILC program it is anticipated that the samples of Z bosons decaying to hadrons where the Z boson mass is currently known to 2.1 MeV should make it feasible to target a 3 MeV error originating from the jet energy scale. The hadronization error is anticipated to be dominated by knowledge of the K_L^0 and neutron fractions. The pile-up entry refers to primarily $\gamma\gamma \to$ hadrons events coincident with W boson events. The contribution of such events to the measured hadronic mass can be mitigated and is not expected to be a dominant systematic error - but it will be more problematic at higher center-of-mass energies. The statistical error depends on the jet energy resolution and the consequent hadronic mass resolution. The hadronic mass resolution for a particular event varies substantially depending primarily on the fractions of energy in charged particles, photons and neutral hadrons in the event. The effective hadronic mass resolution is therefore a strong function of the analysis method. A full convolution fit with more advanced reconstruction techniques like π^0 mass-constrained fitting offers the potential to improve the W boson mass statistical error by a factor of 2.2 over that naively estimated from the observed average jet energy resolution in full simulation studies. In the estimates presented, we have been conservative and

ΔM_W [MeV]	LEP2	ILC	ILC	ILC
$\sqrt{s}$ [GeV]	172-209	250	350	500
$\mathcal{L}$ [fb^{-1}]	3.0	500	350	1000
$P(e^-)$ [%]	0	80	80	80
$P(e^+)$ [%]	0	30	30	30
beam energy	9	0.8	1.1	1.6
luminosity spectrum	N/A	1.0	1.4	2.0
hadronization	13	1.3	1.3	1.3
radiative corrections	8	1.2	1.5	1.8
detector effects	10	1.0	1.0	1.0
other systematics	3	0.3	0.3	0.3
total systematics	21	2.4	2.9	3.5
statistical	30	1.5	2.1	1.8
total	36	2.8	3.6	3.9

Table 19-9. *Current and preliminary estimated experimental uncertainties in the measurement of M_W at e^+e^- colliders from kinematic reconstruction in the $q\bar{q}\ell\nu_\ell$ channel with $\ell = e, \mu$*

have assumed that the actual improvement factor of a realistic and mature analysis is 1.4. This method is likely to be *systematics* dominated.

Prospects at CLIC

CLIC has yet to study the potential precision for a W boson mass measurement from direct reconstruction. However, it is anticipated that with more than 50 million single W boson events, a statistical precision on the W boson mass of a few MeV will be achievable [104]. CLIC does not foresee operation at either 91 GeV or 161 GeV.

Prospects at TLEP

Studies of the prospects at TLEP have just begun and will continue over the next few years. As described in [105], the statistical precision achievable at TLEP using the WW threshold scan is very high, with about 25 million W boson pairs produced at threshold. A statistical precision of about 1 MeV per experiment, leading to 0.5 (0.7) MeV combining four (two) experiments, should be possible.

The key experimental issue is the calibration of the beam energy using the resonant depolarization technique. Using a subset of the collider bunches *in situ* to perform this calibration, the uncertainty on the beam energy of about 100 keV has been projected. The main question is whether this technique can be made operational at a beam energy of 81 GeV, and it is motivated in [105] that it can be.

In Table 19-8, a statistical uncertainty of 0.5 MeV is mentioned (to represent 4 experiments) and a placeholder for other experimental systematics (such as backgrounds) of < 0.5 MeV is also included. Finally, a placeholder for the uncertainty in QED radiative corrections of 1 MeV is included, partly to indicate that this theoretical uncertainty is a major challenge for TLEP; on the other hand, the TLEP potential may provide strong motivation to improve the radiative correction calculations further. A target for the total M_W uncertainty

ΔM_W [MeV]	ILC	ILC	ILC	ILC
$\sqrt{s}$ [GeV]	250	350	500	1000
$\mathcal{L}$ [fb^{-1}]	500	350	1000	2000
$P(e^-)$ [%]	80	80	80	80
$P(e^+)$ [%]	30	30	30	30
jet energy scale	3.0	3.0	3.0	3.0
hadronization	1.5	1.5	1.5	1.5
pileup	0.5	0.7	1.0	2.0
total systematics	3.4	3.4	3.5	3.9
statistical	1.5	1.5	1.0	0.5
total	3.7	3.7	3.6	3.9

Table 19-10. *Preliminary estimated experimental uncertainties in the measurement of M_W at e^+e^- colliders from direct reconstruction of the hadronic mass in single-W and WW events where one W boson decays hadronically. Does not include WW with $q\bar{q}\ell\nu_\ell$ where $\ell = e, \mu$.*

of 0.5 MeV is quoted in [105]; including placeholders for other systematics in Table 19-8, a projected total uncertainty of < 1.2 MeV is obtained. Clearly, more studies are needed to check that the ultimate statistical precision of TLEP can be fully exploited.

19.2.3.3 Experimental aspects: $\sin^2\theta^\ell_{\text{eff}}$

With polarized beams, the left-right asymmetry $A_{\rm LR}$ provides the most sensitive measurement of the effective weak mixing angle. Details of this measurement at a polarized linear collider running at the Z-pole are reported in [106, 107, 108]. With 10^9 Z bosons, an electron polarization of 80% and no positron polarization, a statistical error of $\Delta A_{\rm LR} = 4 \cdot 10^{-5}$ can be realized, although the systematic uncertainty achievable on the absolute polarization measurement will be significantly worse. Extrapolating from the SLD experience, where $\Delta\mathcal{P}/\mathcal{P} = 0.5\%$ has been achieved [109], it is assumed that at a future facility a polarization uncertainty of 0.25% is realistic [110], leading to $\Delta A_{\rm LR} = 3.8 \cdot 10^{-4}$ or $\Delta \sin^2\theta^\ell_{\rm eff} = 5 \cdot 10^{-5}$.

If positron polarization is available, a significantly more precise measurement can be made using a modified Blondel scheme [111] which removes the need for an absolute polarization measurement. The total cross section with both beams being polarized can be written as $\sigma = \sigma_{\rm unpol}[1 - \mathcal{P}_{e^+}\mathcal{P}_{e^-} + A_{\rm LR}(\mathcal{P}_{e^+} - \mathcal{P}_{e^-})]$. If all four helicity combinations are measured, $A_{\rm LR}$ can be determined as

$$A_{\rm LR} = \sqrt{\frac{(\sigma_{++} + \sigma_{-+} - \sigma_{+-} - \sigma_{--})(-\sigma_{++} + \sigma_{-+} - \sigma_{+-} + \sigma_{--})}{(\sigma_{++} + \sigma_{-+} + \sigma_{+-} + \sigma_{--})(-\sigma_{++} + \sigma_{-+} + \sigma_{+-} - \sigma_{--})}},$$

which is independent of the absolute polarization. Only 10% of the total luminosity needs to be delivered in the 'wrong-helicity' combinations $(++, --)$. The statistical uncertainty which can be achieved with $\mathcal{P}_{e^-} = 80\%$ and $\mathcal{P}_{e^+} > 30\%$ is $\Delta A_{\rm LR} < 5 \cdot 10^{-5}$ or $\Delta \sin^2\theta^\ell_{\rm eff} < 6 \cdot 10^{-6}$. The statistical uncertainty improvement for higher positron polarization values is relatively mild, asymptotically approaching $\Delta A_{\rm LR} = 2.5 \cdot 10^{-5}$.

Even though an absolute polarization measurement is not needed, a precise measurement of the polarization difference between the beam helicity states is required. If the polarization in the two helicity states is written as $\mathcal{P}_{e^\pm} = \pm|\mathcal{P}_{e^\pm}| + \delta\mathcal{P}_{e^\pm}$, the dependence of the measured $A_{\rm LR}$ value on the polarization difference

is given by $\mathrm{d}A_{\mathrm{LR}}/\mathrm{d}\delta\mathcal{P}_{\mathrm{e}^\pm} \approx 0.5$. Extrapolating from the SLC experience, it has been estimated that $\delta\mathcal{P}_{e^\pm}$ can be measured to around 10^{-4} [107]. With effort, this uncertainty might be reduced further, although the difficulty of quickly reversing the positron helicity may limit how precisely the relative positron polarization difference can be measured. Several other experimental systematic uncertainties on A_{LR} also need to be controlled at the 10^{-4} level, including asymmetries in the luminosity delivered and backgrounds observed in the different helicity combinations.

Due to $\gamma - Z$ interference, the dependence of A_{LR} on the collision energy $\sqrt{s}$ is given by $\mathrm{d}A_{\mathrm{LR}}/\mathrm{d}\sqrt{s} = 2 \times 10^{-2}/\mathrm{GeV}$. The difference $\sqrt{s} - M_Z$ thus needs to be known to ~ 10 MeV to match the experimental precision achievable with electron polarization only, and to ~ 1 MeV with polarized positrons. A multi-point scan of the Z peak is foreseen to provide the relative calibration of the collision energy $\sqrt{s}$ with respect to m_Z at the ~ 1 MeV level. The collision energy $\sqrt{s}$ must be understood including any beamstrahlung, which causes a significant ≈ 50 MeV shift to the luminosity-weighted mean $\sqrt{s}$, depending on the exact collision parameters. As long as the beamstrahlung distribution is constant throughout the Z scan, however, this effect will be calibrated out to first order by the scan. Direct measurements of this beamstrahlung shape to a few percent should also be possible using Bhabha acolinearity and the di-muon momentum spectrum.

Overall, an uncertainty of $\Delta A_{\mathrm{LR}} = 10^{-4}$ can be achieved at a polarized linear collider with 10^9 Z bosons, corresponding to an uncertainty on the effective weak mixing angle of $\Delta \sin^2\theta^\ell_{\mathrm{eff}} < 1.3 \cdot 10^{-5}$ [106].

Polarized beams can also be produced at circular e^+e^- storage rings, and transverse polarizations of $\sim 50\%$ were observed at LEP [113]. To exploit this polarization for a measurement of A_{LR} requires spin rotators to be installed to provide longitudinal polarization at the interaction points. With the luminosity available at a machine like TLEP, very small statistical uncertainties on A_{LR} can be achieved. The collision energy $\sqrt{s}$ can be measured to a precision of 100 keV using resonant depolarization as was used at LEP for the measurement of the Z boson mass [114]. This uncertainty limits the achievable precision on the effective weak mixing angle to $\Delta \sin^2\theta^\ell_{\mathrm{eff}} = 1 \cdot 10^{-6}$ [105].

In a storage ring, it is difficult to reverse the helicity of the colliding bunches on a short time scale, so the scheme used at a linear collider is not applicable. To avoid being limited by an absolute polarization measurement, the original Blondel scheme has been proposed where four helicity combinations are formed from polarized and unpolarized electron and positron bunches circulating in the same fill [111]. This scheme again relies on the ability to measure the difference in polarization between the electron and positron bunches ($\delta\mathcal{P}_{e^\pm}$), and also to measure or limit any residual polarization in the nominally unpolarized bunches. An added complication is that the longitudinal polarization needs to be known at the interaction point, while the polarization measurements at a storage ring are most easily made on the transversely-polarized beams away from the interaction points, so possible asymmetries in the spin rotators must be carefully considered. Detailed estimates of the other experimental systematic uncertainties achievable at TLEP are not currently available, although in general they are similar to the experimental challenges faced at a linear e^+e^- collider for the same measurement. In Table 19-11, a placeholder for the systematics at TLEP is based on scaling with statistics; a better estimate is needed. Higher order calculations needed for the extraction of $\sin^2\theta^\ell_{\mathrm{eff}}$ also require further study and are absent in this table at the moment. A target of $\Delta \sin^2\theta^\ell_{\mathrm{eff}} = 1 \cdot 10^{-6}$ is quoted in [105]; in Table 19-11 the systematics-dominated target of $\Delta \sin^2\theta^\ell_{\mathrm{eff}} = 3 \cdot 10^{-6}$ is subject to further study of the TLEP potential.

$\Delta \sin^2\theta^l_{\rm eff}$ [10^{-5}]	ILC/GigaZ	TLEP(Z)
$\sqrt{s}$ [GeV]	91	91
$\mathcal{L}$[fb^{-1}]	30	3000×4
systematics	1.1	0.2
statistical	0.5	0.1
higher order corr.	?	?
beam energy	0.5	0.05
total	1.3	0.3

Table 19-11. *Projected target uncertainties in the measurement of* $\sin^2\theta^l_{\rm eff}$ *at* e^+e^- *colliders. Systematic uncertainties for TLEP have been scaled with statistics; whether this scaling can be achieved remains a question to study. Higher-order calculations required for the measurement also need to be investigated.*

19.2.4 Summary of experimental target accuracies and theory uncertainties for $\sin^2\theta^\ell_{\rm eff}$ and M_W

In Table 19-12 we summarize the discussion of the previous sections by showing the target accuracies for the measurements of M_W and $\sin^2\theta^\ell_{eff}$ at the LHC, ILC and TLEP and the estimated future theory uncertainties of their SM predictions.

	LHC	LHC	ILC/GigaZ	ILC	ILC	ILC	TLEP	SM prediction
$\sqrt{s}$ [TeV]	14	14	0.091	0.161	0.161	0.250	0.161	-
$\mathcal{L}$[fb^{-1}]	300	3000		100	480	500	3000×4	-
ΔM_W [MeV]	8	5	-	4.1-4.5	2.3-2.9	2.8	< 1.2	4.2(3.0)
$\Delta \sin^2\theta^\ell_{\rm eff}$ [10^{-5}]	36	21	1.3	-	-	-	0.3	3.0(2.6)

Table 19-12. *Target accuracies for the measurement of* M_W *and* $\sin^2\theta^\ell_{eff}$ *at the LHC, ILC and TLEP, also including estimated future theoretical uncertainties due to missing higher-order corrections, and theory uncertainties of their SM predictions. The uncertainties on the SM predictions are provided for* $\Delta m_t = 0.5(0.1)$ *GeV (see Table 19-3 for details). At present the measured values for* M_W *and* $\sin^2\theta^\ell_{\rm eff}$ *are:* $M_W = 80.385 \pm 0.015$ *GeV [112] and* $\sin^2\theta^\ell_{\rm eff} = (23153 \pm 16) \times 10^{-5}$ *[3] compared to their current SM predictions of Section 19.2.1:* $M_W = 80.360 \pm 0.008$ *GeV and* $\sin^2\theta^\ell_{\rm eff} = (23127 \pm 7.3) \times 10^{-5}$.

19.2.5 Other EWPOs at lepton colliders

Besides M_W and $\sin^2\theta^\ell_{\rm eff}$, other EWPOs of great interest include the Z-pole observables such as the Z boson mass and width, and its hadronic and leptonic partial widths. Estimates of statistical sensitivity and beam energy calibration uncertainty are presented for TLEP in [105]. This machine is capable of producing about a trillion Z bosons. Pending further study, preliminary targets of 0.1 MeV uncertainty have been stated for M_Z and Γ_Z. A relative precision of 5×10^{-5} is stated to be a reasonable target for the ratio of the Z-boson's hadronic-to-leptonic partial widths at TLEP, as well as for the ratios of the Z-boson leptonic widths (as a test of lepton universality). These estimates would represent a factor of ≈ 20 improvement over LEP.

The vertex correction to the $Z \to b\bar{b}$ partial width is also of interest, which is sensitively probed by $R_b = \Gamma_{Z\to b\bar{b}}/\Gamma_{\rm had}$. A precision of $2-5\times10^{-5}$ is stated as a reasonable goal for the measurement of R_b at TLEP, a factor of ≈ 10 improvement over LEP and SLC.

A discussion of present and future anticipated theory errors of predictions for R_b and Γ_Z can be found in Section 19.2.1.

19.2.6 Prospects for determinations of SM parameters from global fits with GFITTER

Measurements at future colliders will increase the experimental precision of key observables sensitive to electroweak loop effects. Among these are the W boson mass, the top quark mass, and the effective weak mixing angle. Alongside the construction of these machines, progress in the calculation of multi-loop corrections to these observables, and also in the determination of $\Delta\alpha_{\rm had}(M_Z^2)$, is expected. Taken together in the global electroweak fit, these improvements will provide tests of the consistency of the SM with unprecedented power.

This section presents a short summary of preliminary studies foreseen to be published soon. To date results of the global electroweak fit are compared with expectations for the Large Hadron Collider (LHC) with $\int Ldt = 300\,{\rm fb}^{-1}$ at $\sqrt{s} = 14\,{\rm TeV}$ and the International Linear Collider (ILC) with GigaZ option [197]. The left columns of Table 19-13 summarize the current and the projected experimental precisions for the observables used in the fit. For the studies of fit prospects at the LHC and ILC presented here, the central values of the assumed future measurements have been adjusted to obtain a common fit value of $M_H \simeq 126\,{\rm GeV}$. We assume that the theoretical uncertainties in the SM predictions of M_W and $\sin^2\theta^\ell_{\rm eff}$ reduce from the current $\delta_{\rm theo}M_W = 4$ MeV and $\delta_{\rm theo}\sin^2\theta^\ell_{\rm eff} = 4.7\cdot10^{-5}$ to 1 MeV and 10^{-5}, respectively. We refer to our past publications [115, 116, 117] for details about the theoretical calculations and the statistical methods used.

Indirect determinations of the SM parameters and observables are obtained by scanning the $\Delta\chi^2$ profile in fits where the corresponding input constraint is ignored. Examples for such profiles of the Higgs boson mass are shown in the left panel of Fig. 19-6. The resulting one-sigma uncertainties are listed in Table 19-13.

The assumed improvements in the experimental precision of M_W and m_t from the LHC lead to a reduction of the uncertainty in the indirect determination of M_H (present: $^{+44}_{-34}\,{\rm GeV}$, LHC: $^{+23}_{-20}\,{\rm GeV}$). Substantial gain is achieved with the ILC/GigaZ with an expected uncertainty of $^{+10}_{-9}\,{\rm GeV}$. In all scenarios the uncertainties on the indirect M_H determination are quoted for a common fit value of $M_H \simeq 126\,{\rm GeV}$.[4]

The current uncertainty on the indirect M_W determination from the fit of 11 GeV will improve to 5.8 GeV with the LHC and to 3.6 MeV at the ILC/GigaZ. A comparison of the direct M_W measurement at the ILC (5 MeV expected precision) with the more precise indirect determination will provide a stringent test of the SM.

The right panel of Fig. 19-6 shows the allowed areas for fits with fixed variable pairs M_W versus m_t in the three scenarios (current fit, LHC prospects, ILC prospects). Also shown by the horizontal and vertical bands are the one-sigma ranges of the current direct measurements (blue), as well as the LHC (green) and ILC/GigaZ expectation (yellow). A significant rise in precision is found for the future scenarios.

[4] A fit using the uncertainties and the central values of the present measurements yields $M_H = 94^{+25}_{-22}\,{\rm GeV}$ [117].

The left panel of Fig. 19-7 shows the corresponding results in the M_W versus $\sin^2\theta^\ell_{\rm eff}$plane. The high precision of the expected $\sin^2\theta^\ell_{\rm eff}$measurement at the ILC will enable a stringent test of the internal SM consistency in this area.

The expected constraints on the oblique parameters [118, 29] S and T, parametrizing possible new physics contributions to the neutral and to the difference between neutral and charged weak current, respectively, for a fixed value of $U = 0$, are shown in the right panel of Fig. 19-7. The blue ellipses indicate the 68% and 95% contours of the current electroweak fit. The light blue ellipses show the results using the current uncertainties with adjusted central values to obtain $M_H \simeq 126\,\text{GeV}$, the green ellipses that of the LHC, and the orange ellipses show the precision expected for the ILC/GigaZ. The corresponding numerical values are given in Table 19-13. The sensitivity to new physics is improved over a factor of three compared with that of today.

19.2.7 EWPOs in the MSSM

Precision measurements of SM observables have proven to be a powerful probe of BSM physics via virtual effects of the additional BSM particles. In general, precision observables (such as particle masses, mixing angles, asymmetries etc.) constitute a test of the model at the quantum-loop level, since they can be calculated within a certain model beyond leading order in perturbation theory, depending sensitively on the other model parameters, and can be measured with equally high precision. Various models predict different values of the same observable due to their different particle content and interactions. This permits to distinguish between, e.g., the SM and a BSM model, via precision observables. Naturally, this requires

	Experimental input $[\pm1\sigma]$			Indirect determination $[\pm1\sigma_{\rm exp} \pm 1\sigma_{\rm theo}]$		
Parameter	Present	LHC	ILC/GigaZ	Present	LHC	ILC/GigaZ
M_H [GeV]	±0.4	$< \pm0.1$	$< \pm0.1$	$^{+32\ +12}_{-26\ -8}$	$^{+20\ +3}_{-18\ -2}$	$^{+6.9\ +2.7}_{-6.6\ -2.4}$
M_W [MeV]	±15	±8	±5	$\pm6.3\ \pm4.2$	$\pm4.8\ \pm1.0$	$\pm1.9\ \pm1.7$
M_Z [MeV]	±2.1	±2.1	±2.1	$\pm11.6\ \pm3.8$	$\pm6.9\ \pm0.8$	$\pm2.6\ \pm1.1$
m_t [GeV]	±0.9	±0.6	±0.1	$\pm2.3\ \pm0.8$	$\pm1.4\ \pm0.2$	$\pm0.7\ ^{+0.3}_{-0.2}$
$\sin^2\theta^\ell_{\rm eff}$ $[\cdot10^{-5}]$	±16	±16	±1.3	$\pm4.8\ \pm5.0$	$\pm2.7\ \pm1.1$	$\pm2.0\ \pm1.2$
$\Delta\alpha^5_{\rm had}M_Z^2$ $[\cdot10^{-5}]$	±10	±4.7	±4.7	$\pm43\ \pm15$	$\pm36\ \pm4$	$\pm5.7\ \pm2.9$
R^0_l $[\cdot10^{-3}]$	±25	±25	±4	–	–	–
$\alpha_S(M_Z)$ $[\cdot10^{-4}]$	–	–	–	$\pm27\ \pm1$	$\pm27\ \pm1$	$^{+6.8\ +0.3}_{-6.3\ -0.2}$
$S\|_{U=0}$	–	–	–	±0.09	±0.09	±0.02
$T\|_{U=0}$	–	–	–	±0.07	±0.06	±0.02

Table 19-13. *Current and estimated future uncertainties in the input observables (left), and the precision obtained from the fit without using a given observable as input (right). The experimental and theoretical uncertainties are separately given, where in the Rfit scheme the total error corresponds to the linear sum of both contributions. The value of $\alpha_s(M_Z^2)$ is not used directly as input in the fit. The exact value of the uncertainties of the future M_H measurements is not relevant for the fit. For all indirect determinations shown in this table (including the present M_H determination) the assumed central values of the input measurements have been adjusted to obtain a common fit value of $M_H \simeq 126$ GeV.*

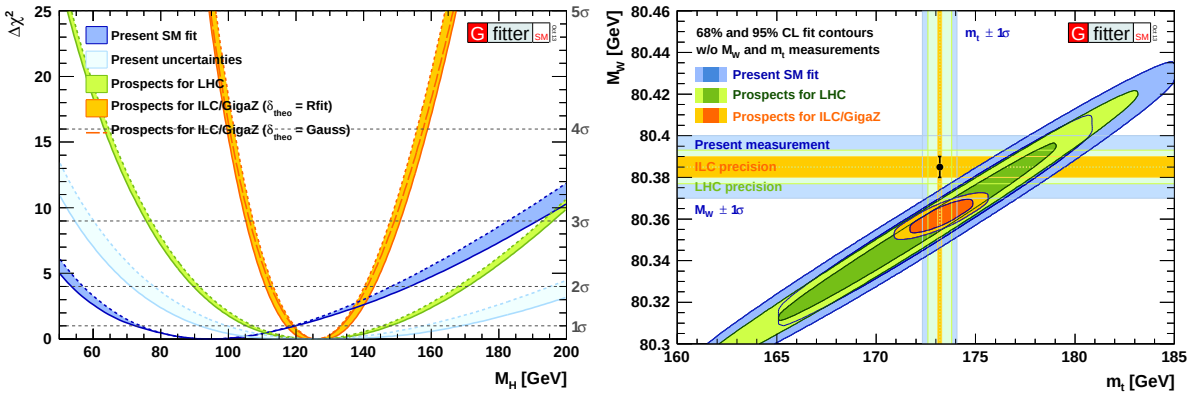

Figure 19-6. *Fit results for the present and assumed future scenarios compared to the direct measurements. For the future scenarios the central values of the input measurements are adjusted to reproduce the SM with $M_H \simeq 126$ GeV. Left: $\Delta\chi^2$ profiles versus M_H; in blue the present result, and in light blue, green and orange the present, LHC and ILC/GigaZ scenarios are shown, respectively, all using the future fit setup with corresponding uncertainties. Right: M_W versus m_t; the horizontal and vertical bands indicate in blue today's precision of the direct measurements, and in light green and orange the extrapolated precisions for LHC and ILC/GigaZ, respectively.*

a very high precision of both the experimental results and the theoretical predictions. (It should be kept in mind that the extraction of precision data often assumes the SM.) Important EWPOs are the W boson mass, M_W, and the effective leptonic weak mixing angle, $\sin^2\theta^\ell_{\rm eff}$, where the top quark mass plays a crucial role as input parameter. As an example for BSM physics the Minimal Supersymmetric Standard Model (MSSM) is a prominent showcase and will be used here for illustration.

The first analysis concerns the W boson mass. The prediction of M_W in the MSSM depends on the masses, mixing angles and couplings of all MSSM particles. Sfermions, charginos, neutralinos and the MSSM Higgs bosons enter already at one-loop level and can give substantial contributions to M_W. The evaluation used here consists of the complete available SM calculation, a full MSSM one-loop calculations and all available MSSM two-loop corrections [119, 120]. Due to the strong MSSM parameter dependencies, it is expected to obtain restrictions on the MSSM parameter space in the comparison of the M_W prediction and the experimental value.

The results for the general MSSM can be obtained in an extensive parameter scan [120]. The ranges of the various SUSY parameters are given in Table 19-14. μ is the Higgsino mixing parameter, $M_{\tilde{F}_i}$ denotes the soft SUSY-breaking parameter for sfermions of the ith family for left-handed squarks ($F = Q$), right-handed up- and down-type squarks ($F = U, D$), left-handed sleptons ($F = L$) and right-handed sleptons ($F = E$). A_f denotes the trilinear sfermion-Higgs couplings, M_3 the gluino mass parameter and M_2 the SU(2) gaugino mass parameter, where the U(1) parameter is fixed as $M_1 = 5/3 s_w^2/c_w^2 M_2$. M_A is the CP-odd Higgs boson mass and $\tan\beta$ the ratio of the two Higgs vacuum expectation values.

All MSSM points included in the results have the neutralino as LSP and the sparticle masses pass the lower mass limits from direct searches at LEP. The Higgs and SUSY masses are calculated using `FeynHiggs` (version 2.9.4) [121, 122, 123, 124, 125]. For every point, it was tested whether it is allowed by direct Higgs searches using the code `HiggsBounds` (version 3.8.0) [126, 127]. This code tests the MSSM points against the limits from LEP, Tevatron and the LHC.

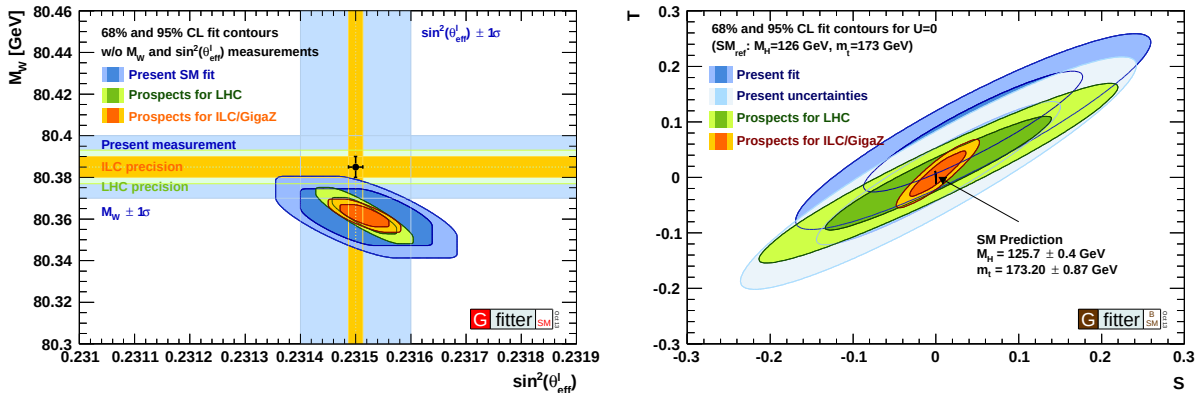

Figure 19-7. *Fit results for the present and assumed future scenarios. Left: fit contours for M_W versus $\sin^2\theta^\ell_{\rm eff}$ compared to the direct measurements; in blue, orange and green the present, LHC and ILC/GigaZ scenarios are shown, respectively. For the future scenarios the central values of the input measurements are adjusted to reproduce the SM with $M_H \simeq 126$ GeV; horizontal and vertical bands indicate today's and the expected future precision of the direct measurements. Right: constraints of the oblique parameters S and T, with $U = 0$ fixed, for the present data (blue), the present uncertainties with central values adjusted to obtain $M_H \simeq 126$ GeV (light blue), the LHC (green) and ILC/GigaZ prospects (orange).*

Parameter	Minimum	Maximum
μ	-2000	2000
$M_{\tilde{E}_{1,2,3}} = M_{\tilde{L}_{1,2,3}}$	100	2000
$M_{\tilde{Q}_{1,2}} = M_{\tilde{U}_{1,2}} = M_{\tilde{D}_{1,2}}$	500	2000
$M_{\tilde{Q}_3}$	100	2000
$M_{\tilde{U}_3}$	100	2000
$M_{\tilde{D}_3}$	100	2000
$A_e = A_\mu = A_\tau$	$-3\, M_{\tilde{E}}$	$3\, M_{\tilde{E}}$
$A_u = A_d = A_c = A_s$	$-3\, M_{\tilde{Q}_{12}}$	$3\, M_{\tilde{Q}_{12}}$
A_b	$-3\max(M_{\tilde{Q}_3}, M_{\tilde{D}_3})$	$3\max(M_{\tilde{Q}_3}, M_{\tilde{D}_3})$
A_t	$-3\max(M_{\tilde{Q}_3}, M_{\tilde{U}_3})$	$3\max(M_{\tilde{Q}_3}, M_{\tilde{U}_3})$
$\tan\beta$	1	60
M_3	500	2000
M_A	90	1000
M_2	100	1000

Table 19-14. *MSSM parameter ranges. All parameters with mass dimension are given in GeV.*

The results for M_W are shown in Fig. 19-8 as a function of m_t, assuming the light CP-even Higgs h in the region $125.6 \pm 0.7(3.1)$ GeV in the SM (MSSM) case. The red band indicates the overlap region of the SM and the MSSM. The leading one-loop SUSY contributions arise from the stop sbottom doublet. However requiring M_h in the region 125.6 ± 3.1 GeV restricts the parameters in the stop sector [128] and with it the possible M_W contribution. Large M_W contributions from the other MSSM sectors are possible, if either charginos, neutralinos or sleptons are light.

The gray ellipse indicates the current experimental uncertainty, whereas the blue and red ellipses shows the anticipated future LHC and ILC/GigaZ precisions, respectively (for each collider experiment separately) of Table 19-12, along with $m_t = 172.3 \pm 0.9$ (0.5, 0.1) GeV for the current (LHC, ILC) measurement of the top quark mass. While, at the current level of precision, SUSY might be considered as slightly favored over the SM by the M_W-m_t measurement, no clear conclusion can be drawn. The smaller blue and red ellipses, on the other hand, indicate the discrimination power of the future LHC and ILC/GigaZ measurements. With the improved precision a small part of the MSSM parameter space could be singled out.

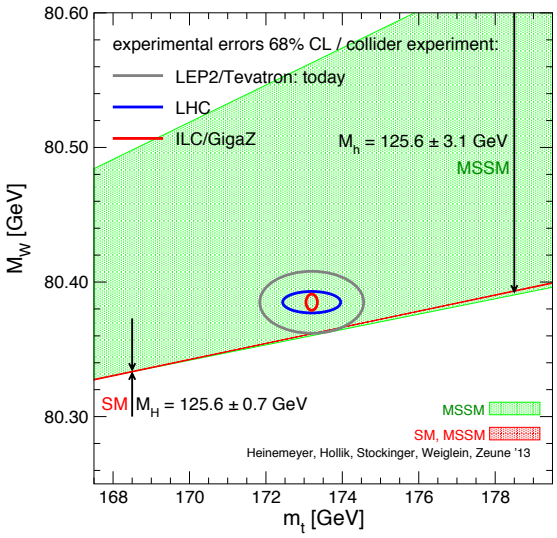

Figure 19-8. *Predictions for M_W as a function of m_t in the SM and MSSM (see text). The gray, blue and red ellipses denote the current, and the target LHC and ILC/GigaZ precision, respectively, as provided in Table 19-12.*

In a second step we apply the precise ILC measurement of M_W to investigate its potential to determine unknown model parameters. Within the MSSM we assume the hypothetical future situation that a light scalar top has been discovered with $m_{\tilde{t}_1} = 400 \pm 40$ GeV at the LHC, but that no other new particle has been observed. We set lower limits of 100 GeV on sleptons, 300 GeV on charginos, 500 GeV on squarks of the third generation and 1200 GeV on the remaining colored particles. The neutralino mass is constrained by the GUT relation $M_1 \approx M_2/2$ so that setting a lower limit of 300 GeV on charginos also sets the lower mass limits on neutralinos of $\sim$ 150 GeV. We have selected the points from our scan accordingly. Any additional particle observation would lead to an even more restricted set of points and thus strengthen the parameter determination. In Fig. 19-9, we show the "surviving" points from our scan. All points fulfil $M_h = 125.6 \pm 3.1$ GeV and $m_{\tilde{t}_1} = 400 \pm 40$ GeV. Orange, red, blue and purple points denote in addition W boson mass values of $M_W = 80.375, 80.385, 80.395, 80.405 \pm 0.005$ GeV, respectively. In the right-hand figure we show the results as a function of the masses of the heavy scalar top and the light scalar bottom. It can be seen that these unknown mass scales are restricted to small intervals if 80.385 GeV or higher M_W values are assumed as central experimental values (i.e. sufficiently different from the SM prediction). In this situation the precise M_W measurement could give clear indications of where to search for these new particles (or how to rule out the simple MSSM picture). For instance, a measurement of $M_W = 80.405 \pm 0.005$ GeV (purple MSSM scenarios) would indicate that $m_{\tilde{b}_1} < 800$ GeV.

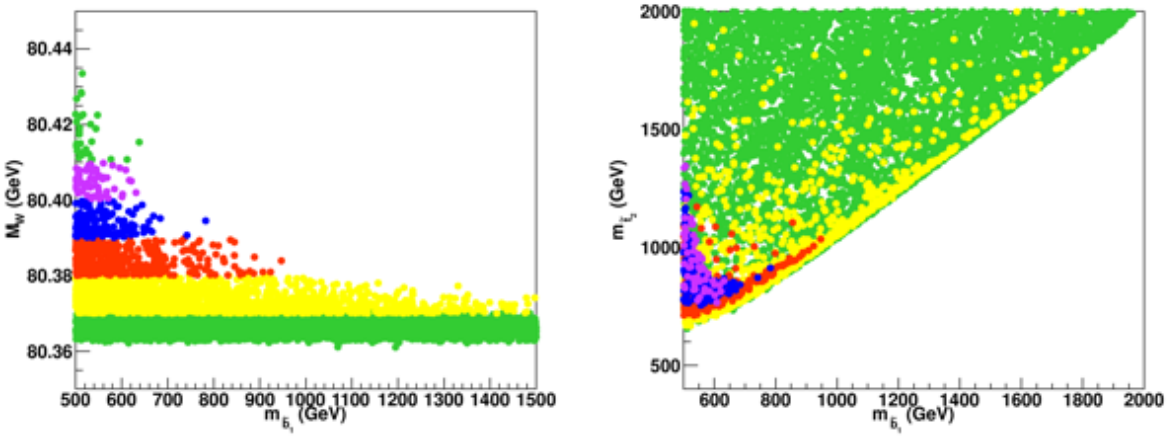

Figure 19-9. *Results of a MSSM parameter scan to illustrate what can be learned from an improved M_W measurement under the assumption a light stop is found with $m_{\tilde{t}_1} = 400 \pm 40$ GeV: green points: all points in the scan with $M_h = 125.6 \pm 3.1$ GeV and $m_{\tilde{t}_1} = 400 \pm 40$ GeV, yellow, red, blue, purple points: $M_W = 80.375 \pm 0.005$ GeV (yellow), $M_W = 80.385 \pm 0.005$ GeV (red), $M_W = 80.395 \pm 0.005$ GeV (blue), and $M_W = 80.405 \pm 0.005$ GeV (purple) .*

The MSSM parameter space could also be constrained by a precise measurement of $\sin^2\theta^\ell_{\rm eff}$. The evaluation of the latter is performed at the same level of accuracy as for M_W [129].

In the first example it is investigated whether the high accuracy achievable at the GigaZ option of the ILC would provide sensitivity to indirect effects of SUSY particles even in a scenario where the superpartners are so heavy that they escape detection at the LHC [129]. We consider in this context a scenario with very heavy squarks and a very heavy gluino. It is based on the values of the SPS 1a′ benchmark scenario [130], but the squark and gluino mass parameters are fixed to 6 times their SPS 1a′ values. The other masses are scaled with a common scale factor given by the light chargino mass, except M_A which we keep fixed at its SPS 1a′ value. In this scenario the strongly interacting particles are too heavy to be detected at the LHC, while, depending on the scale-factor, some colour-neutral particles may be in the ILC reach. In Fig. 19-10 we show the prediction for $\sin^2\theta^\ell_{\rm eff}$ in this scenario as a function of the lighter chargino mass, $m_{\tilde{\chi}_1^\pm}$. The prediction includes the parametric uncertainty, $\sigma^{\rm para-LC}$, induced by the ILC measurement of m_t, $\Delta m_t = 100$ MeV, and the numerically more relevant prospective future uncertainty on $\Delta\alpha^{(5)}_{\rm had}$, $\delta(\Delta\alpha^{(5)}_{\rm had}) = 5 \times 10^{-5}$. The MSSM prediction for $\sin^2\theta^\ell_{\rm eff}$ is compared with the experimental resolution with GigaZ precision, $\sigma^{\rm LC} = 0.000013$, using for simplicity the current experimental central value. The SM prediction (with $M_H^{\rm SM} = M_h^{\rm MSSM}$) is also shown, applying again the parametric uncertainty $\sigma^{\rm para-LC}$. Despite the fact that no coloured SUSY particles would be observed at the LHC in this scenario, the ILC with its high-precision measurement of $\sin^2\theta^\ell_{\rm eff}$ in the GigaZ mode could resolve indirect effects of SUSY up to $m_{\tilde{\chi}_1^\pm} \lesssim 500$ GeV. This means that the high-precision measurements at the LC with GigaZ option could be sensitive to indirect effects of SUSY even in a scenario where SUSY particles have *neither* been directly detected at the LHC nor the first phase of the ILC with a centre of mass energy of up to 500 GeV.

We now analyse the sensitivity of $\sin^2\theta^\ell_{\rm eff}$ together with M_W to higher-order effects in the MSSM by investigating a broad parameter scan range similar as in Tab. 19-14. Only the constraints on the MSSM parameter space from the LEP Higgs searches [131, 132] and the lower bounds on the SUSY particle masses previous to the LHC SUSY searches were taken into account. However, the SUSY particles strongly affected

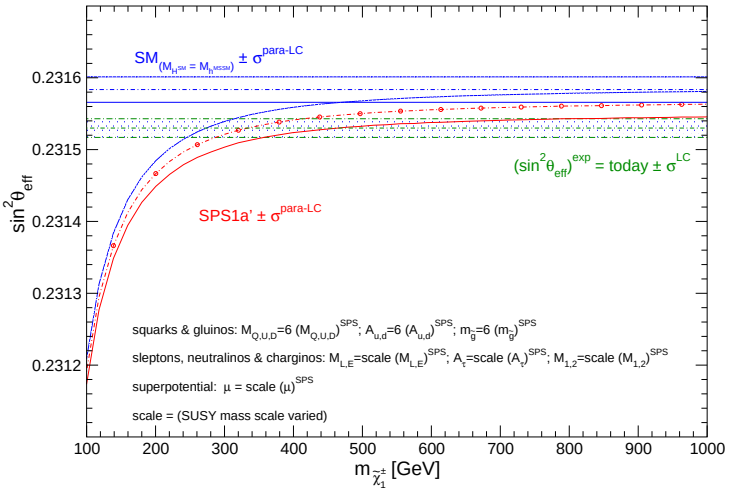

Figure 19-10. *Theoretical prediction for* $\sin^2\theta^\ell_{\rm eff}$ *in the SM and the MSSM (including prospective parametric theoretical uncertainties) compared to the experimental precision at the ILC with GigaZ option. An SPS 1a′ inspired scenario is used, where the squark and gluino mass parameters are fixed to 6 times their SPS 1a′ values. The other mass parameters are varied with a common scale factor (see text).*

by the LHC searches are the squarks of the first and second generation and the gluino. Exactly these particles, however, have a very small effect on the prediction of M_W and $\sin^2\theta^\ell_{\rm eff}$ and thus a negligible effect on this analysis.

In Fig. 19-11 we compare the SM and the MSSM predictions for M_W and $\sin^2\theta^\ell_{\rm eff}$ as obtained from the scatter plot data. The predictions within the two models give rise to two regions in the M_W–$\sin^2\theta^\ell_{\rm eff}$ plane, red for the SM and green for the MSSM. The SM region also forms part of the MSSM-allowed intervals in the decoupling regime. For the SM $M_H^{\rm SM} = 125.6 \pm 0.7$ GeV has been required, whereas for the MSSM the Higgs mass measurement is met with a larger uncertainty due to the still large theory uncertainties in the M_h calculation [122]. The variation with m_t from 170 to 175 GeV is indicated. The 68% C.L. experimental results for M_W and $\sin^2\theta^\ell_{\rm eff}$ are indicated in the plot, given for the current precision and for the target LHC and ILC/GigaZ accuracies, see Tab. 19-12. The center ellipse corresponds to the current world average. Also shown are the error ellipses corresponding to the two individual most precise measurements of $\sin^2\theta^\ell_{\rm eff}$, based on $A^e_{\rm LR}$ by SLD and $A^b_{\rm FB}$ by LEP, corresponding to

$$A^b_{\rm FB}({\rm LEP}) \;:\; \sin^2\theta^{\ell\,{\rm exp,LEP}}_{\rm eff} = 0.23221 \pm 0.00029\ , \tag{19.14}$$

$$A^e_{\rm LR}({\rm SLD}) \;:\; \sin^2\theta^{\ell\,{\rm exp,SLD}}_{\rm eff} = 0.23098 \pm 0.00026\ , \tag{19.15}$$

$$\sin^2\theta^{\ell\,{\rm exp,aver.}}_{\rm eff} = 0.23153 \pm 0.00016\ , \tag{19.16}$$

where the latter one represents the average [3]. The first (second) value prefers a value of $M_H^{\rm SM} \sim 32$ (437) GeV. The two measurements differ by about $3\,\sigma$. The averaged value of $\sin^2\theta^\ell_{\rm eff}$, as given in Eq. 19.16, prefers $M_H^{\rm SM} \sim 110$ GeV. One can see that the current averaged value is compatible with the SM with $M_H^{\rm SM} \sim 125.6$ GeV and with the MSSM. The value of $\sin^2\theta^\ell_{\rm eff}$ obtained from $A^e_{\rm LR}$(SLD) clearly favors the MSSM over the SM. On the other hand, the value of $\sin^2\theta^\ell_{\rm eff}$ obtained from $A^b_{\rm FB}$(LEP) together with the M_W data from LEP and the Tevatron would correspond to an experimentally preferred region that deviates from the predictions of both models. This unsatisfactory solution can only be resolved by new measurements. The anticipated LHC accuracy for $\sin^2\theta^\ell_{\rm eff}$ would have only a limited potential to resolve this discrepancy, as it is larger than the current uncertainty obtained from the LEP/SLD average.

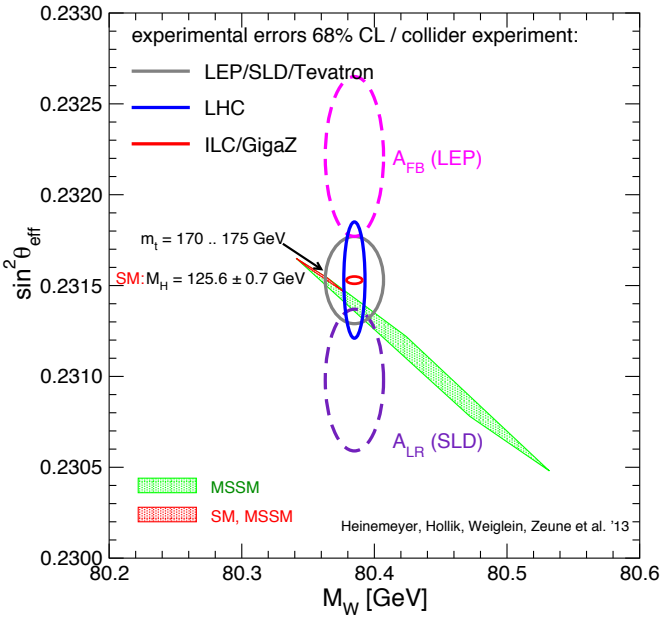

Figure 19-11. *MSSM parameter scan for M_W and $\sin^2\theta^\ell_{\rm eff}$ (see text). Today's 68% C.L. ellipses (from $A^b_{\rm FB}$(LEP), $A^e_{\rm LR}$(SLD) and the world average) are shown as well as the anticipated LHC and ILC/GigaZ precisions, drawn around today's central value.*

On the other hand, a Z factory, i.e. the GigaZ option, would be an ideal solution, as is indicated by the red ellipse. The anticipated ILC/GigaZ precision of the combined M_W–$\sin^2\theta^\ell_{\rm eff}$ measurement could put severe constraints on each of the models and resolve the discrepancy between the $A^b_{\rm FB}$(LEP) and $A^e_{\rm LR}$(SLD) measurements. If the central value of an improved measurement with higher precision should turn out to be close to the central value favored by the current measurement of $A^b_{\rm FB}$(LEP), this would mean that the electroweak precision observables M_W and $\sin^2\theta^\ell_{\rm eff}$ could rule out both the SM and the most general version of the MSSM.

19.2.8 EWPOs and Z' bosons

EWPOs also constrain possible new physics scenarios such as $U(1)'$ gauge extensions of the SM. Current constraints [133] on the associated Z' boson masses, $M_{Z'}$, are generally comparable and in some cases stronger than the direct lower search limits from LEP and the Tevatron. The 8 TeV LHC data have extended the lower limits to roughly 2.5 TeV (depending on the model). However, the LHC dilepton and dijet resonance searches are insensitive to the Z-Z' mass mixing angle, $\theta_{ZZ'}$. Current EWPOs constrain $\theta_{ZZ'}$ to the 10^{-2} level and very often well below this. The EWPOs projected for the ILC including the GigaZ option as shown in Table 19-12 (most importantly the measurements of M_W to 2.3-2.9 MeV, the effective weak mixing angle to 1.3×10^{-5}, and m_t to 0.1 GeV) would improve the $\theta_{ZZ'}$ limits by almost another order of magnitude. This is important, since in specific models, $M_{Z'}$ and $\theta_{ZZ'}$ are not independent. As an example, consider the popular benchmark case of the Z_χ boson (appearing in $SO(10)$ GUT models) with a $U(1)'$ breaking Higgs

sector compatible with Supersymmetry. In this case, the projected EWPOs would experience noticeable shifts for $M_{Z'}$ values of up to 6 TeV, without assuming any improvement in $\Delta\alpha_{\rm had}$. The EWPOs are also important for leptophobic Z' bosons where the LHC sets weaker mass limits.

In the case of a Z' discovery at the LHC, it becomes mandatory to achieve the highest possible accuracy in the EWPOs. As an illustration, suppose a future LHC run discovers a dilepton resonance with an invariant mass of 3 TeV. Even if one would succeed to determine the spin of the resonance, it would not be possible to simultaneously obtain meaningful information on the coupling strength and on $\theta_{ZZ'}$, by using LHC data alone. But the EWPOs would determine the size and the sign of $\theta_{ZZ'}$ which would give valuable information on the $U(1)'$ breaking sector and *simultaneously* constrain the T parameter to the level of ± 0.01, thereby constraining possible additional non-degenerate fermion (or scalar) multiplets that may be necessary to cancel gauge anomalies related to the $U(1)'$.

19.3 New interactions in vector boson scattering and tri-boson processes

Multi-boson production in various topologies provides a unique way to probe new physics. Assuming that the 125 GeV boson discovered at the LHC is the SM Higgs boson, it is natural to assume that electroweak symmetry breaking occurs according to the SM Higgs mechanism. Therefore, deviations from the SM in multi-boson production can be parameterized by $\mathrm{SU}(2)_L{\times}\mathrm{U}(1)_Y$ gauge-invariant operators which do not introduce any new sources of EWSB. If the new physics associated with these operators occurs at a high mass scale, one is motivated to use the formulation of Effective Field Theory (EFT) to organize the operators in order of increasing dimensionality. Here we will consider an EFT, which includes dimension-6 and dimension-8 operators that modify the interactions among electroweak gauge bosons, described by the following Lagrangian:

$$\mathcal{L}_{EFT} = \mathcal{L}_{SM} + \sum_{i=WWW,W,B,\Phi W,\Phi B} \frac{c_i}{\Lambda^2}\mathcal{O}_i + \sum_{j=0,1} \frac{f_{S,j}}{\Lambda^4}\mathcal{O}_{S,j} + \sum_{j=0,\ldots,9} \frac{f_{T,j}}{\Lambda^4}\mathcal{O}_{T,j} + \sum_{j=0,\ldots,7} \frac{f_{M,j}}{\Lambda^4}\mathcal{O}_{M,j} \quad (19.17)$$

A detailed discussion of these operators is provided in Section 19.3.1.

As an example of new physics in the Higgs sector, let us consider the interaction of the Higgs doublet field Φ with a new scalar field S of the form $\Phi^\dagger\Phi S$. This operator can mediate $\Phi\Phi \to \Phi\Phi$ scattering via s and t channel exchange of the S boson. In the limit of the mass of S being much larger than the energy of this scattering process, the lowest dimension effective operator induced is the dimension-4 operator $(\Phi^\dagger\Phi)^2$, which mimics the quartic Higgs potential in the SM. At the next order in the momentum flowing along the S propagator, the effective operator induced is

$$O_{\phi d} = \frac{c_{\phi d}}{M_S^2}\partial_\mu(\Phi^\dagger\Phi)\partial^\mu(\Phi^\dagger\Phi)$$

where the coefficient is enhanced by the coupling of the Φ to the S field and is suppressed by the squared mass of the S boson. This example illustrates a tree-level contribution to a higher-dimension operator due to a new interaction with a massive scalar field. After the Higgs field Φ acquires a vev, the operator $O_{\phi d}$ changes the normalization of the Higgs field and therefore changes its coupling to the electroweak gauge bosons. As a result, the unitarization of the vector boson scattering (VBS) amplitudes is altered and we would expect anomalous contributions.

An example of a dimension-8 operator is provided by the analogue of the QED light-by-light scattering mediated by the electron box loop. In the limit that the electromagnetic field is weak and slowly varying,

this process is described by the Euler-Heisenberg Lagrangian

$$\mathcal{L}_{EH} = \frac{1}{2}(E^2 - B^2) + 2\frac{\alpha^2}{45m^4}[(E^2 - B^2)^2 + 7(E.B)^2]$$

where E and B are the electric and magnetic field strengths, α is the electromagnetic coupling and m is the electron mass. The second term represents the $\gamma\gamma \to \gamma\gamma$ scattering EFT operator induced by the electron box diagram when the photon energies are much smaller than the electron mass. This term can be re-written as a linear combination of the operators $(F_{\mu\nu}F^{\mu\nu})^2$ and $(F_{\mu\rho}F^{\mu\sigma})(F^{\nu\rho}F_{\nu\sigma})$, where F is the electromagnetic field strength tensor.

Similarly, one may imagine a new heavy fermion coupling to the electroweak gauge bosons and inducing a four-boson contact interaction via a box loop. Such an interaction can mediate anomalous triple gauge boson production and anomalous vector boson scattering. The operator would be suppressed by four powers of the heavy fermion mass and enhanced by potentially strong coupling between the new fermion and the longitudinal vector bosons. These dimension-8 operators are described by the operators $\mathcal{O}_{T,i}, i = 0, 1, 2$ of Eqs. 19.33, 19.34 and 19.35.

In the following, a review of studies using VBS and triboson channels is presented. The main purpose of these studies is to estimate the improvement of sensitivity to these operator coefficients as a function of integrated luminosity and collider energy.

19.3.1 Theory of non-standard EW gauge boson interactions

While the translation between simplified new physics models in the EW sector to an EFT is described in [134] and also presented in Section 19.3.6, there are also ambiguities for the low-energy EFT. This results from the choice of operator bases. In the following sections, which are taken from Ref. [135], we give a brief overview of dimension-6 and dimension-8 operators, discuss the EFTs in different operator bases, and provide translations from one basis to another. This should simplify the comparison between many different studies that have been performed for several past, present and future collider experiments. We also address unitarization and discuss the role of higher-order corrections in studies of non-standard EW interactions using VBFNLO and a `POWHEG BOX` implementation of higher-order QCD corrections to $WWjj$ production.

19.3.1.1 Dimension-six operators for electroweak vector boson pair and triple production and scattering

If baryon and lepton numbers are conserved, only operators with even dimension can appear in the EFT. Consequently, the largest new physics contribution is expected from dimension-six operators. Three CP conserving dimension-six operators,

$$\begin{aligned} \mathcal{O}_{WWW} &= \mathrm{Tr}[W_{\mu\nu}W^{\nu\rho}W^{\mu}_{\rho}] \\ \mathcal{O}_{W} &= (D_\mu\Phi)^\dagger W^{\mu\nu}(D_\nu\Phi) \\ \mathcal{O}_{B} &= (D_\mu\Phi)^\dagger B^{\mu\nu}(D_\nu\Phi), \end{aligned} \tag{19.18}$$

and two CP violating dimension-six operators,

$$\begin{aligned} \mathcal{O}_{\tilde{W}WW} &= \mathrm{Tr}[\tilde{W}_{\mu\nu}W^{\nu\rho}W^{\mu}_{\rho}] \\ \mathcal{O}_{\tilde{W}} &= (D_\mu\Phi)^\dagger \tilde{W}^{\mu\nu}(D_\nu\Phi), \end{aligned} \tag{19.19}$$

affect the triple and quartic gauge couplings. Here Φ denotes the Higgs doublet field. The covariant derivative for such a field with hypercharge $Y = 1/2$ is given by

$$D_\mu \equiv \partial_\mu + i\frac{g'}{2}B_\mu + igW_\mu^i\frac{\tau^i}{2} \tag{19.20}$$

where $\tau^i, i = 1, 2, 3$ are the $SU(2)_I$ generators with $\mathrm{Tr}[\tau^i\tau^j] = 2\delta^{ij}$. The field strength tensors of the $SU(2)_I$ (W_μ^i) and $U(1)_Y$ (B_μ) gauge fields read

$$\begin{aligned} W_{\mu\nu} &= \frac{i}{2}g\tau^i(\partial_\mu W_\nu^i - \partial_\nu W_\mu^i + g\epsilon_{ijk}W_\mu^j W_\nu^k) \\ B_{\mu\nu} &= \frac{i}{2}g'(\partial_\mu B_\nu - \partial_\nu B_\mu)\ . \end{aligned} \tag{19.21}$$

As in the SM, trilinear gauge couplings (TGCs) and quartic gauge couplings (QGCs) induced by dimension-six operators are completely related by the requirement to guarantee gauge invariance. In addition, three CP-conserving operators

$$\mathcal{O}_{\Phi d} = \partial_\mu\left(\Phi^\dagger\Phi\right)\partial^\mu\left(\Phi^\dagger\Phi\right) \tag{19.22}$$

$$\mathcal{O}_{\Phi W} = \left(\Phi^\dagger\Phi\right)\mathrm{Tr}[W^{\mu\nu}W_{\mu\nu}] \tag{19.23}$$

$$\mathcal{O}_{\Phi B} = \left(\Phi^\dagger\Phi\right)B^{\mu\nu}B_{\mu\nu} \tag{19.24}$$

and two CP-violating dimension-six operators

$$\begin{aligned} \mathcal{O}_{\tilde{W}W} &= \Phi^\dagger\tilde{W}_{\mu\nu}W^{\mu\nu}\Phi \\ \mathcal{O}_{\tilde{B}B} &= \Phi^\dagger\tilde{B}_{\mu\nu}B^{\mu\nu}\Phi \end{aligned} \tag{19.25}$$

modify the coupling of the Higgs boson to the weak gauge bosons and therefore the four-gauge-boson amplitudes. The list of vertices relevant to three- and four-gauge-boson amplitudes of each operator is displayed in Table 19-15. We have neglected the operators affecting the couplings of the bosons to fermions

	ZWW	AWW	HWW	HZZ	HZA	HAA	WWWW	ZZWW	ZAWW	AAWW
$\mathcal{O}_{WWW}$	X	X					X	X	X	X
$\mathcal{O}_W$	X	X	X	X	X		X	X	X	
$\mathcal{O}_B$	X	X		X	X					
$\mathcal{O}_{\Phi d}$			X	X						
$\mathcal{O}_{\Phi W}$			X	X	X	X				
$\mathcal{O}_{\Phi B}$				X	X	X				
$\mathcal{O}_{\tilde{W}WW}$	X	X					X	X	X	X
$\mathcal{O}_{\tilde{W}}$	X	X	X	X	X					
$\mathcal{O}_{\tilde{W}W}$			X	X	X	X				
$\mathcal{O}_{\tilde{B}B}$				X	X	X				

Table 19-15. *The vertices induced by each operator are marked with X in the corresponding column. The vertices that are not relevant for three- and four-gauge-boson amplitudes have been omitted.*

as they can be measured in other processes such as Z boson decay. This is a minimal set of independent dimension-six operators relevant to amplitudes involving vertices of three and four electroweak gauge bosons. Additional dimension-six operators invariant under SM symmetries can be constructed but they can be shown to be equivalent to a linear combination of the previous operators by using equations of motion. Consequently,

the choice of the basis of operators is not unique. Other choices than the one presented here can be found in the literature. For example, the operators $Q_{\Phi D}$ and $Q_{\Phi WB}$ in Ref. [136] have been replaced in this paper by $\mathcal{O}_W$ and $\mathcal{O}_B$. Our basis avoids the otherwise necessary redefinition of the masses of the gauge bosons and the mixing of the neutral vector bosons. The operator $\mathcal{O}_{\Phi d}$ does not contain any gauge boson since $\Phi^\dagger\Phi$ is a singlet under all the SM gauge groups. However, it contributes to the Higgs field's kinetic term after Φ has been replaced by its value in the unitary gauge, i.e. with

$$\Phi = \left(0, \frac{v+h}{\sqrt{2}}\right)^T \tag{19.26}$$

one finds

$$\mathcal{O}_{\Phi d} \ni v^2 \partial_\mu h \partial^\mu h, \tag{19.27}$$

and it requires a renormalization of the Higgs field,

$$h \to h(1 - \frac{c_{\Phi d}}{\Lambda^2} v^2), \tag{19.28}$$

in the full Lagrangian. The Higgs couplings to all particles including the electroweak gauge bosons are consequently multiplied by the same factor. $\mathcal{O}_{\Phi W}$ and $\mathcal{O}_{\Phi B}$ modify the kinetic term of the gauge bosons after the Higgs doublet has been replaced by its vacuum expectation value (v). Those two operators require a renormalization of the gauge fields and the gauge couplings. As a matter of fact, their part proportional to v^2 is entirely absorbed by those redefinitions and can therefore be removed directly in the definition of the operators, i.e.

$$\begin{aligned} \mathcal{O}_{\Phi W} &= \left(\Phi^\dagger\Phi - v^2\right) \mathrm{Tr}[W^{\mu\nu} W_{\mu\nu}] \\ \mathcal{O}_{\Phi B} &= \left(\Phi^\dagger\Phi - v^2\right) B^{\mu\nu} B_{\mu\nu} \end{aligned} \tag{19.29}$$

It is now clear that those operators affect only the vertices with one or two Higgs bosons and not the TGCs or the QGCs.

19.3.1.2 Dimension-eight operators for genuine QGCs

As can be seen in Table 19-15, the dimension–six operators giving rise to QGCs also exhibit TGCs. In order to separate the effects of the QGCs we shall consider effective operators that lead to QGCs without a TGC associated to them. Moreover, not all possible QGCs are generated by dimension–six operators, for instance, these operators do not give rise to quartic couplings among the neutral gauge bosons [5]. The lowest dimension operator that leads to quartic interactions but does not exhibit two or three weak gauge boson vertices is of dimension eight[6]. The counting is straightforward: we can get a weak boson field either from the covariant derivative (D_μ of Eq. 19.20) of Φ or from the field strength tensor of Eq. 19.21. In either case, the vector field is accompanied by v (after using Eq. 19.26) or a derivative ∂_μ. Therefore, genuine quartic vertices are of dimension 8 or higher.

The idea behind using dimension–eight operators for QGCs is that the anomalous QGCs are to be considered as a straw man to evaluate the LHC potential to study these couplings, without having any theoretical prejudice about their size. There are three classes of genuine QGC operators [138]:

[5] Notice that the lowest order operators leading to neutral TGCs are also of dimension eight.

[6] Effective operators possessing QCGs but no TGCs can be generated at tree level by new physics at a higher scale [137], in contrast with operators containing TGCs that are generated at loop level.

Operators containing only $D_\mu\Phi$

This class contains two independent operators, *i.e.*

$$\mathcal{O}_{S,0} = \left[(D_\mu\Phi)^\dagger D_\nu\Phi\right] \times \left[(D^\mu\Phi)^\dagger D^\nu\Phi\right] , \tag{19.30}$$

$$\mathcal{O}_{S,1} = \left[(D_\mu\Phi)^\dagger D^\mu\Phi\right] \times \left[(D_\nu\Phi)^\dagger D^\nu\Phi\right] , \tag{19.31}$$

where the Higgs covariant derivative is given by the expression in Eq. 19.20. These operators can be generated when we integrate out a spin–one resonance that couples to gauge–boson pairs as discussed in Section 19.3.6.

The operators $\mathcal{O}_{S,0}$ and $\mathcal{O}_{S,1}$ contain quartic $W^+W^-W^+W^-$, W^+W^-ZZ and $ZZZZ$ interactions that do not depend on the gauge boson momenta; for a comparative table showing all QGCs induced by dimension–eight operators see Table 19-16. In our framework, the QGCs are accompanied by vertices with more than 4 particles due to gauge invariance. In order to simply rescale the SM quartic couplings containing $W^\pm$ and Z it is enough to choose $f_{S,0} = -f_{S,1} = f$ which leads to SM quartic couplings modified by a factor $(1 + fv^4/8\Lambda^4)$, where v is the Higgs vacuum expectation value ($v \simeq 246$ GeV).

Operators containing $D_\mu\Phi$ and two field strength tensors

QGCs are also generated by considering two electroweak field strength tensors and two covariant derivatives of the Higgs doublet [138]:

$$\begin{aligned}
\mathcal{O}_{M,0} &= \mathrm{Tr}\left[W_{\mu\nu}W^{\mu\nu}\right] \times \left[(D_\beta\Phi)^\dagger D^\beta\Phi\right] , \\
\mathcal{O}_{M,1} &= \mathrm{Tr}\left[W_{\mu\nu}W^{\nu\beta}\right] \times \left[(D_\beta\Phi)^\dagger D^\mu\Phi\right] , \\
\mathcal{O}_{M,2} &= \left[B_{\mu\nu}B^{\mu\nu}\right] \times \left[(D_\beta\Phi)^\dagger D^\beta\Phi\right] , \\
\mathcal{O}_{M,3} &= \left[B_{\mu\nu}B^{\nu\beta}\right] \times \left[(D_\beta\Phi)^\dagger D^\mu\Phi\right] , \\
\mathcal{O}_{M,4} &= \left[(D_\mu\Phi)^\dagger W_{\beta\nu}D^\mu\Phi\right] \times B^{\beta\nu} , \\
\mathcal{O}_{M,5} &= \left[(D_\mu\Phi)^\dagger W_{\beta\nu}D^\nu\Phi\right] \times B^{\beta\mu} , \\
\mathcal{O}_{M,6} &= \left[(D_\mu\Phi)^\dagger W_{\beta\nu}W^{\beta\nu}D^\mu\Phi\right] , \\
\mathcal{O}_{M,7} &= \left[(D_\mu\Phi)^\dagger W_{\beta\nu}W^{\beta\mu}D^\nu\Phi\right] ,
\end{aligned} \tag{19.32}$$

where the field strengths $W_{\mu\nu}$ and $B_{\mu\nu}$ have been defined above in Eq. (19.21). In this class of effective operators the quartic gauge-boson interactions depend upon the momenta of the vector bosons due to the presence of the field strength in their definitions. Therefore, the Lorentz structure of these operators can not be reduced to the SM one. The complete list of quartic vertices modified by these operators can be found in Table 19-16.

Operators containing only field strength tensors

The following operators containing four field strength tensors also lead to quartic anomalous couplings:

$$\mathcal{O}_{T,0} = \mathrm{Tr}\left[W_{\mu\nu}W^{\mu\nu}\right] \times \mathrm{Tr}\left[W_{\alpha\beta}W^{\alpha\beta}\right] \ , \tag{19.33}$$

$$\mathcal{O}_{T,1} = \mathrm{Tr}\left[W_{\alpha\nu}W^{\mu\beta}\right] \times \mathrm{Tr}\left[W_{\mu\beta}W^{\alpha\nu}\right] \ , \tag{19.34}$$

$$\mathcal{O}_{T,2} = \mathrm{Tr}\left[W_{\alpha\mu}W^{\mu\beta}\right] \times \mathrm{Tr}\left[W_{\beta\nu}W^{\nu\alpha}\right] \ , \tag{19.35}$$

$$\mathcal{O}_{T,5} = \mathrm{Tr}\left[W_{\mu\nu}W^{\mu\nu}\right] \times B_{\alpha\beta}B^{\alpha\beta} \ , \tag{19.36}$$

$$\mathcal{O}_{T,6} = \mathrm{Tr}\left[W_{\alpha\nu}W^{\mu\beta}\right] \times B_{\mu\beta}B^{\alpha\nu} \ , \tag{19.37}$$

$$\mathcal{O}_{T,7} = \mathrm{Tr}\left[W_{\alpha\mu}W^{\mu\beta}\right] \times B_{\beta\nu}B^{\nu\alpha} \ , \tag{19.38}$$

$$\mathcal{O}_{T,8} = B_{\mu\nu}B^{\mu\nu}B_{\alpha\beta}B^{\alpha\beta} \tag{19.39}$$

$$\mathcal{O}_{T,9} = B_{\alpha\mu}B^{\mu\beta}B_{\beta\nu}B^{\nu\alpha} \ . \tag{19.40}$$

It is interesting to note that the two last operators $\mathcal{O}_{T,8}$ and $\mathcal{O}_{T,9}$ give rise to QGCs containing only the neutral electroweak gauge bosons.

Previous analyses [139, 140, 141] of the LHC potential to study QGCs were based on the non–linear realization of the gauge symmetry, *i.e.* using chiral Lagrangians as for instance implemented in WHIZARD. The relation between the above framework and chiral Lagrangians can be found in Section 19.3.1.4.

	WWWW	WWZZ	ZZZZ	WWAZ	WWAA	ZZZA	ZZAA	ZAAA	AAAA
$\mathcal{O}_{S,0}$, $\mathcal{O}_{S,1}$	X	X	X						
$\mathcal{O}_{M,0}$, $\mathcal{O}_{M,1}$,$\mathcal{O}_{M,6}$,$\mathcal{O}_{M,7}$	X	X	X	X	X	X	X		
$\mathcal{O}_{M,2}$,$\mathcal{O}_{M,3}$, $\mathcal{O}_{M,4}$,$\mathcal{O}_{M,5}$		X	X	X	X	X	X		
$\mathcal{O}_{T,0}$,$\mathcal{O}_{T,1}$,$\mathcal{O}_{T,2}$	X	X	X	X	X	X	X	X	X
$\mathcal{O}_{T,5}$,$\mathcal{O}_{T,6}$,$\mathcal{O}_{T,7}$		X	X	X	X	X	X	X	X
$\mathcal{O}_{T,8}$,$\mathcal{O}_{T,9}$			X			X	X	X	X

Table 19-16. *Quartic vertices modified by each dimension-8 operator are marked with X.*

19.3.1.3 Comparison with the anomalous coupling approach and the LEP convention for aQGCs

The anomalous couplings approach is based on the Lagrangian [142]

$$\begin{aligned}\mathcal{L} =& ig_{WWV}\left(g_1^V(W^+_{\mu\nu}W^{-\mu} - W^{+\mu}W^-_{\mu\nu})V^\nu + \kappa_V W^+_\mu W^-_\nu V^{\mu\nu} + \frac{\lambda_V}{M_W^2}W^{\nu+}_\mu W^{-\rho}_\nu V^\mu_\rho\right.\\ &+ig_4^V W^+_\mu W^-_\nu(\partial^\mu V^\nu + \partial^\nu V^\mu) - ig_5^V\epsilon^{\mu\nu\rho\sigma}(W^+_\mu\partial_\rho W^-_\nu - \partial_\rho W^+_\mu W^-_\nu)V_\sigma\\ &\left.+\tilde{\kappa}_V W^+_\mu W^-_\nu\tilde{V}^{\mu\nu} + \frac{\tilde{\lambda}_V}{m_W^2}W^{\nu+}_\mu W^{-\rho}_\nu\tilde{V}^\mu_\rho\right) ,\end{aligned} \tag{19.41}$$

where $V = \gamma, Z$; $W^\pm_{\mu\nu} = \partial_\mu W^\pm_\nu - \partial_\nu W^\pm_\mu$, $V_{\mu\nu} = \partial_\mu V_\nu - \partial_\nu V_\mu$, $g_{WW\gamma} = -e$ and $g_{WWZ} = -e\cot\theta_W$. The first three terms of Eq. 19.41 are C and P invariant while the remaining four terms violate C and/or P. Electromagnetic gauge invariance requires that $g_1^\gamma = 1$ and $g_4^\gamma = g_5^\gamma = 0$. Finally there are five independent C- and P-conserving parameters: $g_1^Z, \kappa_\gamma, \kappa_Z, \lambda_\gamma, \lambda_Z$; and six C and/or P violating parameters:

$g_4^Z, g_5^Z, \tilde{\kappa}_\gamma, \tilde{\kappa_Z}, \tilde{\lambda}_\gamma, \tilde{\lambda_Z}$. This Lagrangian is not the most generic one, since extra derivatives can be added in all of the operators. Furthermore, there is no reason to remove those extra terms, since they are not suppressed by Λ but by M_W.

The effective field theory approach described in the previous section allows one to calculate those parameters in terms of the coefficients of the five dimension-six operators relevant for TGCs, i. e. in terms of the EFT coefficients $c_{WWW}, c_W, c_B, c_{\tilde{W}WW}$ and $c_{\tilde{W}}$. One finds for the anomalous TGC parameters [143, 144]:

$$g_1^Z = 1 + c_W \frac{m_Z^2}{2\Lambda^2} \tag{19.42}$$

$$\kappa_\gamma = 1 + (c_W + c_B)\frac{m_W^2}{2\Lambda^2} \tag{19.43}$$

$$\kappa_Z = 1 + (c_W - c_B \tan^2\theta_W)\frac{m_W^2}{2\Lambda^2} \tag{19.44}$$

$$\lambda_\gamma = \lambda_Z = c_{WWW}\frac{3g^2 m_W^2}{2\Lambda^2} \tag{19.45}$$

$$g_4^V = g_5^V = 0 \tag{19.46}$$

$$\tilde{\kappa}_\gamma = c_{\tilde{W}}\frac{m_W^2}{2\Lambda^2} \tag{19.47}$$

$$\tilde{\kappa}_Z = -c_{\tilde{W}} \tan^2\theta_W \frac{m_W^2}{2\Lambda^2} \tag{19.48}$$

$$\tilde{\lambda}_\gamma = \tilde{\lambda}_Z = c_{\tilde{W}WW}\frac{3g^2 m_W^2}{2\Lambda^2} \tag{19.49}$$

Defining $\Delta g_1^Z = g_1^Z - 1$, $\Delta\kappa_{\gamma,Z} = \kappa_{\gamma,Z} - 1$, the relation [143]

$$\Delta g_1^Z = \Delta\kappa_Z + \tan^2\theta_W \Delta\kappa_\gamma \tag{19.50}$$

and the relation $\lambda_\gamma = \lambda_Z$ reduce the five C and P conserving parameters down to three. For the C and/or P violating parameters, the relation

$$0 = \tilde{\kappa}_Z + \tan^2\theta_W \tilde{\kappa}_\gamma \tag{19.51}$$

and the relations $\tilde{\lambda}_\gamma = \tilde{\lambda}_Z$ and $g_4^Z = g_5^Z = 0$ reduce the six C and/or P violating parameters down to just two.

The Lagrangian of Eq. 19.41 is not $SU(2)_L$ gauge invariant under linear transformations even after imposing those relations because the quartic and higher multiplicity couplings are not included. Furthermore, gauge invariance requires also several relations between vertices with different number of particles. The quartic couplings involving two photons have been parametrized in a similar way. However, the parametrization is not generic enough and does not include the contributions from the dimension-six operators.

The LEP2 constraints on the vertices $\gamma\gamma W^+W^-$ and $\gamma\gamma ZZ$ [145] described in terms of anomalous couplings a_0/Λ^2 and a_c/Λ^2 can be translated into bounds on $f_{M,0}$ – $f_{M,7}$. In Ref. [146] (see also Refs [147, 148]), genuine anomalous quartic couplings involving two photons have been introduced as follows:

$$\begin{aligned}\mathcal{L}_0 &= -\frac{e^2}{16\pi\Lambda^2} a_0 F_{\mu\nu}F^{\mu\nu}\vec{W}^\alpha\vec{W}_\alpha \\ \mathcal{L}_c &= -\frac{e^2}{16\pi\Lambda^2} a_c F_{\mu\alpha}F^{\mu\beta}\vec{W}^\alpha\vec{W}_\beta\end{aligned} \tag{19.52}$$

with

$$F^{\mu\nu} = \partial^\mu A^\nu - \partial^\nu A^\mu$$
$$\vec{W}_\mu = \begin{pmatrix} \frac{1}{\sqrt{2}}(W_\mu^+ + W_\mu^-) \\ \frac{i}{\sqrt{2}}(W_\mu^+ - W_\mu^-) \\ \frac{Z_\mu}{\cos\theta_w} \end{pmatrix} \tag{19.53}$$

where A_μ and $W_\mu^\pm, Z_\mu$ denote the photon and weak fields, respectively. Thus, using the conventions of Eq. (19.21) for the fields in the operators $\mathcal{O}_{M,i}$, and Eq. (19.53) for the fields in the operators $\mathcal{L}_0$ and $\mathcal{L}_c$, the following relations for the $WW\gamma\gamma$ (upper sign) and $ZZ\gamma\gamma$ (lower sign) vertices can be derived:

$$\frac{f_{M,0}}{\Lambda^4} = \frac{a_0}{\Lambda^2}\frac{1}{g^2v^2} \quad \text{and} \quad \frac{f_{M,1}}{\Lambda^4} = -\frac{a_c}{\Lambda^2}\frac{1}{g^2v^2} \tag{19.54}$$
$$\frac{f_{M,2}}{\Lambda^4} = \frac{a_0}{\Lambda^2}\frac{2}{g^2v^2} \quad \text{and} \quad \frac{f_{M,3}}{\Lambda^4} = -\frac{a_c}{\Lambda^2}\frac{2}{g^2v^2} \tag{19.55}$$
$$\frac{f_{M,4}}{\Lambda^4} = \pm\frac{a_0}{\Lambda^2}\frac{1}{g^2v^2} \quad \text{and} \quad \frac{f_{M,5}}{\Lambda^4} = \pm\frac{a_c}{\Lambda^2}\frac{2}{g^2v^2} \tag{19.56}$$
$$\frac{f_{M,6}}{\Lambda^4} = \frac{a_0}{\Lambda^2}\frac{2}{g^2v^2} \quad \text{and} \quad \frac{f_{M,7}}{\Lambda^4} = \frac{a_c}{\Lambda^2}\frac{2}{g^2v^2}\,. \tag{19.57}$$

19.3.1.4 Conventions for non-standard electroweak gauge boson interactions in different MC programs

Dimension-8 operators: VBFNLO and MadGraph5

The convention for the dimension-8-operators in VBFNLO is the same as described in Section 19.3.1.2, and the coefficients f_i/Λ^4 set in the input file are the ones that multiply the operators of Section 19.3.1.2. However, the MadGraph5 implementation by means of a UFO file [149] uses expressions for the field strengths which are slightly different than the ones from Eq.19.21:

$$\begin{aligned} \widehat{W}_{\mu\nu} &= \frac{1}{2}\tau^i(\partial_\mu W_\nu^i - \partial_\nu W_\mu^i + g\epsilon_{ijk}W_\mu^j W_\nu^k) = \frac{1}{ig}W_{\mu\nu} \\ \widehat{B}_{\mu\nu} &= (\partial_\mu B_\nu - \partial_\nu B_\mu) = \frac{2}{ig'}B_{\mu\nu} \end{aligned} \tag{19.58}$$

The resulting changes can be absorbed in a redefinition of the operator coefficients:

$$\begin{aligned}
f_{S,0,1} = f_{S,0,1}^{\text{VBFNLO}} &= f_{S,0,1}^{\text{MG5}} \\
f_{M,0,1} = f_{M,0,1}^{\text{VBFNLO}} &= -\frac{1}{g^2} \cdot f_{M,0,1}^{\text{MG5}} \\
f_{M,2,3} = f_{M,2,3}^{\text{VBFNLO}} &= -\frac{4}{g'^2} \cdot f_{M,2,3}^{\text{MG5}} \\
f_{M,4,5} = f_{M,4,5}^{\text{VBFNLO}} &= -\frac{2}{gg'} \cdot f_{M,4,5}^{\text{MG5}} \\
f_{M,6,7} = f_{M,6,7}^{\text{VBFNLO}} &= -\frac{1}{g^2} \cdot f_{M,6,7}^{\text{MG5}} \\
f_{T,0,1,2} = f_{T,0,1,2}^{\text{VBFNLO}} &= \frac{1}{g^4} \cdot f_{T,0,1,2}^{\text{MG5}} \\
f_{T,5,6,7} = f_{T,5,6,7}^{\text{VBFNLO}} &= \frac{4}{g^2 g'^2} \cdot f_{T,5,6,7}^{\text{MG5}} \\
f_{T,8,9} = f_{T,8,9}^{\text{VBFNLO}} &= \frac{16}{g'^4} \cdot f_{T,8,9}^{\text{MG5}}
\end{aligned} \tag{19.59}$$

Dimension-8 operators: WHIZARD

WHIZARD uses different anomalous coupling operators than the ones described in Section 19.3.1.2, assuming a different symmetry group [150], and so a conversion is in general not possible. However, a vertex-specific conversion exists for the operators $\mathcal{O}_{S,0}$ and $\mathcal{O}_{S,1}$ to their corresponding operators

$$\begin{aligned}
\mathcal{L}_4^{(4)} &= \alpha_4 \left[\text{Tr}\left(V_\mu V_\nu\right)\right]^2 \\
\mathcal{L}_5^{(4)} &= \alpha_5 \left[\text{Tr}\left(V_\mu V^\mu\right)\right]^2, \quad \text{with } V_\mu = \left(D_\mu \Sigma\right) \Sigma^\dagger \, .
\end{aligned} \tag{19.60}$$

The conversion reads:

- for the WWWW-Vertex:

$$\alpha_4 = \frac{f_{S,0}}{\Lambda^4} \frac{v^4}{8} \tag{19.61}$$

$$\alpha_4 + 2 \cdot \alpha_5 = \frac{f_{S,1}}{\Lambda^4} \frac{v^4}{8} \tag{19.62}$$

- for the WWZZ-Vertex:

$$\alpha_4 = \frac{f_{S,0}}{\Lambda^4} \frac{v^4}{16} \tag{19.63}$$

$$\alpha_5 = \frac{f_{S,1}}{\Lambda^4} \frac{v^4}{16} \tag{19.64}$$

- for the ZZZZ-Vertex:

$$\alpha_4 + \alpha_5 = \left(\frac{f_{S,0}}{\Lambda^4} + \frac{f_{S,1}}{\Lambda^4} \right) \frac{v^4}{16} \tag{19.65}$$

Dimension-6 operators: VBFNLO and MadGraph5

The MadGraph model EWdim6 has been generated from FeynRules and contains the operators from Eqs. 19.18, 19.19, 19.22, 19.23 and 19.24, with the exception of $\mathcal{O}_{\tilde{W}W}$, $\mathcal{O}_{\tilde{B}B}$ of Eq. 19.25 and $\mathcal{O}_{D\tilde{W}}$ of Eq. 19.68 [7]. The names of the coefficients is displayed in Table 19-17. All the coefficients include the $1/\Lambda^2$ as reminded by the "L2" at the end of the names and are in TeV^{-2}. The model also has a new coupling order NP counting the power of $1/\Lambda$. Consequently, each vertex from the dimension-six operators has NP=2.

c_{WWW}/Λ^2	CWWWL2
c_W/Λ^2	CWL2
c_B/Λ^2	CBL2
$c_{\tilde{W}WW}/\Lambda^2$	CPWWWL2
$c_{\tilde{W}}/\Lambda^2$	CPWL2
$c_{\Phi d}/\Lambda^2$	CphidL2
$c_{\Phi W}/\Lambda^2$	CphiWL2
$c_{\Phi B}/\Lambda^2$	CphiBL2

Table 19-17. *Names of the couplings of the dimension-six operators present in the EWdim6 model of MadGraph5.*

The operators from Eqs. 19.18 and 19.19 in Section 19.3.1.1 are directly available in VBFNLO. The operators $\mathcal{O}_{\tilde{W}W}$ and $\mathcal{O}_{\tilde{B}B}$ of Eq. 19.25and $\mathcal{O}_{\Phi B}$ of Eq. 19.24 are available as well ($\mathcal{O}_{\Phi B}$ is called $\mathcal{O}_{BB}$ within VBFNLO). Additionally, the operator

$$\mathcal{O}_{WW} = \Phi^\dagger W_{\mu\nu} W^{\mu\nu} \Phi \tag{19.66}$$

from VBFNLO can be related to the operator $\mathcal{O}_{\Phi W}$ of Eq. 19.23 by choosing the coefficient as

$$c_{WW} = 2 \cdot c_{\Phi W} \tag{19.67}$$

In addition to those operators, VBFNLO also provides the following CP-odd operators:

$$\begin{aligned} \mathcal{O}_{\tilde{B}} &= (D_\mu \Phi)^\dagger \tilde{B}^{\mu\nu} (D_\nu \Phi) \\ \mathcal{O}_{B\tilde{W}} &= \Phi^\dagger B_{\mu\nu} \tilde{W}^{\mu\nu} \Phi \\ \mathcal{O}_{D\tilde{W}} &= \text{Tr}\left([D_\mu, \tilde{W}_{\nu\rho}][D^\mu, W^{\nu\rho}] \right) . \end{aligned} \tag{19.68}$$

However, only 4 of the 7 CP-odd operators are linearly independent, so the additional operators can be expressed in terms of the operators of Eqs. 19.19 and 19.25 as follows:

$$\begin{aligned} \mathcal{O}_{\tilde{B}} &= \mathcal{O}_{\tilde{W}} + \frac{1}{2}\mathcal{O}_{\tilde{W}W} - \frac{1}{2}\mathcal{O}_{\tilde{B}B} \\ \mathcal{O}_{B\tilde{W}} &= -2\,\mathcal{O}_{\tilde{W}} - \mathcal{O}_{\tilde{W}W} \\ \mathcal{O}_{D\tilde{W}} &= -4\,\mathcal{O}_{\tilde{W}WW} \,. \end{aligned} \tag{19.69}$$

The CP-conserving anomalous couplings implementation is also available in VBFNLO with the parameters Δg_1^Z, $\Delta\kappa_Z$, $\Delta\kappa_\gamma$, and λ_γ, defined in Section 19.3.1.3.

[7] We have neglected the CP violating operators with the dual strength tensors affecting only the gauge boson Higgs couplings, since measuring CP violation in the four-weak-boson amplitude would be very challenging.

19.3.1.5 Discussion of unitarity bounds and usage of form factors

The effective field theory is valid only below the new physics scale Λ and no violation of unitarity occurs in this regime. In the regime where EFT is valid, the new physics contributions to a SM process, i.e. the interference of the SM amplitude with the higher-dimensional operators and the square of the new physics amplitudes, are suppressed by increasing powers of $1/\Lambda$,

$$|\mathcal{M}_{SM} + \mathcal{M}_{dim6} + \mathcal{M}_{dim8} + \ldots|^2 = \underbrace{|\mathcal{M}_{SM}|^2}_{\Lambda^0} + \underbrace{2\mathcal{R}e\,(\mathcal{M}_{SM}\mathcal{M}_{dim6})}_{\Lambda^{-2}} + \underbrace{|\mathcal{M}_{dim6}|^2 + 2\mathcal{R}e\,(\mathcal{M}_{SM}\mathcal{M}_{dim8})}_{\Lambda^{-4}} + \ldots \tag{19.70}$$

For illustration we show in Figs. 19-12, 19-13 the invariant mass distribution of the W-pair, m_{WW}, produced at the 14 TeV LHC, with and without the contribution of the dimension six operator $\mathcal{O}_{WWW}$ of Eq. 19.18. As can be seen in Figs. 19-12, the prediction for m_{WW} including $\mathcal{O}_{WWW}$ is well below the unitarity bound [151] for this process in the relevant energy regime. However, as illustrated in Fig. 19-13, the contributions of this operator to the amplitude squared for $W_L W_T$ production reach similar magnitude at $m_{WW} \approx 1.3$ TeV and above this energy the $1/\Lambda^4$ suppressed term overtakes the $1/\Lambda^2$ suppressed contribution. Clearly, the $1/\Lambda$ expansion is only valid below this energy. In typical analyses for anomalous couplings, the EFT does not break down for m_{VV} as low as 1 TeV.

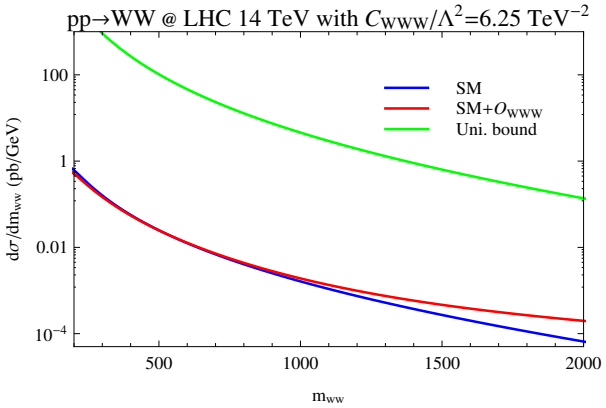

Figure 19-12. *m_{WW} distributions in W-pair production at the 14 TeV LHC are displayed for the SM (in blue) and for the SM plus the dimension six operator $\mathcal{O}_{WWW}$ with $c_{WWW}/\Lambda^2 = 6.25$ TeV (in red). Also shown is the unitarity bound [151] (in green).*

For dimension eight operators, the effect from unitarity violation typically sets in earlier due to the higher exponent in Λ in the denominator. Hence, the task to avoid unphysical contributions from regions where unitarity is violated becomes more important. In these regions the EFT expansion in terms of suppressed additional contributions to the SM part, our starting point, is no longer valid, as each order becomes similarly important.

In experimental searches one has to ensure that the sensitivity to anomalous gauge couplings is not driven by parameter regions where unitarity is violated. As nature will ensure unitarity conservation in the full model, such results would not be meaningful. Thereby, one can take advantage of the fact that only energies up to the center-of-mass energy of the collider are probed. For hadron colliders like the LHC, the steep fall-off of the parton distribution functions means that the effective probed energy range is even smaller, as the expected number of signal events will be smaller than one above a certain energy and therefore this region will not contribute. However, if the bound for unitarity violation is lower than that, some method to ensure that no sensitivity comes from this energy range needs to be employed. One possibility is to use

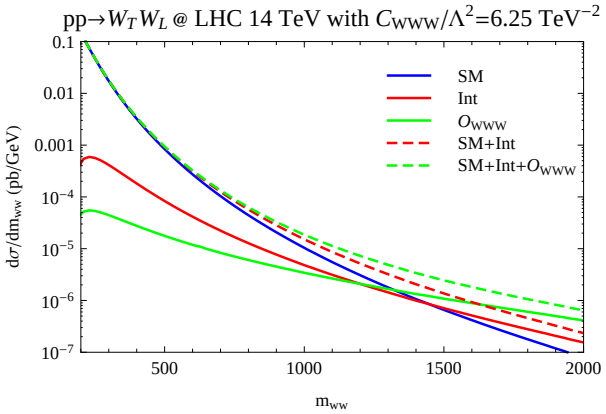

Figure 19-13. *m_{WW} distributions in W-pair production at the 14 TeV LHC are displayed for the production of one longitudinally and one transversally polarized W boson, when considering the SM (solid blue line), only the interference between the SM and the dimension-six operator (solid red line), the sum of the two (dashed red line), only the square of the new physics amplitude (solid green line), and finally the total contribution from the SM and the dimension-six operator (dashed green line).*

appropriate experimental cuts. However, often processes will contain neutrinos and so the full reconstruction of the partonic energy is not possible. Another option is to use form factors. These are introduced to model an energy-dependent cutoff, which in the full theory would be accomplished by new-physics states at the scale Λ, which have been integrated out in the EFT description. Various options are possible, for example a sharp cut-off of the higher-dimensional contributions at a fixed energy scale, or a dipole-like form factor as used in VBFNLO, that gives a smoother cut-off. The exact choice depends on the full model, so for an effective theory description all choices are equally well motivated from the theory side. The last possibility to ensure no unitarity violation happens is a unitarity projection, like the K-matrix method implemented in WHIZARD (see also Section 19.3.6). There the amplitude A is moved onto the unitarity circle along a line connecting $\mathcal{R}e(A)$ and the imaginary unit i. Physically, this corresponds to introducing an infinitely heavy and wide resonance. This scheme maximizes the contributions from anomalous couplings while ensuring unitarity for all energies.

19.3.1.6 The role of higher order corrections in multi-boson processes at the LHC

Higher-order corrections play an important role for accurate predictions at the LHC. In this section we study the impact of NLO QCD corrections in vector-boson fusion and triboson processes and how they impact the extraction of anomalous quartic gauge couplings. As example of these two process classes we take the processes W^+W^+jj and $W^+\gamma\gamma$, respectively. The NLO results including anomalous QGCs presented in Sections 19.3.1.6 and 19.3.1.6 have been obtained with VBFNLO. We discuss the impact of a parton shower on the example of W^+W^+jj production with `POWHEG+PYTHIA` [152] in Section 19.3.1.6. Finally, in Section 19.3.1.6 we discuss the impact of NLO electroweak corrections in triboson processes.

Vector-boson-fusion process W^+W^+jj with VBFNLO

The production of a vector-boson pair via vector-boson fusion [153, 154, 155, 156, 157] has a characteristic signature of two high-energetic, so-called tagging jets in the forward region of the detector, which are defined as the two jets with the largest transverse momentum. This can be exploited experimentally by requiring that there is a large rapidity separation ($\Delta\eta_{jj} > 4$) between the tagging jets, they are in opposite detector hemispheres ($\eta_{j_1} \times \eta_{j_2} < 0$) and they possess a large invariant mass ($M_{jj} > 600$ GeV). Additional central jet

	σ_{LO}	σ_{NLO}
SM	1.169 fb	1.176 fb
anom.coupl.	1.399 fb	1.388 fb

Table 19-18. *Total cross sections at LO and NLO for the process $pp \to e^+\nu_e\mu^+\nu_\mu jj$ in the SM and with anomalous coupling $\frac{f_{T,1}}{\Lambda^4} = 200\ TeV^{-4}$. Statistical errors from Monte Carlo integration are below the per mille level.*

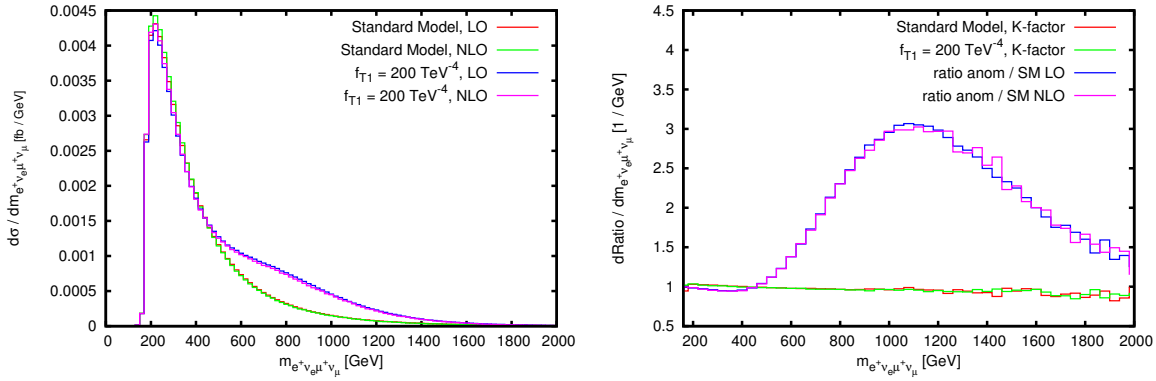

Figure 19-14. *Invariant-mass distribution of the two lepton, two neutrino system. Left: Differential cross section for the SM and with anomalous coupling T_1 at LO and NLO. Right: Differential K-factors for the SM and with anomalous coupling as well as the cross-section ratio between anomalous coupling and SM for LO and NLO.*

radiation at higher orders is strongly suppressed due to the exchange of a color-singlet in the t-channel, in contrast to typical QCD-induced backgrounds. Higher-order corrections are typically small, below the 10% level, and reduce the residual scale uncertainty to about 2.5%. Choosing the momentum transfer between an incoming and an outgoing parton along a fermion line proves to be particularly advantageous, as then also corrections to important distributions are small and flat over the whole range.

As example we take the process $pp \to e^+\nu_e\mu^+\nu_\mu jj$ with anomalous coupling $\frac{f_{T,1}}{\Lambda^4} = 200\ \text{TeV}^{-4}$ and form factor scale $\Lambda = 1188$ GeV and exponent $p = 4$. The results for the total cross sections at LO and NLO are shown in Table 19-18. Switching on the anomalous couplings increases the cross section by just under 20%, and NLO QCD corrections hardly change this number. This can also be seen in Fig. 19-14 where we show the differential distribution with respect to the invariant mass of the two leptons and the two neutrinos. In the left-hand plot we present the differential cross section in the SM and with anomalous couplings switched on both at LO and NLO. Similar to the integrated cross section, the difference between LO and NLO is small in both cases. In contrast the anomalous couplings yield a positive contribution to the cross section over the SM, which starts at an invariant mass of about 500 GeV, before the formfactor, introduced to preserve unitarity, damps the contributions again at higher invariant masses. On the right-hand side we present two groups of ratios. The differential K factor is flat and close to one both for the SM and the anomalous coupling scenario. The second set shows the ratio of differential anomalous-coupling over SM cross section both at LO and NLO. The two curves agree well and show enhancements of the cross section up to a factor of three. Hence, in this process higher-order corrections do not influence the extraction of anomalous couplings.

Vector-boson-fusion process W^+W^+jj in the POWHEG BOX

NLO-QCD calculations are a crucial prerequisite for precision analyses at the LHC, reducing theoretical uncertainties associated with hard scattering processes significantly. On the other hand, a realistic description of the additional hadronic activity that occurs in any collider environment crucially relies on parton-shower Monte Carlo generators such as HERWIG [64] or PYTHIA [66]. The perturbative accuracy of these programs is, however, limited to leading logarithmic accuracy. The most realistic yet accurate predictions available to date for processes with many particles in the final state are thus obtained by combining NLO-QCD calculations for the hard scattering with parton shower programs, for example in the framework of the POWHEG formalism [158, 159]. Such a matching can be performed with the help of the POWHEG BOX [160], a repository that provides all process-independent building blocks of the matching procedure, while process-specific elements have to be provided by the user.

Building on existing NLO-QCD calculations [161, 162, 156, 153], recently various VBF processes have been implemented in the POWHEG BOX [163, 164, 165, 152, 166]. The code developed is publicly available from the project webpage, http://powhegbox.mib.infn.it/, and can be tailored to the user's needs for any dedicated study. In order to assess the impact of parton-shower effects on NLO-QCD predictions for VBF-induced W^+W^+jj production at the LHC, numerical analyses for a representative setup have been performed for the $e^+\nu_e\mu^+\nu_\mu jj$ final state [152]. At a collision energy of $\sqrt{s} = 7$ TeV, the MSTW2008 parton distribution functions [77] are used for incoming protons and the FASTJET package [167] for the reconstruction of jets via the k_T algorithm with a resolution parameter of $R = 0.4$. Events are showered with PYTHIA 6.4.21, including hadronization corrections and underlying event with the Perugia 0 tune. At least two hard jets are required with $p_{T,j} \geq 20$ GeV and $|y_j| \leq 4.5$, well-separated from each other such that $|y_{j_1} - y_{j_2}| > 4$, $y_{j_1} \times y_{j_2} < 0$, and $M_{j_1 j_2} > 600$ GeV. In addition, an e^+ and a μ^+ with $p_{T,\ell} \geq 20$ GeV, $|y_\ell| \leq 2.5$, $\Delta R_{j\ell} \geq 0.4$, $\Delta R_{\ell\ell} \geq 0.1$, located between the two tagging jets, are requested. For the renormalization and factorization scales dynamical choices bound to the kinematics of the underlying Born configuration are made.

In this setup distributions related to the tagging jets or the hard leptons turn out to be rather insensitive to parton-shower effects. As illustrated by Fig. 19.3.1.6 (left panel) for the invariant mass distribution of the charged-lepton pair, the NLO-QCD and the POWHEG+PYTHIA results are very similar, both in normalization and shape. More pronounced effects of the parton shower occur in observables related to the emission of an extra hard jet, c.f. Fig. 19.3.1.6 (right panel) for $d\sigma/dy_{j_3}$. When the rapidity distribution of a third jet is used in order to estimate central-jet veto efficiencies, this effect should be carefully taken into account.

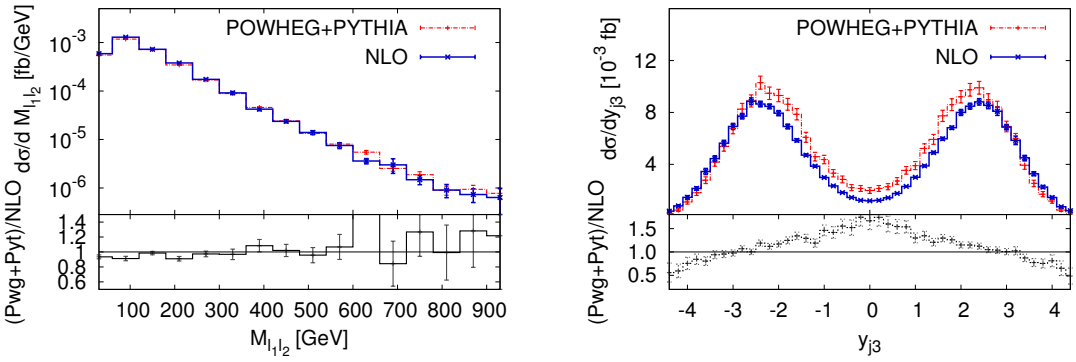

Figure 19-15. *Invariant mass distribution of the charged lepton pair (left) and rapidity distribution of the third jet (right) in VBF-induced $e^+\nu_e\mu^+\nu_\mu jj$ production at the LHC with $\sqrt{s} = 7$ TeV and the selection cuts described in the text. The lower panels show the respective ratios of the* POWHEG+PYTHIA *and the NLO-QCD results. Horizontal bars indicate statistical errors in each case.*

	σ_{LO}	σ_{NLO}
SM	1.124 fb	3.674 fb
anom.coupl.	1.216 fb	3.787 fb

Table 19-19. *Total cross sections at LO and NLO for the process $pp \to e^+\nu_e\gamma\gamma$ in the SM and with anomalous coupling $\frac{f_{T,6}}{\Lambda^4} = 2000\ TeV^{-4}$. Statistical errors from Monte Carlo integration are below the per mille level.*

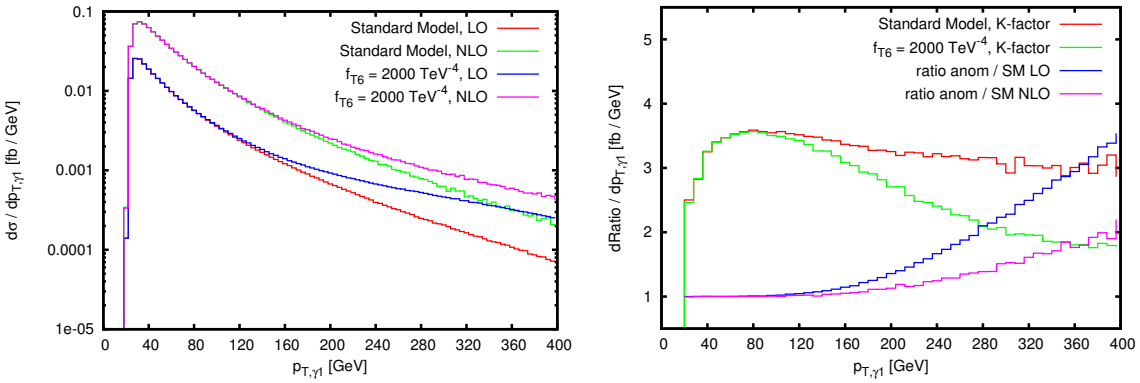

Figure 19-16. *Transverse-momentum distribution of the harder photon. Left: Differential cross section for the SM and with anomalous coupling T_6 at LO and NLO. Right: Differential K-factors for the SM and with anomalous coupling as well as the cross-section ratio between anomalous coupling and SM for LO and NLO.*

Triboson process $W^+\gamma\gamma$ with VBFNLO

The second group of process where anomalous quartic gauge couplings can be tested are the triboson processes [168, 169, 170, 171, 172, 173, 174, 175, 176, 177, 178]. The quartic vertex enters via an s-channel vector boson, which decays into three vector bosons, while diagrams with two or three bosons attached to the quark line as well as non-resonant contributions form an irreducible background. These processes have been shown to possess quite large K factors, typically between 1.5 and 1.8, mostly due to the additional quark-gluon–induced production processes first entering in the real-emission process. They also have a considerable scale dependence. While the dependence on the factorization scale can be reduced by NLO QCD corrections, the strong coupling constant first enters in the real emission part and therefore shows a large variation with the scale.

The example process we are considering here is $pp \to e^+\nu_e\gamma\gamma$ [174, 175]. In this process the K factor with a numerical value of about 3 is particularly large. This is due to the fact that the SM amplitude vanishes when the two photons are collinear and $\cos\theta_W = \frac{1}{3}$, where θ_W is the angle between the W boson and the incoming quark in the partonic center-of-mass frame. This so-called radiation zero [179, 180, 181] is spoiled by the extra jet emission at NLO, therefore giving huge K factors in these phase-space regions. The numerical values for the integrated cross section are tabulated in Table 19-19. As anomalous coupling we choose the operator T_6 with $\frac{f_{T,6}}{\Lambda^4} = 2000\ \mathrm{TeV}^{-4}$, form factor scale $\Lambda = 1606$ GeV and exponent $p = 4$.

Turning to differential distributions, we show the transverse momentum distribution of the harder photon in Figure 19-16. The left-hand side shows again the differential integrated cross section. Both the SM and the anomalous-coupling scenario show differential NLO cross sections which are significantly larger than their

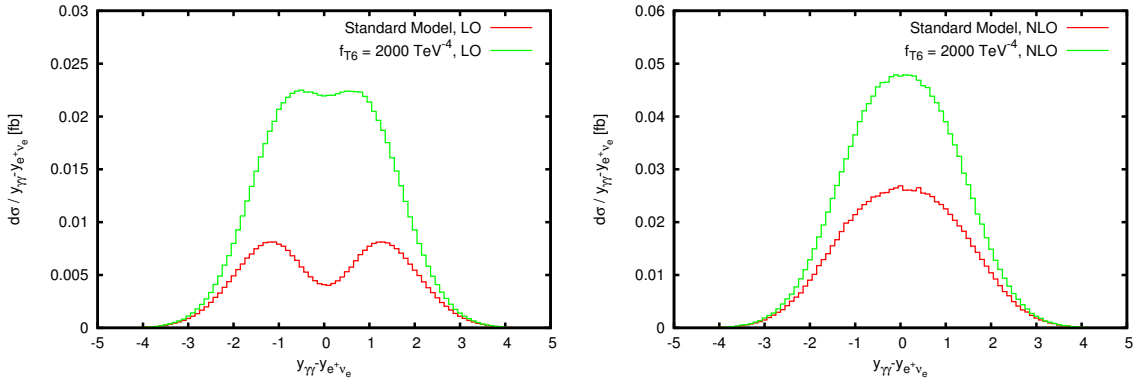

Figure 19-17. *Rapidity difference of the diphoton system and the lepton-neutrino system for the SM and the anomalous coupling scenario. Left: LO distributions Right: NLO distributions*

LO counterpart. Contributions from anomalous couplings start to contribute for transverse photon momenta above 100 GeV and their relative size becomes gradually larger when going to higher momenta as expected.

On the right-hand side one can see that the K-factor behavior differs for the SM and the anomalous coupling scenario. While, in the SM, the K factor is almost constant and only slightly decreases when going to larger transverse momenta, there is a much stronger decrease when anomalous couplings are switched on. At the high end of the shown range, the K factor has reached a value of around 1.8, which is the number typically observed in other triboson processes involving W bosons. As the effect of the anomalous coupling increases, the cancellation between different amplitudes gets gradually destroyed and the radiation zero filled up. Only the effects from additional jet radiation remain, yielding the smaller K factor.

That this is indeed the case can be seen in Fig. 19-17. Here we require additionally that the transverse momentum of the harder photon exceeds 200 GeV and the invariant mass of the lepton-neutrino system exceeds 75 GeV to suppress radiation off the final-state lepton. The effect of the radiation zero should be visible as a dip at zero in the rapidity difference between the diphoton system and the lepton-neutrino system, which can be indeed observed for the LO SM curve. In contrast the anomalous-coupling curve shows no such behavior even at LO, and at NLO the dip is filled in both cases.

Turning back to the right-hand plot of Fig. 19-16, the ratio between anomalous-coupling and SM prediction decreases when going from LO to NLO. This is due to the same effect, as part of the additional contribution is caused by filling up the radiation zero, which is no longer present at NLO because there already QCD effects have caused this. Hence, for this process group, higher-order corrections play an important role and cannot be neglected when determining the size of or limits on anomalous quartic gauge couplings.

Electroweak corrections to triboson processes

The first calculation of electroweak NLO corrections for a triboson processes at hadron colliders has appeared only very recently. Hence, no publicly available Monte Carlo implementation is available at the present stage. For gauge boson pair production via vector-boson fusion electroweak corrections no results exist in the literature at the current stage.

In Ref. [182] the full NLO corrections to on-shell WWZ production have been considered. Besides the QCD corrections already calculated in Refs. [169, 171], additional virtual electroweak diagrams with loops up to the pentagon level appear as well as real-emission processes with an additional external photon. There, processes with both photon radiation and initial-state photons are taken into account. The latter appear

when using PDFs with photons [81, 82]. Additionally, in this case the photon-initiated contribution of $\gamma\gamma \to WWZ$ is added at tree-level. The electroweak corrections are typically quite small for integrated cross sections, of about -2%. They can, however, get significant in differential distributions. For example, looking at the transverse-momentum distribution of the Z boson, at the 14 TeV LHC, one observes corrections of up to -30% for transverse momenta of 1 TeV. Thereby, the photon-initiated processes play an important role to partly cancel large Sudakov virtual corrections.

19.3.2 Current bounds on triple and quartic gauge boson couplings

Current bounds on the aTGCs of Eq. 19.41 from LEP, Tevatron and LHC searches in $WW\gamma, WWZ, ZZ$ and $Z\gamma$ events are summarized in Figs. 19-18, 19-19, 19-20, and 19-21. Constraints from a combined analysis of EWPOs and LEP data on aTGCs can be found in Ref. [183], for instance.

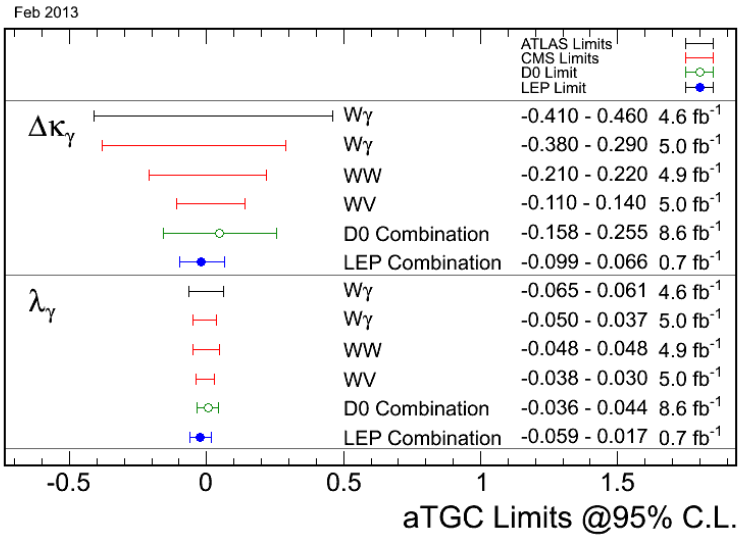

Figure 19-18. *Limits on anomalous $WW\gamma$ couplings. Tevatron limits use a form factor with the cut-off parameter $\Lambda = 2$ TeV. Taken from Ref. [184].*

A review of current bounds on quartic gauge couplings from LEP can be found in Ref. [145]. Recently, stringent bounds on anomalous quartic gauge couplings involving two photons, a_0 and a_c of Eq. 19.52, have been obtained from two-photon production of a W^+W^- pair at the LHC, as reported by CMS [187] (95% CL intervals): $|a_0/\Lambda^2| < 0.00015$ GeV^{-2}, $|a_c/\Lambda^2| < 0.0005$ GeV^{-2} with a dipole form factor and $\Lambda_{cutoff} = 500$ GeV, and $|a_0/\Lambda^2| < 4.0 \times 10^{-6}$ GeV^{-2}, $|a_c/\Lambda^2| < 1.5 \times 10^{-5}$ GeV^{-2} without using a form factor.

19.3.3 Multi-boson processes at the 14 TeV LHC

Studies on vector boson scattering (VBS) and triboson production have been presented by ATLAS collaboration for $\sqrt{s} = 14$ TeV and integrated luminosities of 300 fb^{-1} and 3 ab^{-1} respectively [188, 189]. These studies showcase the greatly increased sensitivity for new physics in these channels.

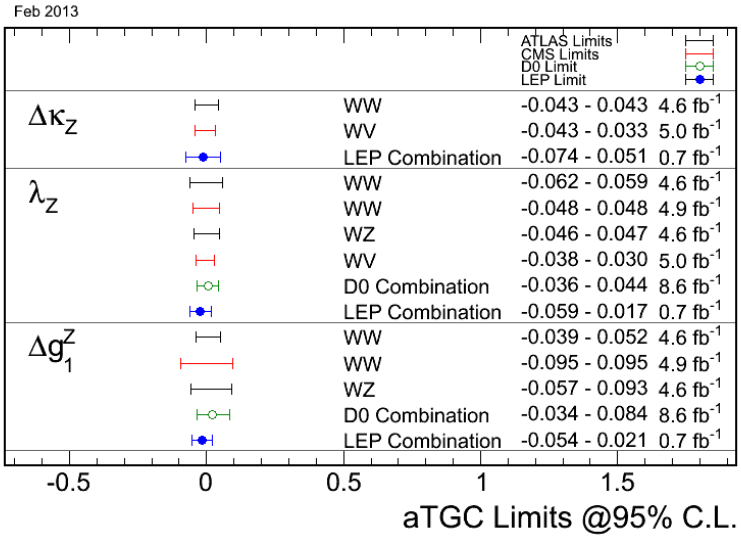

Figure 19-19. *Limits on anomalous WWZ couplings. Tevatron limits use a form factor with the cut-off parameter $\Lambda = 2$ TeV. Taken from Ref. [184].*

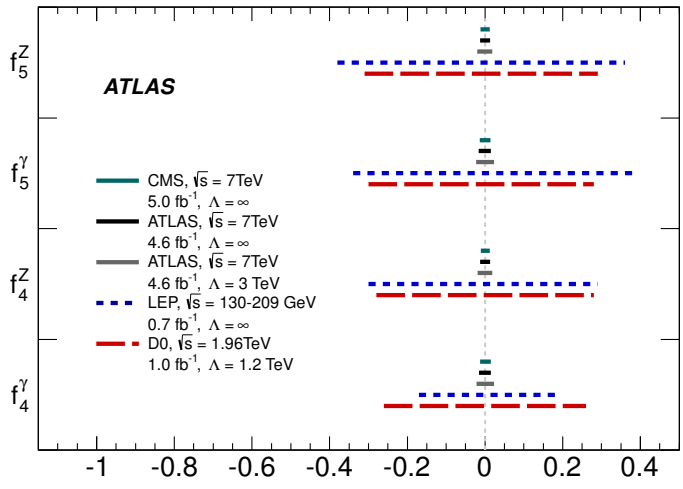

Figure 19-20. *Anomalous $ZZ\gamma$ and ZZZ 95% CL intervals from ZZ production at ATLAS, CMS, LEP and the Tevatron experiments. If a form factor is used, the cut-off parameter Λ is also shown. Taken from Ref. [185].*

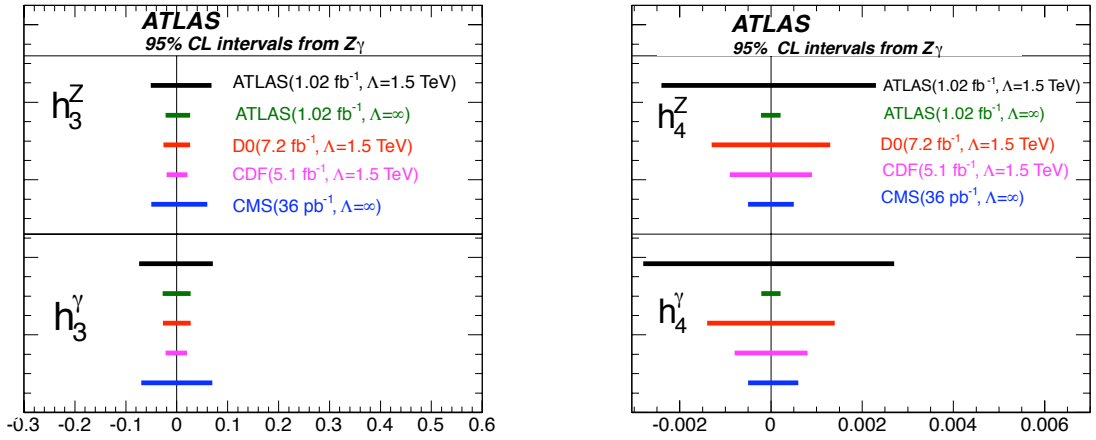

Figure 19-21. *The 95% CL intervals for neutral aTGCs from ATLAS, CMS, LEP and the Tevatron experiments as obtained from $Z\gamma$ events. If a form factor is used, the cut-off parameter Λ is also shown. Taken from Ref. [186].*

parameter	300 fb^{-1}	1 ab^{-1}	3 ab^{-1}
α_4	0.066	0.025	0.016

Table 19-20. *Summary of expected upper limits for α_4 at the 95% confidence level using the $pp \to W^+W^- + 2j \to e\mu + 2\nu + 2j$ VBS search at pp collision center-of-mass energy of 14 TeV at ATLAS [188]. See Table 19-32 for corresponding resonance mass limits in a dimension-8 operator formulation and considering simplified models of electroweak resonances.*

Studies of vector boson scattering in the $W^+W^-jj \to \ell^+\nu\ell^-\nu jj$ have been presented based on the comparison of the m_{lljj} distribution from backgrounds (including $t\bar{t}$ production, diboson production with ISR jets, and SM VBS) and anomalous VBS signal. The statistical sensitivity has been parameterized using the electroweak chiral lagrangian operator with coefficient α_4 (see Eq. 19.60). In this formulation of new physics, this particular operator is one of the least constrained since it preserves the CP symmetry and the electoweak SU(2) custodial symmetry, does not induce oblique corrections in the gauge boson propagators, and only induces anomalous quartic couplings which have not been constrained by past studies on trilinear guage couplings. Unitarity is maintained by using the inverse amplitude method [190, 191]. Table 19-20 shows the results of this ATLAS study, as reproduced from their report. The sensitivity to the α_4 (referred to as a_4 in [188]) coefficient is increased by more than a factor of 4 in the high-luminosity upgrade of the LHC. Using a dimension-8 operator formulation and considering simplified models of electroweak resonances, these α_4 limits are converted to corresponding masses of heavy resonances in Table 19-32.

ATLAS has also presented a study of VBS in the $ZZ \to 4\ell$ channel which has a clean and fully reconstructible final state. In this study, the K-matrix unitarization approach is used to model anomalous quartic couplings and unitarization is achieved by including TeV-scale resonances. Such resonances would be clearly visible in the 4ℓ invariant mass distribution. Table 19-21, reproduced from the ATLAS report, shows the statistical significance of potential resonant signals given the background-only hypothesis, for a number of resonance masses and couplings. The comparison of the two scenarios with integrated luminosities of 300 fb^{-1} and 3000 fb^{-1} respectively showcases the discovery potential of the high-luminosity upgrade.

ATLAS has estimated the precision on the measurement of the integrated cross section for the purely-electroweak SM process $pp \to ZZ + 2j \to 4\ell + 2j$. In the kinematic region where the tagging forward jets have $m_{jj} > 1$ TeV and the 4-lepton invariant mass $m_{4\ell} > 200(500)$ GeV, a statistical precision of 10(15)% is achievable with 3000 fb^{-1}, compared to 30(45)% with 300 fb^{-1}. Since a key prediction of the SM is that the Higgs boson unitarizes longitudinal VBS, it is important to make the definitive measurements of this cross section, which is only possible with the high-luminosity upgrade in this clean and robust channel.

model	300 fb^{-1}	3000 fb^{-1}
$m_{\text{resonance}} = 500$ GeV, $g = 1.0$	2.4σ	7.5σ
$m_{\text{resonance}} = 1$ TeV, $g = 1.75$	1.7σ	5.5σ
$m_{\text{resonance}} = 1$ TeV, $g = 2.5$	3.0σ	9.4σ

Table 19-21. *Summary of the expected sensitivity to anomalous VBS signal, quoted in terms of the background-only p_0-value expected for signal+background. The p_0-value has been converted to the corresponding number of Gaussian σ in significance. These results are given for the $pp \to ZZ{+}2j \to \ell\ell\ell\ell{+}2j$ channel at $\sqrt{s} = 14$ TeV. The increase in significance with integrated luminosity is shown for different resonance masses and couplings g.*

ATLAS has also shown sensitivity studies using the fully-leptonic decay modes of $W^{\pm}W^{\pm}$, WZ and ZZ channels in the VBS mode as well as triboson results in the $Z\gamma\gamma$ channel. These results are quoted in the language of EFT higher-dimension operators. The studies are performed in the kinematic regions where unitarity is perserved. In this context, ATLAS has studied one dimension-6 operator, $\mathcal{O}_{\Phi W}$ of Eq. 19.23 and four dimension-8 operators, $\mathcal{O}_{S,0}$ of Eq. 19.30 and $\mathcal{O}_{T,i}, i = 1, 8, 9$ of Eqs. 19.34, 19.39, and 19.40. Their values for 5σ-significance discovery are summarised in Table 19-22, reproduced from the ATLAS report. The high-luminosity upgrade increases the discovery potential for the operator coefficients by factors of 2-3, with further increases possible using analysis optimizations. If an anomaly is discovered with 300 fb^{-1}, the corresponding operator coefficient can be measured with a precision of 5% or better with 3000 fb^{-1} of integrated luminosity, allowing detailed studies of the underlying physics in this arena.

Parameter	dimension	channel	Λ_{UV} [TeV]	300 fb^{-1}		3000 fb^{-1}	
				5σ	95% CL	5σ	95% CL
$c_{\Phi W}/\Lambda^2$	6	ZZ	1.9	34 TeV^{-2}	20 TeV^{-2}	16 TeV^{-2}	9.3 TeV^{-2}
$f_{S,0}/\Lambda^4$	8	$W^{\pm}W^{\pm}$	2.0	10 TeV^{-4}	6.8 TeV^{-4}	4.5 TeV^{-4}	0.8 TeV^{-4}
$f_{T,1}/\Lambda^4$	8	WZ	3.7	1.3 TeV^{-4}	0.7 TeV^{-4}	0.6 TeV^{-4}	0.3 TeV^{-4}
$f_{T,8}/\Lambda^4$	8	$Z\gamma\gamma$	12	0.9 TeV^{-4}	0.5 TeV^{-4}	0.4 TeV^{-4}	0.2 TeV^{-4}
$f_{T,9}/\Lambda^4$	8	$Z\gamma\gamma$	13	2.0 TeV^{-4}	0.9 TeV^{-4}	0.7 TeV^{-4}	0.3 TeV^{-4}

Table 19-22. *5σ-significance discovery values and 95% CL limits for coefficients of higher-dimension operators. Madgraph5 is used for the event generation. Λ_{UV} is the unitarity violation bound corresponding to the sensitivity with 3000 fb^{-1} of integrated luminosity. See Table 19-33 for resonance mass limits corresponding to the $f_{S,0}/\Lambda^4$ sensitivity above, in a dimension-8 operator formulation and considering simplified models of electroweak resonances.*

The substantially improved sensitivity to these higher dimensional operators highlights the potential of the LHC to probe one of the most important aspects of the electroweak sector of the SM, namely, the unitarization of the vector boson scattering amplitudes by the Higgs mechanism. Since the "Mexican hat" Higgs potential is essentially just a parameterization, a more "dynamical" explanation of this potential in

terms of the Higgs' interaction with new scalar, vector or fermion fields involving strong dynamics can easily induce higher-dimension operators as precursors to the more complete theory of the Higgs sector.

Another example of the impact of the HL-LHC in studying the unitarization mechanism is provided by the improved sensitivity to the $\mathcal{O}_{\Phi d}$ operator of Eq. 19.22 shown in Table 19-24. The threshold of interest in the magnitude of this operator is provided by v^{-2} where v is the Higgs field's vacuum expectation value, thus $v^{-2} = 16$ TeV^{-2}. As the sensitivity to the magnitude of this operator falls below 16 TeV^{-2}, we obtain a direct test of the SM unitarization mechanism. Table 19-24 shows that this threshold is crossed by increasing the LHC integrated luminosity from 300 fb^{-1} to 3000 fb^{-1}.

Vector boson scattering and triboson production are unique probes of the possible high-energy dynamics underlying the Higgs potential. Furthermore, the different operators reflect directly in different energy dependencies of VBS and triboson production, and the study of these processes can not only detect the presence of new underlying dynamics but also distinguish between the operators through the differences in the kinematic shapes.

19.3.4 Multi-boson processes at HE pp colliders

Additional sensitivity studies have been performed using the Snowmass-DELPHES detector simulation [192]. These studies extend the ATLAS investigations to higher energy *pp* colliders, and also include additional final states and higher-dimension operators. Madgraph5 has been used for the event generation and the relations of Eqn. 19.59 apply. The results presented in [192] are summarized here and tables of numerical results have been reproduced from this reference. The main area of interest is anomalous quartic gauge couplings which are only probed by vector boson scattering and triboson production. Access to these processes has only opened up with the availability of LHC data, and therefore they are promising new avenues for discovery, for instance, of the composite nature of the Higgs sector.

In the following, a review of studies using VBS and triboson channels is presented. A number of different combinations of operators and final states are investigated. The main purpose of these studies is to estimate the improvement of sensitivity to coefficients of higher-dimension operators as a function of integrated luminosity and collider energy. In cases where the same operator is used with different final states, we also learn which of these final states are more sensitive.

Using the VBS $ZZ \to 4\ell$ final state, the sensitivity to the following operators was quantified for 14 TeV and 33 TeV *pp* colliders; the dimension-6 operator $\mathcal{O}_{\Phi W}$ of Eqn. 19.23 and the dimension-8 operators $\mathcal{O}_{T,8}$ of Eqn. 19.39 and $\mathcal{O}_{T,9}$ of Eqn. 19.40, with the results shown in Table 19-23. As the sensitivity to these operators is probed with higher-energy colliders, the regime where the amplitude violates unitarity is probed more deeply. This is an indication of the colliders' ability to directly produce the particle excitations of the ultraviolet-complete field theory underlying the EFT. The results in [192] are quoted both with and without the application of a unitarity-violating (UV) upper bound on the invariant mass of the multi-boson system. When the bound is applied, the surviving events are restricted to the low-mass region where the corresponding beyond-SM amplitude does not violate unitarity.

Similarly, the studies of the VBS $WZ \to 3\ell\nu$ were extended to 14 TeV and 33 TeV *pp* colliders using the following operators; the dimension-8 operator $\mathcal{O}_{T,1}$ of Eqn. 19.34 and the dimension-6 operator $\mathcal{O}_{\Phi d}$ of Eqn. 19.22. The results are shown in Table 19-24.

Another sensitive channel is the VBS production of same-sign W bosons, which unlike VBS W^+W^- is not dominated by $t\bar{t}$ production. Sensitivity studies to the $\mathcal{O}_{T,1}$ operator (Eqn. 19.34) produce the results shown

Parameter	Luminosity [fb^{-1}]	14 TeV		33 TeV	
		5σ	95% CL	5σ	95% CL
$c_{\Phi W}/\Lambda^2$ [TeV^{-2}]	3000	16.2 (16.2)	9.7 (9.7)	13.2 (13.2)	8.2 (8.2)
	300	31.3 (31.5)	18.2 (18.3)	23.8 (23.8)	14.7 (14.7)
$f_{T,8}/\Lambda^4$ [TeV^{-4}]	3000	2.9 (4.7)	1.7 (2.4)	1.6 (1.7)	1.0 (1.3)
	300	5.5 (8.4)	3.2 (5.3)	2.8 (2.3)	1.8 (1.8)
$f_{T,9}/\Lambda^4$ [TeV^{-4}]	3000	5.7 (6.3)	3.9 (4.6)	3.8 (6.6)	2.5 (3.5)
	300	8.7 (9.0)	6.2 (6.7)	6.3 (10.1)	4.2 (8.2)

Table 19-23. *In $pp \to ZZ + 2j \to 4\ell + 2j$ processes, 5σ-significance discovery values and 95% CL limits are shown for coefficients of high-dimension operators with 300 fb^{-1}/3000 fb^{-1} of integrated luminosity. To show the impact of the UV bound, the corresponding results are shown in parentheses.*

Parameter	Luminosity [fb^{-1}]	14 TeV		33 TeV	
		5σ	95% CL	5σ	95% CL
$c_{\Phi d}/\Lambda^2$ [TeV^{-2}]	3000	15.2 (15.2)	9.1 (9.1)	12.6 (12.7)	7.7 (7.7)
	300	28.5 (28.7)	17.1 (17.1)	23.1 (23.3)	14.1 (14.2)
$f_{T,1}/\Lambda^4$ [TeV^{-4}]	3000	0.6 (0.9)	0.4 (0.5)	0.3 (0.6)	0.2 (0.3)
	300	1.1 (1.6)	0.7 (1.0)	0.6 (0.9)	0.3 (0.6)

Table 19-24. *In $pp \to WZ + 2j \to \ell\nu\ell\ell + 2j$ processes, 5σ-significance discovery values and 95% CL limits are shown for coefficients of higher-dimension operators with 300 fb^{-1}/3000 fb^{-1} of integrated luminosity at 14 TeV and 33 TeV. The results obtained after applying the UV bounds are shown in parentheses.*

in Table 19-25. As part of this exercise, different pileup configurations were investigated and found not to have a significant effect, as shown in Table 19-25. The implication is that none of the fully-leptonic channels considered in these studies are very sensitive to pileup. In this channel, the studies are extended to a 100 TeV pp collider.

Good sensitivity to higher-dimension operators is also obtainable from triboson production. Using the $WWW \to 3\ell + 3\nu$ final state, the following operators were investigated: the dimension-8 operator $\mathcal{O}_{T,0}$ of Eqn. 19.33 and the dimension-6 operator $\mathcal{O}_{WWW}$ of Eqn. 19.18. The sensitivity to these operators is presented in Table 19-26.

Finally, the final state $Z\gamma\gamma \to \ell\ell\gamma\gamma$ is used to investigate the sensitivity for the dimension-8 operators $\mathcal{O}_{M,i}, i = 0, 1, 2, 3$ of Eqn. 19.32, and the results are presented in Table 19-27.

The conclusions that can draw from these numerical results, have been stated in [192] and reproduced verbatim in this report for convenience, below;

- The VBS ZZ final state, when used to probe the $\mathcal{O}_{\Phi W}$ dimension-6 operator, increases in sensitivity to the operator coefficient by a factor of ≈ 1.9 when the luminosity is increased by a factor of 10 from 300 fb^{-1} to 3000 fb^{-1}, and by a factor of ≈ 1.2 when the collider energy is increased from 14 TeV to 33 TeV. When considering the dimension-8 operators $\mathcal{O}_{T,8}$ ($\mathcal{O}_{T,9}$), the sensitivity increases by a factor of 1.9 (1.5) due to the same luminosity increase and by a factor of ≈ 1.8 (1.5) due to the energy increase. The sensitivity to the dimension-6 operator is not affected by imposing a UV bound, while the sensitivity to the dimension-8 operator is reduced by a factor of about 1.8 when the bound is applied.

Parameter	$\sqrt{s}$ [TeV]	Luminosity [fb^{-1}]	pileup	5σ [TeV^{-4}]	95% CL [TeV^{-4}]
$f_{T,1}/\Lambda^4$	14	300	50	0.2 (0.4)	0.1 (0.2)
$f_{T,1}/\Lambda^4$	14	3000	140	0.1 (0.2)	0.06 (0.1)
$f_{T,1}/\Lambda^4$	14	3000	0	0.1 (0.2)	0.06 (0.1)
$f_{T,1}/\Lambda^4$	100	1000	40	0.001 (0.001)	0.0004 (0.0004)
$f_{T,1}/\Lambda^4$	100	3000	263	0.001 (0.001)	0.0008 (0.0008)
$f_{T,1}/\Lambda^4$	100	3000	0	0.001 (0.001)	0.0008 (0.0008)

Table 19-25. *In $pp \to W^{\pm}W^{\pm} + 2j \to \ell\nu\ell\nu + 2j$ processes, 5σ-significance discovery values and 95% CL limits are shown for coefficients the higher-dimension operator, $f_{T,1}/\Lambda^4$, for different machine scenarios without the UV cut and with the UV cut in parenthesis. Pileup refers to the number of pp interactions per crossing.*

Parameter	dim.	Luminosity [fb^{-1}]	14 TeV	33 TeV	100 TeV
c_{WWW}/Λ^2 [TeV^{-2}]	6	300	4.8 (8)	-	-
		1000	-	-	1.3 (1.5)
		3000	2.3 (2.5)	1.7 (2.0)	0.9 (1.0)
$f_{T,0}/\Lambda^4$ [TeV^{-4}]	8	300	1.2	-	-
		1000	-	-	0.004
		3000	0.6	0.05	0.002

Table 19-26. *In the $pp \to WWW \to 3\ell + 3\nu$ process, the 5σ-significance discovery values are shown for the coefficients of higher order operators. The values in parentheses are obtained with the UV bound applied. pp colliders at $\sqrt{s} = 14$, 33 and 100 TeV are studied.*

- The VBS WZ final state, when used to probe the $\mathcal{O}_{\Phi d}$ dimension-6 operator, increases in sensitivity to the operator coefficient by a factor of ≈ 1.9 when the luminosity is increased from 300 fb^{-1} to 3000 fb^{-1}, and by a factor of ≈ 1.2 when the collider energy is increased from 14 TeV to 33 TeV. When considering the dimension-8 operator $\mathcal{O}_{T,1}$, the sensitivity increases by a factor of ≈ 1.8 due to the same luminosity increase and by a factor of ≈ 2 due to the energy increase. The sensitivity to the dimension-6 operator is not affected by imposing a UV bound, while the sensitivity to the dimension-8 operator is reduced by a factor of about 1.8 when the bound is applied.

- The VBS same-sign WW final state, when used to probe the $\mathcal{O}_{T,1}$ dimension-8 operator, increases in sensitivity to the operator coefficient by a factor of ≈ 2 when the luminosity is increased from 300 fb^{-1} to 3000 fb^{-1} at $\sqrt{s} = 14$ TeV. An increase in collider energy from 14 TeV to 100 TeV increases the sensitivity by a factor of 100. The sensitivity is not affected at $\sqrt{s} = 100$ TeV by imposing a UV bound because the bound is very high for the value of the coefficient probed. The sensitivity at $\sqrt{s} = 14$ TeV is reduced by a factor of about 2 when the bound is applied.

- The triboson WWW final state, when used to probe the $\mathcal{O}_{WWW}$ dimension-6 operator, increases in sensitivity to the operator coefficient by a factor of ≈ 2 when the luminosity is increased from 300 fb^{-1} to 3000 fb^{-1} at $\sqrt{s} = 14$ TeV. An increase in collider energy from 14 TeV to 33 TeV (100 TeV) increases the sensitivity by a factor of 1.3 (2.5). These results are affected at the 10% level by the application of the UV bound. When probing the dimension-8 operator $\mathcal{O}_{T,0}$, the sensitivity to the operator coefficient increases by a factor of ≈ 2 when the luminosity is increased from 300 fb^{-1} to 3000

Parameter	$\sqrt{s}$	14 TeV	14 TeV	33 TeV	100 TeV
	Lum.	300 fb^{-1}	3000 fb^{-1}		
$f_{M,0}/\Lambda^4$ [TeV^{-4}]	5σ	7300 (830)	3600 (310)	1900 (190)	750 (120)
	95% CL	4200 (360)	1200 (160)	660 (120)	71 (59)
$f_{M,1}/\Lambda^4$ [TeV^{-4}]	5σ	7600 (1600)	3600 (680)	2100 (340)	1000 (220)
	95% CL	4500 (800)	1200 (290)	770 (160)	240 (126)
$f_{M,2}/\Lambda^4$ [TeV^{-4}]	5σ	3300 (130)	510 (48)	310 (26)	120 (16)
	95% CL	670 (56)	160 (21)	110 (13)	25 (10)
$f_{M,3}/\Lambda^4$ [TeV^{-4}]	5σ	2400 (250)	720 (120)	320 (66)	180 (34)
	95% CL	820 (133)	210 (52)	130 (23)	38 (15)

Table 19-27. *In $pp \to Z\gamma\gamma \to l^+l^-\gamma\gamma$ processes, 5σ-significance discovery values and 95% CL limits are shown for coefficients of dimension-8 operators with integrated luminosity of 300 fb^{-1} at $\sqrt{s} = 14$ TeV and 3000 fb^{-1} at $\sqrt{s} = 14$ TeV, 33 TeV and 100 TeV, respectively. To show the impact without the UV bound, the corresponding results are shown in parentheses.*

fb^{-1} at $\sqrt{s} = 14$ TeV. An increase in collider energy from 14 TeV to 33 TeV (100 TeV) increases the sensitivity by a factor of 12 (300). This dramatic increase is tamed by the UV bound; we take this as an indication that WWW triboson production is a sensitive channel for direct production of new particles as the collider energy is raised.

- The triboson $Z\gamma\gamma$ final state, when used to probe the $\mathcal{O}_{M,i}$ dimension-8 operators, increases in sensitivity to the operator coefficient by a factor of $2-6$ (depending the operator considered) when the luminosity is increased from 300 fb^{-1} to 3000 fb^{-1} at $\sqrt{s} = 14$ TeV. An increase in collider energy from 14 TeV to 33 TeV (100 TeV) increases the sensitivity by a factor of ≈ 2 (4 to 5). These results are strongly affected by the application of the UV bound.

It is important to note that the sensitivities for the 33 TeV and 100 TeV colliders are based on analyses that have not been re-optimized for higher energy colliders; the analyses were optimized for 14 TeV only. Optimization of the analyses for higher collider energies is important and should be revisited in the future, as it will lead to further improvements of the sensitivity to new physics at those machines. The leptonic channels studied in [192] have been shown to be relatively insensitive to pileup effects.

19.3.5 Multi-boson processes at lepton colliders

Di-boson processes, in particular $e^+e^- \to W^+W^-$, were used very successfully at LEP to probe TGCs, and multi-boson processes have also been studied at ILC and CLIC to estimate the sensitivity to TGCs and QGCs. Table 19-28 provides projected sensitivities to the TGCs of Eq. 19.41 at a 500 GeV and 800 GeV ILC with polarized beams. As shown in Fig. 19-22 (see Ref. [193]), most TGCs will be better constrained at ILC than at the LHC, though the LHC will improve significantly upon LEP and the Tevatron. For one specific anomalous coupling parameter, $\Delta\lambda_\gamma$, the LHC and especially the HL-LHC (with 3000 fb^{-1}) is competitive with ILC800.

Estimates of sensitivities to CP-even aTGCs in W-boson pair production at CLIC have been provided in Ref. [195] and reproduced for the Snowmass study in Ref. [104], as shown in Table 19-29. The TGCs

coupling	error $\times 10^{-4}$	
	$\sqrt{s} = 500$ GeV	$\sqrt{s} = 800$ GeV
Δg_1^{Z}	15.5	12.6
$\Delta\kappa_\gamma$	3.3	1.9
λ_γ	5.9	3.3
$\Delta\kappa_{\mathrm{Z}}$	3.2	1.9
λ_{Z}	6.7	3.0
g_5^Z	16.5	14.4
g_4^Z	45.9	18.3
$\tilde{\kappa}_{\mathrm{Z}}$	39.0	14.3
$\tilde{\lambda}_{\mathrm{Z}}$	7.5	3.0

Table 19-28. *Results of the single parameter fits (1σ) to the different triple gauge couplings at the ILC for $\sqrt{s} = 500$ GeV with $\mathcal{L} = 500$ fb^{-1} and $\sqrt{s} = 800$ GeV with $\mathcal{L} = 1000$ fb^{-1}; $\mathcal{P}_{e^-} = 80\%$ and $\mathcal{P}_{e^+} = 60\%$ has been used. Taken from Ref. [194].*

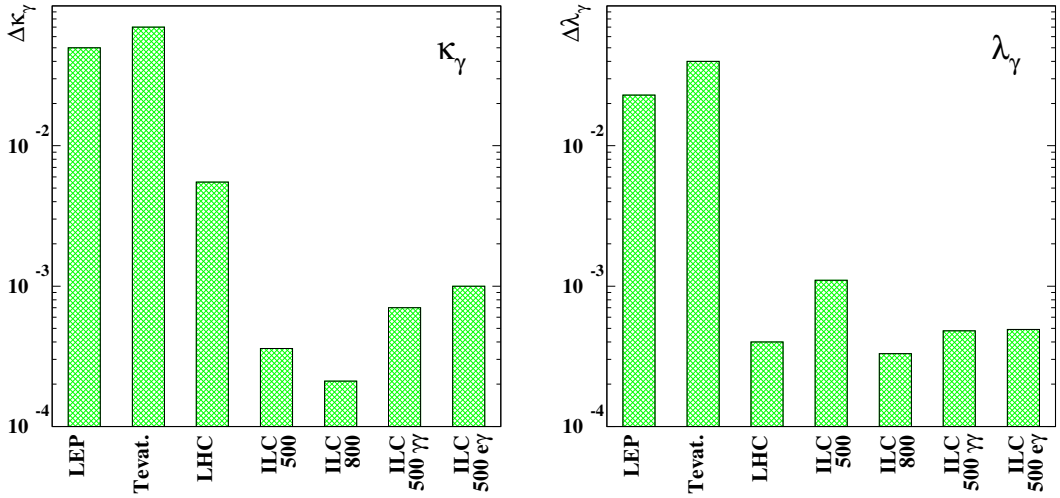

Figure 19-22. *Comparison of $\Delta\kappa_\gamma$ and $\Delta\lambda_\gamma$ at different machines. For LHC and ILC three years of running are assumed (LHC: 300 fb^{-1}, ILC $\sqrt{s} = 500$ GeV: 500 fb^{-1}, ILC $\sqrt{s} = 800$ GeV: 1000 fb^{-1}). If available the results from multi-parameter fits have been used. Taken from Ref. [193, 194].*

$g_i^{L,R}, \lambda_{L,R}$ and $\Delta\kappa_{L,R}$ are defined in terms of the TGCs of Eq. 19.41. The superscripts L (R) refer to the values obtained for amplitudes with left (right) handed electrons and right (left) handed positrons. The definitions for g_1, for example, are

$$g_1^{\mathrm{L}} = 4\sin^2\theta_{\mathrm{W}} g_1^\gamma + (2 - 4\sin^2\theta_{\mathrm{W}}) g_1^Z \xi \tag{19.71}$$

$$g_2^{\mathrm{R}} = 4\sin^2\theta_{\mathrm{W}} g_1^\gamma - 4\sin^2\theta_{\mathrm{W}} g_1^Z \xi \tag{19.72}$$

where $\xi = s/(s - m_Z^2)$. For more details, see [195].

Prospects for precision studies of anomalous quartic couplings at the ILC have been studied in $e^+e^- \to WWZ$ and $e^+e^- \to ZZZ$ and VBS processes with and without beam polarization in Ref. [196] (see also Ref. [197] for a review), and the results for WWZ, ZZZ production are presented in Table 19-30. The aQGCs have been parametrized in the effective chiral Lagrangian approach as described in Section 19.3.6.

$\sqrt{s}$ [GeV]	$\mathrm{Re}(\Delta g_1^L)$	$\mathrm{Re}(\Delta\kappa_L)$	$\mathrm{Re}(\lambda_L)$	$\mathrm{Re}(g_5^L)$	$\mathrm{Re}(g_1^R)$	$\mathrm{Re}(\Delta\kappa_R)$	$\mathrm{Re}(\lambda_R)$	$\mathrm{Re}(g_5^R)$
500	2.6	0.85	0.59	2.0	10	2.4	3.6	6.7
800	1.6	0.35	0.24	1.4	6.2	0.92	1.8	4.8
3000	0.93	0.051	0.036	0.88	3.1	0.12	0.36	3.2

Table 19-29. *Sensitivity of CLIC to the real parts of CP-even TGCs in units of* 10^{-3}*, defined in [195]. The integrated luminosities for the* 500 *GeV,* 800 *GeV and* 3000 *GeV stages are assumed here to be* 500 fb^{-1}, 1 ab^{-1} *and* 3 ab^{-1} *respectively. Taken from Ref. [104]*

		WWZ			ZZZ	best
		no pol.	e^- pol.	both pol.	no pol.	
$16\pi^2\Delta\alpha_4$	σ^+	9.79	4.21	1.90	3.94	1.78
	σ^-	−4.40	−3.34	−1.71	−3.53	−1.48
$16\pi^2\Delta\alpha_5$	σ^+	3.05	2.69	1.17	3.94	1.14
	σ^-	−7.10	−6.40	−2.19	−3.53	−1.64

Table 19-30. *Sensitivity of the 1 TeV ILC (with 1* ab^{-1}*) to the aQGC coupling parameters* α_4 *and* α_5 *in* WWZ *and* ZZZ *production, expressed as* 1σ *errors. WWZ: two-parameter fit; ZZZ: one-parameter fit; best: best combination of both. Taken from Ref. [196].*

In Section 19.3.1.4 we provide a conversion of the aQGCs coupling parameters α_4, α_5 of this approach to the EFT coefficients $f_{S,0}, f_{S,1}$ for $WWWW, WWZZ$ and $ZZZZ$ vertices. Using this translation, we can convert the α_4, α_5 sensitivity from ILC in Table 19-30 to the $f_{S,0}, f_{S,1}$ basis used by the ATLAS studies in Section 19.3.3 and the LHC and higher-energy pp collider studies in Setion. 19.3.4. Using Eq. 19.61, we find that the ILC sensitivity translates to 90% CL limits on $f_{S,0}/\Lambda^4 \approx 20$ TeV^{-4}, which are about a factor of 20 weaker than the 95% CL limit estimated by the ATLAS study using 3000 fb^{-1}, as shown in Table 19-22. The sensitivity to the other dimension-8 operators, which induce purely quartic anomalous couplings, is even higher at the LHC, as shown in Sec. 19.3.3 and Sec. 19.3.4. This is likely because the $\mathcal{O}_{S,0(1)}$ operators do not contain derivatives of the gauge boson fields, while such derivatives in other dimension-8 operators enhance the anomalous production at the higher LHC energy.

We arrive at the preliminary conclusion that aTGC's, which are induced by dimension-6 operators, are significantly better probed by the high-energy ILC options compared to the LHC. On the other hand, aQGC's, which are induced by dimension-8 operators, are significantly better probed (by 1-2 orders of magnitude) by the LHC, due to the stronger growth of the anomalous cross section with energy. This conclusion is supported by the comparison of 95% CL limits in Table 19-33 for the LHC and Table 19-34 for the ILC. The LHC is sensitive to resonance masses that are higher by more than a factor of two, as compared to ILC1000. Note further that this comparison is based on the $\mathcal{O}_{S,0}$ operator of Eqn. 19.30, for which the LHC sensitivity is not as strong as for the other operators (such as $\mathcal{O}_{T,i}, i = 1, 8, 9$ of Eqn. 19.34, 19.39, and 19.40) due to the difference in the number of derivatives of gauge fields.

19.3.6 Simplified Models for New Physics in Vector Boson Scattering

Here we briefly describe the translation of very heavy resonances that arise in simplified models and leave only traces in the form of deviations in the SM couplings into higher-dimensional operators leading to such deviations. A detailed discussion can be found in Ref. [134].

The simplified models discussed here contain the SM supplemented by all possible resonances that could couple to the sector of EW gauge bosons according to their spin and isospin quantum numbers. Such simplified models cover cases ranging from Two- or Multi-Higgs doublet models, extended scalar sectors, Technicolor models, models of complete or partial compositeness, Little Higgs models, Twin Higgs models and many more. Cases where there is only a single resonance present could be described along these lines as well as cases where there are more resonances (but maybe only one of them accessible to LHC). The resonances are just parametrized by their mass, possibly their width, as well as their couplings to the electroweak sector. As simplified models are like any effective field theory not UV-complete, perturbative unitarity of tree-level amplitudes in that setup are not guaranteed (see also Section 19.3.1). To give a prescription that can be used by the experiments in a model-independent setup and does not yield overly optimistic results due to unphysical amplitude contributions within exclusion limits, a unitarization formalism has been introduced in Ref. [134] that projects back on amplitudes that are genuinely unitary. This is insured by giving additive corrections to the SM vector boson scattering augmented by the BSM resonances. A simple implementation has been performed in the event generator WHIZARD [199].

Here we define a simplified model that is able to describe the essence of a new physics sector that couples to the EW sector in an approach as model-independent as possible. We refrain from discussing fermionic resonances here as those would contribute only at the 1-loop order to vector boson scattering, and concentrate on new bosonic resonances. To do so, one needs to supplement the Lagrangian of the EW SM (accounting for the discovery of the 125 GeV state as the SM Higgs boson but maybe allowing its couplings to deviate within the limits of the EW perturbation theory (EWPT) from their SM values). As the main signatures to study the EW sector of the SM are diboson, triboson and generically multi-boson production as well as vector-boson scattering (VBS), and here particularly scattering of longitudinal gauge bosons, it is convenient to use an operator basis containing explicitly the longitudinal degrees of freedom (DOFs) of the EW gauge bosons. This effective Lagrangian is basically identical to the chiral EW Lagrangian [198], except that we linearize the Lagrangian by adding the Higgs particle, and all higher-dimensional operators stem from BSM contributions. So we implement $SU(2)_L \times U(1)_Y$ gauge invariance, where the building blocks are the SM fermions, ψ, the EW (transversal) gauge boson fields W_μ^a $(a = 1, 2, 3)$ and B_μ as well as the longitudinal DOFs, $\Sigma = \exp\left[\frac{-i}{v} w^a \tau^a\right]$.

The effective Lagrangian is obtained by adding to the minimal (SM) Lagrangian of Ref. [134] deviations from that Lagrangian in the form of higher-dimensional operators allowed by gauge symmetry as well as CP as follows:

$$\mathcal{L}_{\text{eff}} = \mathcal{L}_{\text{min}} + \beta_1 \mathcal{L}_0' + \sum_i \alpha_i \mathcal{L}_i + \frac{1}{\Lambda} \sum_i \alpha_i^{(5)} \mathcal{L}_i^{(5)} + \frac{1}{\Lambda^2} \sum_i \alpha_i^{(6)} \mathcal{L}_i^{(6)} + \dots \tag{19.73}$$

where Λ is (up to $\mathcal{O}(1)$ constants) the scale where BSM physics potentially enters. The operators are

$$\mathcal{L}_0' = \frac{v^2}{4} \operatorname{tr}[\mathbf{T}\mathbf{V}_\mu] \operatorname{tr}[\mathbf{T}\mathbf{V}^\mu] \tag{19.74}$$

$$\mathcal{L}_1 = \operatorname{tr}[\mathbf{B}_{\mu\nu}\mathbf{W}^{\mu\nu}] \qquad \mathcal{L}_6 = \operatorname{tr}[\mathbf{V}_\mu \mathbf{V}_\nu] \operatorname{tr}[\mathbf{T}\mathbf{V}^\mu] \operatorname{tr}[\mathbf{T}\mathbf{V}^\nu] \tag{19.75}$$

$$\mathcal{L}_2 = \mathrm{i} \operatorname{tr}[\mathbf{B}_{\mu\nu}[\mathbf{V}^\mu, \mathbf{V}^\nu]] \qquad \mathcal{L}_7 = \operatorname{tr}[\mathbf{V}_\mu \mathbf{V}^\mu] \operatorname{tr}[\mathbf{T}\mathbf{V}_\nu] \operatorname{tr}[\mathbf{T}\mathbf{V}^\nu] \tag{19.76}$$

$$\mathcal{L}_3 = \mathrm{i} \operatorname{tr}[\mathbf{W}_{\mu\nu}[\mathbf{V}^\mu, \mathbf{V}^\nu]] \qquad \mathcal{L}_8 = \tfrac{1}{4} \operatorname{tr}[\mathbf{T}\mathbf{W}_{\mu\nu}] \operatorname{tr}[\mathbf{T}\mathbf{W}^{\mu\nu}] \tag{19.77}$$

$$\mathcal{L}_4 = \operatorname{tr}[\mathbf{V}_\mu \mathbf{V}_\nu] \operatorname{tr}[\mathbf{V}^\mu \mathbf{V}^\nu] \qquad \mathcal{L}_9 = \tfrac{\mathrm{i}}{2} \operatorname{tr}[\mathbf{T}\mathbf{W}_{\mu\nu}] \operatorname{tr}[\mathbf{T}[\mathbf{V}^\mu, \mathbf{V}^\nu]] \tag{19.78}$$

$$\mathcal{L}_5 = \operatorname{tr}[\mathbf{V}_\mu \mathbf{V}^\mu] \operatorname{tr}[\mathbf{V}_\nu \mathbf{V}^\nu] \qquad \mathcal{L}_{10} = \tfrac{1}{2} \left(\operatorname{tr}[\mathbf{T}\mathbf{V}_\mu] \operatorname{tr}[\mathbf{T}\mathbf{V}^\mu]\right)^2 \tag{19.79}$$

Here, the field strength tensors are defined in terms of W_μ^a $(a = 1, 2, 3)$ and B_μ as

$$\mathbf{W}_{\mu\nu} = \partial_\mu \mathbf{W}_\nu - \partial_\nu \mathbf{W}_\mu + ig\,[\mathbf{W}_\mu, \mathbf{W}_\nu] \tag{19.80}$$

$$\mathbf{B}_{\mu\nu} = \partial_\mu \mathbf{B}_\nu - \partial_\nu \mathbf{B}_\mu \tag{19.81}$$

with

$$\mathbf{W}_\mu = W_\mu^a \frac{\tau^a}{2} \qquad \text{and} \qquad \mathbf{B}_\mu = B_\mu \frac{\tau^3}{2}. \tag{19.82}$$

Using the covariant derivative

$$\mathbf{D}_\mu \Sigma = \partial_\mu + ig\mathbf{W}_\mu \Sigma - ig'\Sigma \mathbf{B}_\mu \tag{19.83}$$

one defines $\mathbf{V}$ as a field representing longitudinal vectors, $\mathbf{V} = \Sigma(\mathbf{D}\Sigma)^\dagger$ that will be used shortly to write down operators giving rise to modified couplings. In order to write down operators projecting out the neutral component, one uses $\mathbf{T} = \Sigma\tau^3\Sigma^\dagger$. For more technical details about this formalism interpreted in that context of simplified models for extended EW symmetry breaking, cf. [150, 200]. Indirect information on new physics is encoded in the operator coefficients β_1, α_i. From EWPT (SLC/LEP/Tevatron measurements), one knows that $\alpha_i \ll 1$, while on the other hand from naive dimensional analysis one would assume $\alpha_i \sim 1/16\pi^2 \approx 0.006$ as they have to renormalize divergences in an effective field theoretic simplified model of a UV-complete BSM model. Using such a bottom-up approach, it is notoriously difficult, as the usual setup as a ratio of the EW and the BSM scale $\alpha_i = v^2/\Lambda^2$ is only valid up to unknown operator normalization coefficients (that are in general coupling constants of the UV-complete model), furthermore the power counting can be highly nontrivial, producing unexpected scaling behavior of operators.

Higher-dimensional operators do lead to deviations of the triple and quartic gauge couplings from their SM values. For completeness, we repeat the formulae for triple and quartic gauge couplings, and how they depend on the SM parameters as well as on the operator coefficients of the effective Lagrangian above:

$$\begin{aligned}
\mathcal{L}_{TGC} = {} & \mathrm{i}e \left[g_1^\gamma A_\mu \left(W_\nu^- W^{+\mu\nu} - W_\nu^+ W^{-\mu\nu} \right) + \kappa^\gamma W_\mu^- W_\nu^+ A^{\mu\nu} + \frac{\lambda^\gamma}{M_W^2} W_\mu^{-\nu} W_{\nu\rho}^+ A^{\rho\mu} \right] \\
& + \mathrm{i}e \frac{c_\mathrm{w}}{s_\mathrm{w}} \left[g_1^Z Z_\mu \left(W_\nu^- W^{+\mu\nu} - W_\nu^+ W^{-\mu\nu} \right) + \kappa^Z W_\mu^- W_\nu^+ Z^{\mu\nu} + \frac{\lambda^Z}{M_W^2} W_\mu^{-\nu} W_{\nu\rho}^+ Z^{\rho\mu} \right] \qquad (19.84) \\
\mathcal{L}_{QGC} = {} & e^2 \left[g_1^{\gamma\gamma} A^\mu A^\nu W_\mu^- W_\nu^+ - g_2^{\gamma\gamma} A^\mu A_\mu W^{-\nu} W_\nu^+ \right] \\
& + e^2 \frac{c_\mathrm{w}}{s_\mathrm{w}} \left[g_1^{\gamma Z} A^\mu Z^\nu \left(W_\mu^- W_\nu^+ + W_\mu^+ W_\nu^- \right) - 2 g_2^{\gamma Z} A^\mu Z_\mu W^{-\nu} W_\nu^+ \right] \\
& + e^2 \frac{c_\mathrm{w}^2}{s_\mathrm{w}^2} \left[g_1^{ZZ} Z^\mu Z^\nu W_\mu^- W_\nu^+ - g_2^{ZZ} Z^\mu Z_\mu W^{-\nu} W_\nu^+ \right] \\
& + \frac{e^2}{2 s_\mathrm{w}^2} \left[g_1^{WW} W^{-\mu} W^{+\nu} W_\mu^- W_\nu^+ - g_2^{WW} \left(W^{-\mu} W_\mu^+ \right)^2 \right] + \frac{e^2}{4 s_\mathrm{w}^2 c_\mathrm{w}^4} h^{ZZ} (Z^\mu Z_\mu)^2 \qquad (19.85)
\end{aligned}$$

In these equations, the SM values are $g_1^{\gamma,Z} = \kappa^{\gamma,Z} = 1$, $\lambda^{\gamma,Z} = 0$, and $g_{1/2}^{VV'} = 1$, $h^{ZZ} = 0$. The quantity $\delta_Z = \frac{\beta_1 + g'^2 \alpha_1}{c_\mathrm{w}^2 - s_\mathrm{w}^2}$ takes into account the definition of the EW scheme as well as the oblique corrections through the ρ parameter. In the presence of the operators Eq. 19.74, one gets the following shifts:

$$\Delta g_1^\gamma = 0 \qquad \Delta\kappa^\gamma = g^2(\alpha_2 - \alpha_1) + g^2\alpha_3 + g^2(\alpha_9 - \alpha_8) \tag{19.86}$$

$$\Delta g_1^Z = \delta_Z + \tfrac{g^2}{c_\mathrm{w}^2}\alpha_3 \qquad \Delta\kappa^Z = \delta_Z - g'^2(\alpha_2 - \alpha_1) + g^2\alpha_3 + g^2(\alpha_9 - \alpha_8) \tag{19.87}$$

as well as

$$\Delta g_1^{\gamma\gamma} = \Delta g_2^{\gamma\gamma} = 0 \qquad \Delta g_2^{ZZ} = 2\Delta g_1^{\gamma Z} - \tfrac{g^2}{c_\mathrm{w}^4}(\alpha_5 + \alpha_7) \tag{19.88}$$

$$\Delta g_1^{\gamma Z} = \Delta g_2^{\gamma Z} = \delta_Z + \tfrac{g^2}{c_\mathrm{w}^2}\alpha_3 \qquad \Delta g_1^{WW} = 2c_\mathrm{w}^2 \Delta g_1^{\gamma Z} + 2g^2(\alpha_9 - \alpha_8) + g^2\alpha_4 \tag{19.89}$$

$$\Delta g_1^{ZZ} = 2\Delta g_1^{\gamma Z} + \tfrac{g^2}{c_\mathrm{w}^4}(\alpha_4 + \alpha_6) \qquad \Delta g_2^{WW} = 2c_\mathrm{w}^2 \Delta g_1^{\gamma Z} + 2g^2(\alpha_9 - \alpha_8) - g^2(\alpha_4 + 2\alpha_5) \tag{19.90}$$

$$h^{ZZ} = g^2 \left[\alpha_4 + \alpha_5 + 2(\alpha_6 + \alpha_7 + \alpha_{10}) \right] \tag{19.91}$$

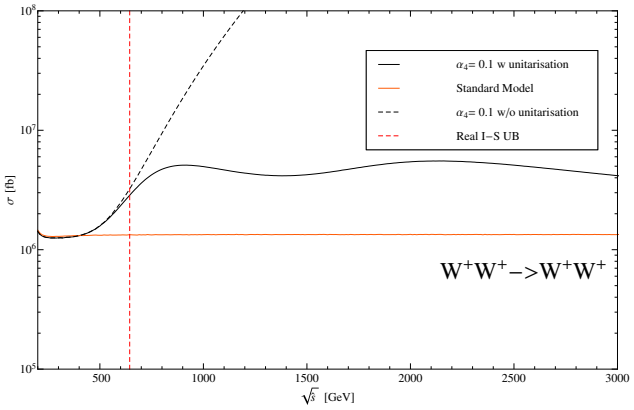

Figure 19-23. *Cross section of VBS with anomalous quartic gauge coupling α_4 in $W^+W^+ \to W^+W^+$. The orange line represents the Standard Model. Above the unitarity bound (red dashed line) one can clearly see that the cross section without unitarization scheme (black dashed line) violates unitarity. The unitarized cross section (black solid line) is going to saturate above the unitarity bound.*

The energy range of testing these anomalous couplings is bound by unitarity. Using α_4 as example the invariant mass of VBS is constrained by $\sqrt{s} \leq \sqrt[4]{\frac{6}{7\alpha_4}}v$. Beyond this energy bound Monte-Carlo generators would generate too many unphysical events and a useful statement about the tested anomalous coupling is not possible. Therefore dependent on the anomalous coupling only a small part of the energy range of LHC can be used. A possible formalism to utilize nevertheless events in the complete energy range is the K-Matrix scheme, which is described in [134]. Following this scheme the isospin-spin eigenamplitude will saturate for energies above the unitarity bound (cf figure 19-23). Therefore Monte Carlo generators using K-Matrix generate the maximal number of events allowed by unitarity.

We now make the connection to how BSM models in their incarnation as EW resonances, coupling to the SM EW gauge boson sector (particularly the longitudinal DOFs), generate such anomalous couplings. To be as general as possible, we include weakly interacting cases (e.g. Little Higgs models) where the new resonances are narrow (proper particles), as well as strongly interacting cases (e.g. compositeness or Technicolor models) where the new resonances are rather wide and could even approach the case of a continuum (e.g. unparticles or conformal sectors). As we know from EWPT, $\beta_1 \ll 1$, so the $SU(2)_c$ custodial symmetry of weak isospin (that in the SM is only broken by hypercharge $g' \neq 0$ and the fermion masses) is valid to a very good approximation. From the spin and isospin quantum numbers, only the resonances in the following table can couple to system of two EW vector bosons,

	$J=0$	$J=1$	$J=2$
$I=0$	σ^0 ("Higgs")	$[\omega^0]$ (γ'/Z')	f^0 (KK graviton)
$I=1$	$[\pi^\pm, \pi^0]$ (2HDM)	$\rho^\pm, \rho^0$ (W'/Z')	$[a^\pm, a^0]$
$I=2$	$\phi^{\pm\pm}, \phi^\pm, \phi^0$ (Higgs triplet)	—	$t^{\pm\pm}, t^\pm, t^0$

So only the scalars, vector or tensors can couple, and only the weak isospins $I = 0, 1, 2$ are allowed. The table shows prime examples for the corresponding combinations where a specific choice for the hypercharge has been made. The entries in brackets are combinations that are only possible with $SU(2)_c$-violating couplings, and are not further discussed here. The scalar isoscalar has the same quantum numbers as the SM Higgs boson. The scalar isovector appears in Technicolor models, while the isotensor can be found in the Littlest

Higgs model, e.g. Vector resonances appear in extra-dimensional models, Technicolor, Little Higgs models and many more. Tensor resonances without EW quantum numbers can be thought of as a recurrence of the graviton, while the isovector and -tensor are quite exotic and appear only, e. g., in extended compositeness models.

As a next step, we relate these resonances from our simplified models to anomalous couplings. Consider any kind of heavy resonance with generic Lagrangian $\mathcal{L}_\Phi = z\Big[\Phi\left(M_\Phi^2 + DD\right)\Phi + 2\Phi J\Big]$. Here, z is a (wavefunction re)normalization constant of the Lagrangian, and D is the gauge-covariant derivative. J is the EW current to which that particular resonance couples. Integrating out the resonance leads to $\mathcal{L}_\Phi^{\text{eff}} = -\frac{z}{M^2}JJ + \frac{z}{M^4}J(DD)J + \mathcal{O}(M^{-6})$. We now specialize to a scalar isoscalar resonance σ, whose Lagrangian is given by $\mathcal{L}_\sigma = -\frac{1}{2}\Big[\sigma(M_\sigma^2+\partial^2)\sigma - g_\sigma v\,\text{tr}\left[\mathbf{V}_\mu\mathbf{V}^\mu\right] - h_\sigma\,\text{tr}\left[\mathbf{TV}_\mu\right]\text{tr}\left[\mathbf{TV}^\mu\right]\Big]$. Integrating out the scalar, leads to the effective Lagrangian

$$\mathcal{L}_\sigma^{\text{eff}} = \frac{v^2}{8M_\sigma^2}\left[g_\sigma\,\text{tr}\left[\mathbf{V}_\mu\mathbf{V}^\mu\right] + h_\sigma\,\text{tr}\left[\mathbf{TV}_\mu\right]\text{tr}\left[\mathbf{TV}^\mu\right]\right]^2$$

From this one can read off that integrating out a scalar isoscalar generates the following anomalous quartic couplings

$$\alpha_5 = g_\sigma^2\left(\frac{v^2}{8M_\sigma^2}\right) \qquad \alpha_7 = 2g_\sigma h_\sigma\left(\frac{v^2}{8M_\sigma^2}\right) \qquad \alpha_{10} = 2h_\sigma^2\left(\frac{v^2}{8M_\sigma^2}\right) \tag{19.92}$$

One sees immediately, that a heavy SM Higgs would have fit into that scheme, using the special couplings $g_\sigma = 1$ and $h_\sigma = 0$.

When one tries to turn constraints on anomalous couplings into direct constraints on new physics, one faces the problem that there are too many free parameters to over-constrain the system. There is however one limiting case where one can do that which has been applied in the context of studies of the possible search power of a 1 TeV ILC on anomalous quartic couplings and their interpretation in terms of resonances [196]: In the limit of a very broad resonance (that couples rather strongly to the EW sector), the resonance is close to a broad continuum: $\Gamma \sim M \gg \Gamma(\text{non}-WW,ZZ) \sim 0$. Also, in that case the decays of such a particular resonance into non-W/Zs can be ignored. From the functional relation between the resonance width, its couplings and its mass (again in the case of a scalar isoscalar)

$$\Gamma_\sigma = \frac{g_\sigma^2 + \frac{1}{2}(g_\sigma^2+2h_\sigma^2)^2}{16\pi}\left(\frac{M_\sigma^3}{v^2}\right) + \Gamma(\text{non}-WW,ZZ) \tag{19.93}$$

one can then translate bounds for anomalous couplings directly into those of the effective Lagrangian:

$$\alpha_5 \leq \frac{4\pi}{3}\left(\frac{v^4}{M_\sigma^4}\right) \approx \frac{0.015}{(M_\sigma \text{ in TeV})^4} \quad \Rightarrow \quad 16\pi^2\alpha_5 \leq \frac{2.42}{(M_\sigma \text{ in TeV})^4} \tag{19.94}$$

Note that because of the different dependence of scalar and tensor widths compared to vector widths, the limits behave differently depending on the spin of the resonance:

Scalar:	$\Gamma \sim g^2M^3$, $\alpha \sim g^2/M^2$	$\Rightarrow$	$\alpha_{\max} \sim 1/M^4$
Vector:	$\Gamma \sim g^2M$, $\alpha \sim g^2/M^2$	$\Rightarrow$	$\alpha_{\max} \sim 1/M^2$
Tensor:	$\Gamma \sim g^2M^3$, $\alpha \sim g^2/M^2$	$\Rightarrow$	$\alpha_{\max} \sim 1/M^4$

Table 19-31 shows the width of the five different possible non-$SU(2)_c$ violating resonances for their decays into longitudinal EW gauge bosons, as well as their contributions to the anomalous quartic couplings parameters

Resonance	σ	ϕ	ρ	f	t
$\Gamma[g^2M^2/(64\pi v^2)]$	6	1	$\frac{4}{3}(\frac{v^2}{M^2})$	$\frac{1}{5}$	$\frac{1}{30}$
$\Delta\alpha_4[(16\pi\Gamma/M)(v^4/M^4)]$	0	$\frac{1}{4}$	$\frac{3}{4}$	$\frac{5}{2}$	$-\frac{5}{8}$
$\Delta\alpha_5[(16\pi\Gamma/M)(v^4/M^4)]$	$\frac{1}{12}$	$-\frac{1}{12}$	$-\frac{3}{4}$	$-\frac{5}{8}$	$\frac{35}{8}$

Table 19-31. *Width Γ of the five different possible non-$SU(2)_c$ violating resonances for their decays into longitudinal EW gauge bosons, as well as their contributions to the anomalous quartic couplings parameters α_4 and α_5.*

Type of resonance	LHC 300 fb^{-1}	LHC 3000 fb^{-1}
scalar ϕ	0.9 TeV	1.3 TeV
vector ρ	1.2 TeV	1.7 TeV
tensor f	1.6 TeV	2.3 TeV

Table 19-32. *95% CL limits for the mass M of a broad resonance in simplified models obtained from limits on α_4 of Table 19-20 and using the widths of Table 19-31 with $\Gamma \sim M$.*

α_4 and α_5. In Table 19-32 we provide limits on M based on the ATLAS limits on α_4 presented in Table 19-20 (assuming $\Gamma \sim M$, $v = 0.246$ TeV). The ATLAS limits on $f_{S,0}/\Lambda^4$ (see Table 19-22) can also be translated into limits on the mass M of a broad EW resonance ($\Gamma \sim M$) as follows (using Eq. 19.61):

$$M = \left(\frac{nc_R 16\pi}{f_{S,0}/\Lambda^4}\right)^{\frac{1}{4}} \tag{19.95}$$

where c_R are the contributions to $\Delta\alpha_4$ of Table 19-31 and $n = 8, 16$ for the $WWWW$ and $ZZWW$ case, respectively. These equivalent resonance mass sensitivities are shown in Table 19-33. Note that the sensitivities shown in Table 19-33 are better than those in Table 19-32 because the latter were derived from the W^+W^- VBS channel which has a significant $t\bar{t}$ background, whereas the channels used for Table 19-33 do not suffer from this large background.

Type of resonance	LHC 300 fb^{-1}		LHC 3000 fb^{-1}	
	5σ	95% CL	5σ	95% CL
scalar ϕ	1.8 TeV	2.0 TeV	2.2 TeV	3.3 TeV
vector ρ	2.3 TeV	2.6 TeV	2.9 TeV	4.4 TeV
tensor f	3.2 TeV	3.5 TeV	3.9 TeV	6.0 TeV

Table 19-33. *5σ-significance discovery values and 95% CL limits for the mass M of a broad resonance in simplified models. These values are obtained from the $f_{S,0}/\Lambda^4$ values of Table 19-22 and using Eq. 19.95 for the $WWWW$ case ($n = 8$). These studies are more sensitive than those in Table 19-32 because of the absence of the large $t\bar{t}$ background in the $W^\pm W^\pm$ VBS channel used for these studies, while there is a large $t\bar{t}$ background in the W^+W^- VBS channel used for Table 19-32.*

In Ref. [196], 1 σ sensitivities on the anomalous couplings α_i from VBS studies at a 1 TeV ILC (with 1 ab^{-1}) have been translated into 1 σ limits on masses of pure EW resonances (M). Table 19-34 shows the corresponding 95% CL exclusion limits on M in the $SU(2)_c$ conserving case and assuming $\Gamma/M = 1$.

Type of resonance	95% CL
scalar ϕ	1.64 TeV
vector ρ	2.09 TeV
tensor f	2.76 TeV

Table 19-34. *95% CL exclusion limits for the mass M of a pure EW resonance from α_4 sensitivity studies in VBS at a 1 TeV ILC (with 1 ab^{-1}) in the $SU(2)_c$ conserving case and assuming a single resonance with $\Gamma/M = 1$. The 95% CL limits have been obtained from the 1 σ limits of Ref. [196], $M_{\phi,\rho,f} = 1.95, 2.49, 3.29$ TeV, which are based on $16\pi^2\Delta\alpha_4 = 0.5026, 0.5671, 0.6437$ for ϕ, ρ, f resonances. The latter have been doubled to 2 σ, which are then interpreted as 95% CL limits for M using Table 19-31.*

19.3.7 TGCs from a global fit to Higgs data

In this Section, we discuss the limits on higher-dimension operator coefficients in EFT from measurements of the Higgs boson properties.

As discussed earlier in this report, effective Lagrangians can be used to parametrize in a model-independent way the low–energy effects of possible extensions of the standard model (SM) [201, 202, 203, 204, 205]. There is a freedom in the choice of the operator basis since operators connected by the equations of motion lead to the same S–matrix elements [206]. Taking advantage of the freedom in the choice of the operator basis, it is convenient to include in the basis used to analyze the Higgs couplings, operators that are directly related to the existing data, in particular to triple gauge couplings (TGCs), as well as, to the precision electroweak observables [202, 203, 207]. Neglecting, for the moment, modifications of the Higgs couplings to the first and second families and CP violating interactions[8], a useful basis is [203]

$$\begin{aligned}\mathcal{L}_{eff} = & -\frac{\alpha_s v}{8\pi}\frac{f_g}{\Lambda^2}\mathcal{O}_{GG} + \frac{f_{WW}}{\Lambda^2}\mathcal{O}_{WW} + \frac{f_{\rm bot}}{\Lambda^2}\mathcal{O}_{d\Phi,33} + \frac{f_{\rm top}}{\Lambda^2}\mathcal{O}_{u\Phi,33} \\ & + \frac{f_\tau}{\Lambda^2}\mathcal{O}_{e\Phi,33} + \frac{f_W}{\Lambda^2}\mathcal{O}_W + \frac{f_B}{\Lambda^2}\mathcal{O}_B + \frac{f_{WWW}}{\Lambda^2}\mathcal{O}_{WWW}\end{aligned} \tag{19.96}$$

with

$$\begin{aligned}&\mathcal{O}_{GG} = \Phi^\dagger\Phi\, G^a_{\mu\nu}G^{a\mu\nu}\ , \ \ \mathcal{O}_{WW} = \Phi^\dagger\hat{W}_{\mu\nu}\hat{W}^{\mu\nu}\Phi\ , \\ &\mathcal{O}_W = (D_\mu\Phi)^\dagger\hat{W}^{\mu\nu}(D_\nu\Phi)\ , \ \ \mathcal{O}_B = (D_\mu\Phi)^\dagger\hat{B}^{\mu\nu}(D_\nu\Phi)\ , \\ &\mathcal{O}_{WWW} = \mathrm{Tr}[\hat{W}_{\mu\nu}\hat{W}^{\nu\rho}\hat{W}^\mu_\rho]\ , \ \ \mathcal{O}_{u\Phi,ij} = (\Phi^\dagger\Phi)(\bar{L}_i\Phi u_{R_j})\ , \\ &\mathcal{O}_{e\Phi,ij} = (\Phi^\dagger\Phi)(\bar{L}_i\Phi e_{R_j})\ , \ \ \mathcal{O}_{d\Phi,ij} = (\Phi^\dagger\Phi)(\bar{Q}_i\Phi d_{Rj})\ ,\end{aligned} \tag{19.97}$$

$$\tag{19.98}$$

where Φ stands for the Higgs doublet with covariant derivative $D_\mu\Phi = \left(\partial_\mu + i\frac{1}{2}g'B_\mu + ig\frac{\sigma_a}{2}W^a_\mu\right)\Phi$ and $v = 246$ GeV is its vacuum expectation value. $\hat{B}_{\mu\nu} = i\frac{g'}{2}B_{\mu\nu}$ and $\hat{W}_{\mu\nu} = i\frac{g}{2}\sigma^a W^a_{\mu\nu}$ with $SU(2)_L$ ($U(1)_Y$) gauge coupling g (g') and Pauli matrices σ^a. We also use the notation of L for the lepton doublet, Q for the quark doublet and f_R for the $SU(2)$ singlet fermions, where i, j are flavor indices. $\mathcal{O}_B$ and $\mathcal{O}_W$ contribute both to Higgs physics and TGCs which means that some changes of the couplings of the Higgs field to the vector gauge bosons are related to TGCs due to gauge invariance in a model independent fashion [207]. In fact, the TGCs γW^+W^- and ZW^+W^- can be parametrized as [142]

$$\mathcal{L}_{WWV} = -ig_{WWV}\Big\{g_1^V\left(W^+_{\mu\nu}W^{-\,\mu}V^\nu - W^+_\mu V_\nu W^{-\,\mu\nu}\right) + \kappa_V W^+_\mu W^-_\nu V^{\mu\nu} + \frac{\lambda_V}{m_W^2}W^+_{\mu\nu}W^{-\,\nu\rho}V_\rho{}^\mu\Big\}\ , \tag{19.99}$$

[8] We have neglected in the analysis the effects of the operators $\mathcal{O}_{\phi d}$ and $\mathcal{O}_{\phi B}$ which, strictly speaking, are not bounded by the EWPT even after the use of equations of motion.

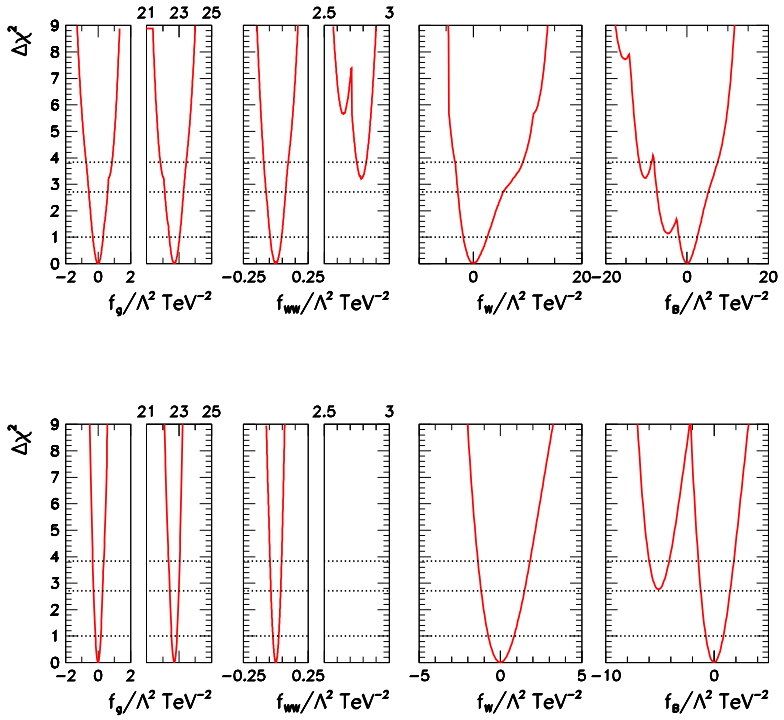

Figure 19-24. $\Delta\chi^2$ *as a function of* f_g, f_{WW}, f_W, *and* f_B *assuming* $f_{\rm bot} = f_\tau = f_{\rm top} = 0$, *after marginalizing over the three undisplayed ones. The three horizontal dashed lines stand for the* $\Delta\chi^2$ *values associated to 68%, 90% and 95% from bottom to top respectively. The upper (lower) row was obtained for an integrated luminosity of 300 (3000)* fb^{-1}.

where $g_{WW\gamma} = e = gs$ and $g_{WWZ} = gc$ with $s(c)$ being the sine (cosine) of the weak mixing angle. In general these vertices involve six C and P conserving couplings [142]. Nevertheless, the electromagnetic gauge invariance requires that $g_1^\gamma = 1$, while the five remaining couplings are related to the dimension–six operators $\mathcal{O}_B$, $\mathcal{O}_W$ and $\mathcal{O}_{WWW}$

$$\Delta\kappa_\gamma = \frac{g^2v^2}{8\Lambda^2}\Big(f_W + f_B\Big)\,,\ \lambda_\gamma = \lambda_Z = \frac{3g^2M_W^2}{2\Lambda^2}f_{WWW}\ ,\Delta g_1^Z = \frac{g^2v^2}{8c^2\Lambda^2}f_W\,,\ \Delta\kappa_Z = \frac{g^2v^2}{8c^2\Lambda^2}\Big(c^2f_W - s^2f_B\Big)\,, \tag{19.100}$$

where we wrote $\kappa^V = 1 + \Delta\kappa^V$ and $g_1^Z = 1 + \Delta g_1^Z$.

Here we assess the impact of Higgs physics on the TGC determination at the LHC with a center–of-mass energy of 14 TeV and integrated luminosities of 300 fb^{-1} and 3000 fb^{-1}. We fit the ATLAS and CMS expected sensitivities [208, 209] for the Higgs signal strength using four independent parameters $\{f_g\ ,\ f_W\ ,\ f_B\ ,\ f_{WW}\}$ and setting the Yukawa couplings to the fermions to their SM values. This scenario captures most of the features of fits using a larger set of free parameters since the addition of fermionic operators has little impact on the Higgs couplings to gauge–boson pairs and TGCs [202, 203].

	68% CL allowed range		95% CL allowed range	
	300 fb^{-1}	3000 fb^{-1}	300 fb^{-1}	3000 fb^{-1}
f_g/Λ^2 (TeV^{-2})	$(-0.33, 0.31) \cup (22.40, 23.04)$	$(-0.17, 0.17) \cup (22.54, 22.88)$	$(-0.74, 0.86) \cup (21.85, 23.45)$	$(-0.33, 0.34) \cup (22.36, 23.04)$
f_{WW}/Λ^2 (TeV^{-2})	$(-0.043, 0.044)$	$(-0.023, 0.022)$	$(-0.093, 0.096) \cup (2.75, 2.82)$	$(-0.045, 0.044)$
f_W/Λ^2 (TeV^{-2})	$(-1.9, 2.5)$	$(-0.75, 0.83)$	$(-3.4, 9.1)$	$(-1.39, 1.82)$
f_B/Λ^2 (TeV^{-2})	$(-2.0, 2.5)$	$(-0.78, 0.85)$	$(-11.7, 7.5)$	$(-6.0, -4.1) \cup (-1.5, 1.8)$

Table 19-35. *68% CL and 95% expected allowed ranges for 300 and 3000 fb^{-1} of integrated luminosity.*

Figure 19-24 displays $\Delta\chi^2$ as a function of the four fitting parameters [9] for integrated luminosities of 300 fb^{-1} (upper row) and 3000 fb^{-1} (lower row). The corresponding 68% CL and 95% expected allowed ranges can be found in Table 19-35. We can observe in the upper and lower left panels that the $\Delta\chi^2$ as a function of f_g exhibits two degenerate minima due to the interference between SM and anomalous contributions to $gg \to H$ production . In the case of the χ^2 dependence on f_{WW} there is also an interference between anomalous and SM contributions to $H \to \gamma\gamma$, however, the degeneracy of the minima is lifted since the f_{WW} coupling contributes also to Higgs decays into WW^*, ZZ^* and γZ, as well as in Vh associated and vector boson fusion production mechanisms. Clearly a larger statistics helps eliminating the degeneracy in f_{WW}. The interference between f_B and the SM contribution to $H \to \gamma Z$ is responsible for the two local minima with smaller $\Delta\chi^2$ while the additional minima in the upper right panel originates from the marginalization of f_{WW}. Comparing the upper and lower rows, we can see that a larger integrated luminosity also helps to significantly reduce the errors in the determination of the anomalous couplings.

Figure 19-25 depicts the χ^2 dependence on branching ratios and production cross sections for integrated luminosities of 300 fb^{-1} and 3000 fb^{-1}. As we can see these quantities can be determined with a precision better than 20% (5%) with 300 (3000) fb^{-1}. The only exception is the Higgs branching ratio into $Z\gamma$ that can be measured within 20% with 3000 fb^{-1}. These results show the consistency of the extracted accuracies in the production cross sections and branching ratios in the dim-6 operator framework with those obtained by the experimental collaborations in their simulations [208, 209] assuming a shift of the SM couplings.

Next we focus our attention to the expected TGC bounds derived from this analysis of the Higgs data. Eq. 19.100 allows us to translate the constraints on f_W and f_B coming from the Higgs measurements to bounds on $\Delta\kappa_\gamma$, $\Delta\kappa_Z$ and Δg_1^Z of which only two are independent. Fig. 19-26 displays the result of our fit to the Higgs data where we plot the 90%, 95%, 99%, and 3σ CL allowed region in the plane $\Delta\kappa_\gamma \otimes \Delta g_1^Z$ after marginalizing over the other two parameters relevant to the Higgs analysis, *i.e.* f_g and f_{WW}. Notice that the two almost degenerate local minima in f_B lead to the appearance of two narrow disconnected regions due to the high precision achieved with 3000 fb^{-1}.

Clearly the analysis of the Higgs data alone can improve the present best bounds on TGC which are still coming from LEP. Further improvement will come from combining the Higgs results with those from direct study of the TGC couplings. Unfortunately the study of the capabilities of the LHC14 runs on the constraints of the TGC couplings from di-boson production in this scenario is still missing.

In summary, indirect new physics effects associated with extensions of the electroweak symmetry breaking sector can be written in terms of an effective Lagrangian whose lowest order operators are of dimension six. The coefficients of these dimension–six operators parametrize our ignorance of these effects. In the above

[9] Details of the fitting procedure can be seen in Refs. [202, 203]

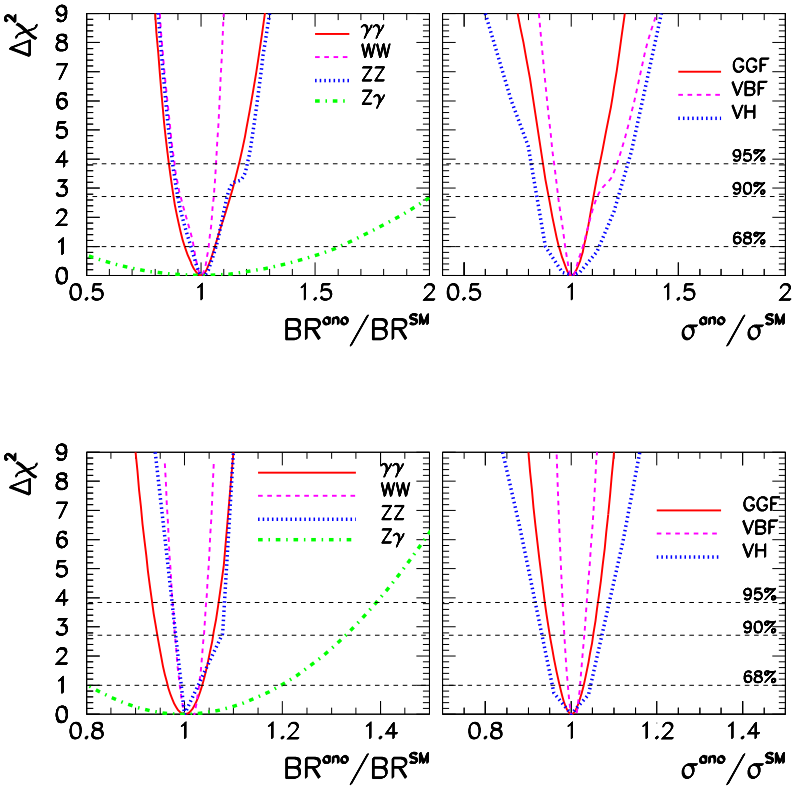

Figure 19-25. $\Delta\chi^2$ *as a function of branching ratios (left panels) and production cross sections (right panels) when we use only the expected ATLAS and CMS sensitivity on the Higgs signal strengths for integrated luminosities of 300 fb*$^{-1}$ *(upper row) and 3000 fb*$^{-1}$ *(lower row).*

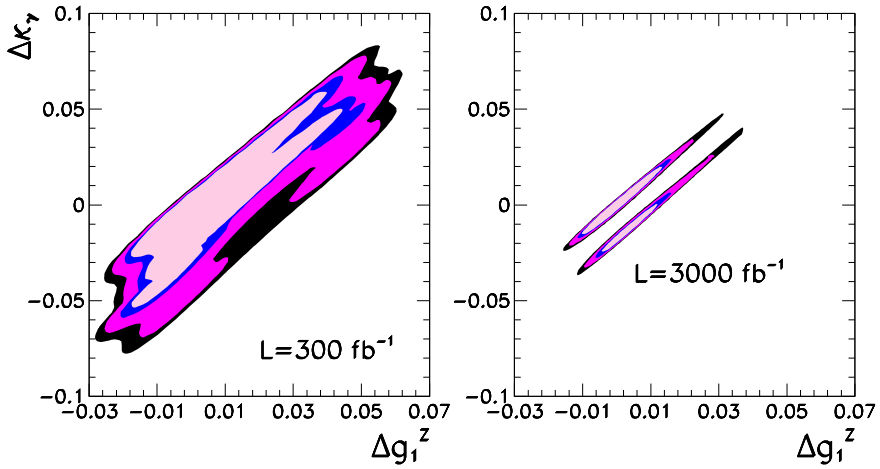

Figure 19-26. *We present the expected 90%, 95%, 99%, and 3σ allowed regions for the $\Delta\kappa_\gamma \otimes \Delta g_1^Z$ plane from the analysis of the Higgs data from LHC at 14 TeV with integrated luminosities of 300 fb^{-1} (left panel) and 3000 fb^{-1} (right panel).*

framework changes of the couplings of the Higgs to electroweak gauge bosons are related to the anomalous triple gauge–boson vertices [210]. Therefore, the analysis of the Higgs boson data at LHC can be used to constrain TGCs. Moreover, the combination of future TGC and Higgs measurements have the potential to lead to the strongest constraints on new physics effects associated with this sector.

19.4 Conclusions

With the discovery of the Higgs boson and the measurement of its mass at the LHC, the last missing component of the SM has been determined. However, the big question related to the origin of the Higgs "Mexican hat" potential remains to be answered. This question is exacerbated by the instability of this potential under quantum corrections.

The role of precision electroweak measurements is of increasing importance in over-constraining the Higgs sector of the SM. The two themes we have investigated in the arena of precision electroweak measurements are (a) the electroweak precision observables (EWPOs) that test the particle content and couplings in the SM and BSM scenarios, and (b) the measurements involving multiple gauge bosons in the final state which provide unique probes of the basic tenets of electroweak symmetry breaking.

In the case of EWPOs, we have focused on the measurement of M_W and $\sin^2\theta^l_{\rm eff}$. Other EWPOs should be available, in particular at ILC/GigaZ and TLEP; for instance, the $Z \to b\bar{b}$ partial width and the leptonic partial width are equally worthy of consideration. Our conclusions are as follows:

- The knowledge of the Higgs mass has sharpened the predictions of these EWPOs such that the predictions are a factor of 2-4 more precise than the experimental measurements.

- In almost all extensions of the SM, which are associated with the electroweak symmetry-breaking sector, these EWPOs receive corrections due to quantum loops (due to e.g. supersymmetric particles or techni-fermions), or due to effective operators (induced for example in strongly-interacting light Higgs models), or due to Kaluza-Klein modes in extra-dimensional models.

- M_W and $\sin^2\theta^l_{\rm eff}$ typically have different sensitivities to the sources of new physics. This may be demonstrated by the parametrization of new physics in the gauge boson self-energies in terms of the S, T and U "oblique" corrections. Fixed values of M_W and $\sin^2\theta^l_{\rm eff}$ correspond to lines in the $S-T$ plane with different slopes. Thus, improved measurements of both EWPOs can constrain all of the above sources of new physics in a relatively model-independent fashion.

- The current world average M_W has a precision of 15 MeV, dominated by the combined Tevatron measurement, which has a precision of 16 MeV based on the analysis of partial datasets. CDF and DO have projected that analyses of the full Tevatron statistics can yield a 10 MeV measurement, assuming a factor of two improvement in the uncertainty due to parton distribution functions, improvement in the calculation of radiative corrections and improved understanding of the trackers and calorimeters.

- Studies based on pseudo-data have demonstrated that measurements of boson distributions with the 2011-2012 LHC data may be able to improve the PDFs relevant for the M_W measurement by a factor of two in the near future, enabling the Tevatron potential for M_W to be realized.

- Enormous statistics of W bosons and control samples at the LHC offer the prospect of higher M_W precision. Studies based on pseudo-data have shown that the PDF uncertainty in M_W is about twice as big at the LHC as the Tevatron, due mainly to the larger fraction of sea quark-initiated production. Thus, further improvement by a factor of 2-3 in the PDFs will be required, beyond what is needed for the Tevatron. Furthermore, additional improvements in the QED and electroweak radiative correction calculations and NNLO+NNLL generators for W and Z bosons will likely also be required. However, considering the 15-year time scale for the ultimate M_W measurement from the LHC, we consider a target precision of 5 MeV to be appropriate for the LHC.

- Studies of the M_W measurement at the ILC using the threshold scan and final state reconstruction have been updated. It is projected that the ILC will be able to perform the M_W measurement with a precision of 4-5 MeV with $\mathcal{L} = 100\,\text{fb}^{-1}$ and of 2.5 MeV with $\mathcal{L} \approx 500\,\text{fb}^{-1}$.

- The circular electron-positron TLEP machine, running at the WW threshold, can produce very high statistics for the M_W measurement, and is likely to achieve energy calibration at the level of a fraction of an MeV. This potential motivates further studies of longitudinal beam polarization and control of other systematics achievable at TLEP. Given an integrated luminosity that can enable a statistical precision of ~ 0.5 MeV, further investigations of related issues are clearly warranted. Assuming a systematic uncertainty contribution of 1 MeV from missing higher-order corrections, TLEP could achieve an M_W precision of < 1.2 MeV. One of the goals of the ongoing TLEP study is to ensure that the W mass can be measured with a precision better that 1 MeV; this includes a program of improvements in the theoretical calculations.

- The measurement of $\sin^2\theta_{\rm eff}$ from LEP and SLC have averaged to a precision of 16×10^{-5}, albeit with a $\sim 3\sigma$ difference between them. Additional, especially improved, measurements will be valuable to shed light on this difference.

- A measurement of $\sin^2\theta^l_{\rm eff}$ using the full Tevatron dataset is projected with a precision of 41×10^{-5}. This measurement will be interesting to compare with LEP and SLC.

- Compared to the Tevatron, measurement of $\sin^2\theta^l_{\rm eff}$ at the LHC is handicapped by a larger sensitivity to PDFs due to the dilution of the quark and antiquark directions. As with the M_W measurement,

considerable control of the experimental and production model uncertainties will be required. Under the condition that a factor of 6-7 improvement on PDFs is achieved (a condition also required for the M_W target for the LHC), a projected uncertainty on $\sin^2\theta^\ell_{\rm eff}$ of 21×10^{-5} is obtained. This precision is similar to the current LEP and SLC measurements and is valuable before the advent of future lepton colliders.

- Considerably more precise measurements of $\sin^2\theta^\ell_{\rm eff}$ are highly desirable for taking the stringency of the SM tests to the next order of magnitude. Such measurements are possible at future lepton colliders running on the $Z-$pole such as ILC/GigaZ and TLEP.
- The ILC/GigaZ projection for the precision on $\sin^2\theta^\ell_{\rm eff}$ is 1.3×10^{-5}, a factor of 10 improvement on the current world average.
- TLEP has the potential to go beyond ILC/GigaZ in the precision on $\sin^2\theta^\ell_{\rm eff}$. This warrants a more detailed study. TLEP can produce 10^{12} Z bosons and could target improvements of a factor of $\sim$100 in $\sin^2\theta^\ell_{\rm eff}$ and a factor of 10-20 in other Z-pole observables beyond LEP and SLC. The precision at TLEP would be high enough that all aspects of EWPOs, both theoretical and experimental, need to be revisited. Further studies on experimental and theory systematics, and beam energy calibration and polarization are needed to understand if this TLEP potential can be realized.
- Measurements of M_W at the few MeV level, and $\sin^2\theta^\ell_{\rm eff}$ at the level of 10^{-5}, require that the parametric uncertainties from m_{top}, M_Z, and $\Delta\alpha_{had}$ (the contribution to the running of α_{EM} from hadronic loops) as well as the missing higher order calculations be addressed. Parametric uncertainties from m_{top} and $\Delta\alpha_{had}$, if reduced by a factor of 2 compared to current uncertainties, will prevent them from exceeding the anticipated total precision on M_W at the LHC. At the ILC and TLEP a factor of 5 and 10 improvement, respectively, in the parametric uncertainties is needed, which is only achievable if the precision on M_Z is considerably improved as well. TLEP can improve the M_Z precision by a factor of at least 10. It is anticipated that calculations in the coming years will reduce the effect of missing higher-order calculations by a factor of 4 which is sufficient for the LHC and ILC target uncertainties, but further effort will be needed for TLEP.

The second aspect of precision electroweak measurements we have emphasized is vector boson scattering and the related process of triboson production. Vector boson scattering addresses one of the crucial big questions that still needs to be tested experimentally, ie. the unitarization of longitudinal vector boson scattering at high energy. In the SM, the unitarization is achieved when Higgs boson exchange amplitudes are included, and this mechanism relies on the longitudinal modes of the massive gauge bosons being the would-be Goldstone modes of the symmetry-breaking Higgs potential. A direct demonstration of this mechanism is required, and is a prime motivation for the HL-LHC.

Models which explain the lightness of the discovered Higgs boson by describing it as a pseudo-Goldstone boson associated with the breaking of a larger symmetry, often introduce higher-dimension operators as an effective field theory (EFT) approximation of the new dynamics. Testing for these operators in vector boson scattering and triboson production can answer one of the outstanding questions in the Higgs sector: is the dynamics associated with the stabilization of the Higgs potential under quantum corrections, weakly coupled (e.g. SUSY) or strongly coupled (e.g. SILH models)?

The EFT formulation is not limited to specific models; any high energy theory can be reduced to a low-energy EFT and the former will specify the values of operator coefficients in the latter. Therefore, EFT operators provide a general method of parameterizing the effects of new physics at a high scale.

Some of these higher-dimension operators can alter the Higgs boson couplings, some can affect the values of EWPOs while others have no impact on these observables but still strongly affect multi-boson production.

The study of the latter processes can provide direct evidence of new SILH dynamics through the energy-dependence of the anomalous production. Further clarification of the new dynamics can be provided by comparing final states involving different combinations of W and Z bosons and photons, which can elucidate the group structure of the new dynamics.

Our conclusions in the area of multi-boson production are as follows:

- Studies of vector boson scattering and triboson production have become possible, for the first time, at the LHC. These processes probe quartic couplings which offer a new and promising avenue of research into electroweak symmetry breaking.
- For the next decade, the LHC will continue to be the facility to explore these processes at higher levels of precision.
- The LHC will improve the sensitivity to anomalous trilinear gauge couplings by 1-2 orders of magnitude beyond LEP and the Tevatron.
- The HL-LHC is needed to demonstrate that the Higgs couplings to the electroweak vector bosons is an essential component of the unitarization mechanism for vector boson scattering. An integrated luminosity of 300 fb^{-1} is not enough.
- The sensitivity to higher-dimension operators improves by a factor of 2-3 with the HL-LHC, in comparison with the 300 fb^{-1} at the LHC.
- Triboson production and vector boson scattering are sensitive and complementary probes of dimension-8 operators. These processes becomes rapidly more sensitive with increasing beam energy, providing strong motivation for a 100 TeV pp collider.
- Anomalous trilinear gauge couplings, which are induced by dimension-6 operators, are significantly better probed by the high-energy ILC options compared to the LHC. On the other hand, anomalous quartic gauge couplings, which are induced by dimension-8 operators, are significantly better probed (by 1-2 orders of magnitude) by the LHC, due to the stronger growth of the anomalous cross section with energy. Interpreting the latter as being induced by electroweak resonances, the LHC is sensitive to resonance masses that are higher by more than a factor of two, as compared to ILC1000.

ACKNOWLEDGEMENTS

We are grateful to the many scientists who assisted us in various ways through the process. We have benefited from those who have given us technical advice, and from those who took time to help us with individual tasks.

We acknowledge the support of the U.S. Department of Energy and the National Science Foundation.

C. Degrande is supported in part by the U. S. Department of Energy under Contract No. DE-FG02-13ER42001.

The work of the Gfitter collaboration is funded by the German Research Foundation (DFG) in the Collaborative Research Centre (SFB) 676 “Particles, Strings and the Early Universe” located in Hamburg.

J. Reuter has been partially supported by the Strategic HGF Alliance ”Physics at the Terascale”.

O. Eboli acknowledges support from Fundação de Amparo à Pesquisa do Estado de São Paulo (FAPESP) and Conselho Nacional de Desenvolvimento Científico e Tecnológico (CNPq).

The work of J. Erler was supported by PAPIIT (DGAPA–UNAM) project IN106913 and CONACyT (Mexico) project 151234, and grateful acknowledges the hospitality and support by the Mainz Institute for Theoretical Physics (MITP) where part of his work was completed.

B. Feigl and M. Rauch acknowledge support by the BMBF under Grant No. 05H09VKG ("Verbundprojekt HEP-Theorie").

The work of S. Heinemeyer was supported in part by CICYT (Grant No. FPA 2010–22163-C02-01), and by the Spanish MICINN's Consolider-Ingenio 2010 Program under Grant MultiDark No. CSD2009-00064.

B. Jaeger would like to thank the Research Center Elementary Forces and Mathematical Foundations (EMG) of the Johannes Gutenberg University Mainz. B. Jaeger and D. Wackeroth would also like to thank the hospitality of the Aspen Center for Physics where part of this work was done and supported in part by the National Science Foundation under Grant No. PHYS-1066293.

O. Mattelaer is a chercheur logistique post-doctoral of F.R.S-FNRS.

A. Vicini is supported by an italian PRIN 2010 grant.

The work of D. Wackeroth is supported in part by the U.S. National Science Foundation under grant no. PHY-1118138.

References

[1] ALEPH and CDF and D0 and DELPHI and L3 and OPAL and SLD and LEP Electroweak Working Group and Tevatron Electroweak Working Group and SLD Electroweak and Heavy Flavour Groups Collaborations, arXiv:1012.2367 [hep-ex].

[2] G. F. Giudice, C. Grojean, A. Pomarol and R. Rattazzi, JHEP **0706**, 045 (2007) [hep-ph/0703164], and references therein.

[3] The ALEPH, DELPHI, L3, OPAL, SLD Collaborations, the LEP Electroweak Working Group, the SLD Electroweak and Heavy Flavour Groups, Phys. Rept. **427** 257, (2006) [hep-ex/0509008].

[4] T. Aaltonen *et al.* [CDF Collaboration], Phys. Rev. Lett. **106**, 241801 (2011) [arXiv:1103.5699 [hep-ex]];
V. M. Abazov *et al.* [DO Collaboration], Phys. Rev. D **84**, 012007 (2011) [arXiv:1104.4590 [hep-ex]].

[5] S. Chatrchyan *et al.* [CMS Collaboration], Phys. Lett. B **718**, 752 (2013) [arXiv:1207.3973 [hep-ex]].
G. Aad *et al.* [ATLAS Collaboration], ATLAS-CONF-2013-043.

[6] M. Awramik, M. Czakon, A. Freitas, G. Weiglein, Phys. Rev. Lett. **93**, 201805 (2004) [hep-ph/0407317];
M. Awramik, M. Czakon and A. Freitas, Phys. Lett. B **642**, 563 (2006) [hep-ph/0605339];
W. Hollik, U. Meier and S. Uccirati, Nucl. Phys. B **731**, 213 (2005) [hep-ph/0507158], Nucl. Phys. B **765**, 154 (2007) [hep-ph/0610312].

[7] M. Awramik, M. Czakon and A. Freitas, JHEP **0611**, 048 (2006) [hep-ph/0608099].

[8] L. Avdeev, J. Fleischer, S. Mikhailov and O. Tarasov, Phys. Lett. B **336**, 560 (1994) [Erratum-ibid. B **349**, 597 (1994)] [hep-ph/9406363];
K. G. Chetyrkin, J. H. Kühn and M. Steinhauser, Phys. Lett. B **351**, 331 (1995) [hep-ph/9502291];
K. G. Chetyrkin, J. H. Kühn and M. Steinhauser, Phys. Rev. Lett. **75**, 3394 (1995) [hep-ph/9504413];
K. G. Chetyrkin, J. H. Kühn and M. Steinhauser, Nucl. Phys. B **482**, 213 (1996) [hep-ph/9606230].

[9] Y. Schröder and M. Steinhauser, Phys. Lett. B **622**, 124 (2005) [hep-ph/0504055];
K. G. Chetyrkin, M. Faisst, J. H. Kühn, P. Maierhoefer and C. Sturm, Phys. Rev. Lett. **97**, 102003 (2006) [hep-ph/0605201];
R. Boughezal and M. Czakon, Nucl. Phys. B **755**, 221 (2006) [hep-ph/0606232].

[10] J. J. van der Bij, K. G. Chetyrkin, M. Faisst, G. Jikia and T. Seidensticker, Phys. Lett. B **498**, 156 (2001) [hep-ph/0011373];
M. Faisst, J. H. Kühn, T. Seidensticker and O. Veretin, Nucl. Phys. B **665**, 649 (2003) [hep-ph/0302275].

[11] R. Boughezal, J. B. Tausk and J. J. van der Bij, Nucl. Phys. B **713**, 278 (2005) [hep-ph/0410216], Nucl. Phys. B **725**, 3 (2005) [hep-ph/0504092].

[12] D. Y. Bardin, P. Christova, M. Jack, L. Kalinovskaya, A. Olchevski, S. Riemann and T. Riemann, Comput. Phys. Commun. **133**, 229 (2001) [hep-ph/9908433].

[13] M. Böhm and W. Hollik, Nucl. Phys. B **204**, 45 (1982);
S. Jadach, J. H. Kühn, R. G. Stuart and Z. Wąs, Z. Phys. C **38**, 609 (1988) [Erratum-ibid. C **45**, 528 (1990)].

[14] M. Greco, G. Pancheri-Srivastava and Y. Srivastava, Nucl. Phys. B **171**, 118 (1980) [Erratum-ibid. B **197**, 543 (1982)];
F. A. Berends, R. Kleiss and S. Jadach, Nucl. Phys. B **202**, 63 (1982).

[15] W. Hollik, *Predictions for e^+e^- Processes*, in *Precision Tests of the Standard Model*, ed. P. Langacker (World Scientific, Singapur, 1993), p. 117.

[16] A. Czarnecki and J. H. Kühn, Phys. Rev. Lett. **77**, 3955 (1996) [hep-ph/9608366];
R. Harlander, T. Seidensticker and M. Steinhauser, Phys. Lett. B **426**, 125 (1998) [hep-ph/9712228].

[17] A. Freitas and Y.-C. Huang, JHEP **1208**, 050 (2012) [Erratum arXiv:1205.0299v3 [hep-ph]].

[18] R. Barbieri, M. Beccaria, P. Ciafaloni, G. Curci and A. Vicere, Phys. Lett. B **288**, 95 (1992) [Erratum-ibid. B **312**, 511 (1993)] [hep-ph/9205238];
R. Barbieri, M. Beccaria, P. Ciafaloni, G. Curci and A. Vicere, Nucl. Phys. B **409**, 105 (1993);
J. Fleischer, O. V. Tarasov and F. Jegerlehner, Phys. Lett. B **319**, 249 (1993);
J. Fleischer, O. V. Tarasov and F. Jegerlehner, Phys. Rev. D **51**, 3820 (1995);
G. Degrassi and P. Gambino, Nucl. Phys. B **567**, 3 (2000) [hep-ph/9905472].

[19] T. van Ritbergen and R. G. Stuart, Phys. Rev. Lett. **82**, 488 (1999) [hep-ph/9808283];
M. Steinhauser and T. Seidensticker, Phys. Lett. B **467**, 271 (1999) [hep-ph/9909436].

[20] A. Freitas, W. Hollik, W. Walter and G. Weiglein, Phys. Lett. B **495**, 338 (2000) [Erratum-ibid. B **570**, 260 (2003)] [hep-ph/0007091];
M. Awramik and M. Czakon, Phys. Rev. Lett. **89**, 241801 (2002) [hep-ph/0208113];
A. Onishchenko and O. Veretin, Phys. Lett. B **551**, 111 (2003) [hep-ph/0209010];
M. Awramik and M. Czakon, Phys. Lett. B **568**, 48 (2003) [hep-ph/0305248].

[21] M. Awramik, M. Czakon, A. Freitas and G. Weiglein, Phys. Rev. D **69**, 053006 (2004) [hep-ph/0311148].

[22] A. B. Arbuzov, M. Awramik, M. Czakon, A. Freitas, M. W. Grünewald, K. Mönig, S. Riemann, T. Riemann, Comput. Phys. Commun. **174**, 728 (2006) [hep-ph/0507146].

[23] H. Flächer, M. Goebel, J. Haller, A. Höcker, K. Mönig and J. Stelzer, Eur. Phys. J. C **60**, 543 (2009) [Erratum-ibid. C **71**, 1718 (2011)] [arXiv:0811.0009 [hep-ph]].

[24] R. G. Stuart, Phys. Lett. B **262**, 113 (1991);
H. Veltman, Z. Phys. C **62**, 35 (1994).

[25] M. Davier, A. Hoecker, B. Malaescu and Z. Zhang, Eur. Phys. J. C **71**, 1515 (2011) [Erratum-ibid. C **72**, 1874 (2012)] [arXiv:1010.4180 [hep-ph]].

[26] K. Hagiwara, R. Liao, A. D. Martin, D. Nomura and T. Teubner, J. Phys. G **38**, 085003 (2011) [arXiv:1105.3149 [hep-ph]].

[27] The Tevatron Electroweak Working Group and the CDF and DO Collaborations, arXiv:1107.5255 [hep-ex].

[28] J. Beringer *et al.* [Particle Data Group Collaboration], Phys. Rev. D **86**, 010001 (2012).

[29] M. E. Peskin and T. Takeuchi, Phys. Rev. D **46**, 381 (1992).

[30] A. V. Kotwal and J. Stark, Ann. Rev. Nucl. Part. Sci. **58**, 147 (2008).

[31] C. Balazs and C. P. Yuan, Phys. Rev. D **56**, 5558 (1997) [arXiv:hep-ph/9704258]; R. K. Ellis and S. Veseli, Nucl. Phys. B **511**, 649 (1998) [arXiv:hep-ph/9706526].

[32] F. Landry, R. Brock, G. Ladinsky and C. P. Yuan, Phys. Rev. D **63**, 013004 (2001) [arXiv:hep-ph/9905391].

[33] S. Frixione and B. R. Webber, JHEP **0206**, 029 (2002) [arXiv:hep-ph/0204244]; S. Frixione, F. Stoeckli, P. Torrielli, B. R. Webber and C. D. White, [arXiv:hep-ph/1010.0819].

[34] S. Alioli, P. Nason, C. Oleari and E. Re, JHEP **0807**, 060 (2008) [arXiv:hep-ph/0805.4802].

[35] K. Hamilton, P. Richardson and J. Tully, JHEP **0810**, 015 (2008) [arXiv:0806.0290 [hep-ph]]

[36] C. Anastasiou, L. J. Dixon, K. Melnikov and F. Petriello, Phys. Rev. D **69**, 094008 (2004) [arXiv:hep-ph/0312266].

[37] K. Melnikov and F. Petriello, Phys. Rev. Lett. **96**, 231803 (2006) [arXiv:hep-ph/0603182].

[38] S. Catani, L. Cieri, G. Ferrera, D. de Florian and M. Grazzini, Phys. Rev. Lett. **103**, 082001 (2009) [arXiv:0903.2120 [hep-ph]].

[39] T. Aaltonen *et al.* [CDF Collaboration], Phys. Rev. D **77**, 112001 (2008) [arXiv:0708.3642 [hep-ex]].

[40] V. M. Abazov *et al.* [D0 Collaboration], Phys. Rev. Lett. **103**, 141801 (2009) [arXiv:0908.0766 [hep-ex]].

[41] F. Abe *et al.* [CDF Collaboration], Phys. Rev. Lett. **75**, 11 (1995) and Phys. Rev. D **52**, 4784 (1995); T. Affolder *et al.* [CDF Collaboration], Phys. Rev. D **64**, 052001 (2001).

[42] S. Abachi *et al.* [D0 Collaboration], Phys. Rev. Lett. **77**, 3309 (1996), B. Abbott *et al.* [D0 Collaboration], Phys. Rev. D **58**, 012002 (1998); Phys. Rev. D **58**, 092003 (1998); Phys. Rev. Lett. **80**, 3008 (1998); Phys. Rev. Lett. **84**, 222 (2000); Phys. Rev. D **62** 092006 (2000); V. M. Abazov *et al.* [D0 Collaboration], Phys. Rev. D **66**, 012001 (2002).

[43] W. Ashmanskas *et al.* [TEVEWWG], arXiv:hep-ex/0311039 and references therein.

[44] F. Abe *et al.* [CDF Collaboration], Phys. Rev. Lett. **74**, 341 (1995).

[45] T. Affolder *et al.* [CDF Collaboration], Phys. Rev. Lett. **85**, 3347 (2000).

[46] V. M. Abazov *et al.* [D0 Collaboration], Phys. Rev. D **66**, 032008 (2002).

[47] D. Wackeroth and W. Hollik, Phys. Rev. D **55**, 6788 (1997) [arXiv:hep-ph/9606398].

[48] U. Baur, S. Keller and D. Wackeroth, Phys. Rev. D **59**, 013002 (1999) [arXiv:hep-ph/9807417].

[49] S. Dittmaier and M. Krämer, Phys. Rev. D **65**, 073007 (2002) [arXiv:hep-ph/0109062].

[50] U. Baur and D. Wackeroth, Phys. Rev. D **70**, 073015 (2004) [arXiv:hep-ph/0405191].

[51] A. Arbuzov, D. Bardin, S. Bondarenko, P. Christova, L. Kalinovskaya, G. Nanava and R. Sadykov, Eur. Phys. J. C **46**, 407 (2006) [Erratum-ibid. C **50**, 505 (2007)] [arXiv:hep-ph/0506110].

[52] C. M. Carloni Calame, G. Montagna, O. Nicrosini and A. Vicini, JHEP **0612**, 016 (2006) [arXiv:hep-ph/0609170].

[53] V. A. Zykunov, Phys. Atom. Nucl. **71**, 732 (2008); Eur. Phys. J. direct C **3**, 9 (2001) [arXiv:hep-ph/0107059].

[54] C. Buttar *et al.*, [arXiv:hep-ph/0604120.]

[55] C. E. Gerber *et al.* [TeV4LHC-Top and Electroweak Working Group], [arXiv:hep-ph/0705.3251].

[56] C. M. Carloni Calame, G. Montagna, O. Nicrosini and M. Treccani, Phys. Rev. D **69**, 037301 (2004).

[57] W. Placzek and S. Jadach, Eur. Phys. J. C **29**, 325 (2003).

[58] P. Golonka and Z. Was, Eur. Phys. J. C **45**, 97 (2006) [arXiv:hep-ph/0506026].

[59] K. Hamilton and P. Richardson, JHEP **0607**, 010 (2006) [arXiv:hep-ph/0603034].

[60] S. Brensing, S. Dittmaier, M. Krämer and A. Mück, Phys. Rev. D **77**, 073006 (2008) [arXiv:0710.3309 [hep-ph]].

[61] E. Laenen and D. Wackeroth, Ann. Rev. Nucl. Part. Sci. **59**, 367 (2009).

[62] Q. H. Cao and C. P. Yuan, Phys. Rev. Lett. **93**, 042001 (2004) [arXiv:hep-ph/0401026].

[63] G. Balossini *et al.*, JHEP **1001**, 013 (2010) [arXiv:hep-ph/0907.0276].

[64] G. Corcella *et al.*, JHEP **0101** (2001) 010. [hep-ph/0011363].

[65] A. Arbuzov, D. Bardin, S. Bondarenko, P. Christova, L. Kalinovskaya, G. Nanava, R. Sadykov, Eur. Phys. J. C **54**, 451 (2008) [arXiv:0711.0625 [hep-ph]].

[66] T. Sjostrand, S. Mrenna, P. Z. Skands, JHEP **0605** (2006) 026. [hep-ph/0603175].

[67] P. Richardson, R. R. Sadykov, A. A. Sapronov, M. H. Seymour and P. Z. Skands, arXiv:1011.5444 [hep-ph].

[68] C. Bernaciak and D. Wackeroth, Phys. Rev. D **85**, 093003 (2012) [arXiv:1201.4804 [hep-ph]].

[69] L. Barze, G. Montagna, P. Nason, O. Nicrosini and F. Piccinini, JHEP **1204**, 037 (2012) [arXiv:1202.0465 [hep-ph]].

[70] L. Barze, G. Montagna, P. Nason, O. Nicrosini, F. Piccinini and A. Vicini, Eur. Phys. J. C **73**, 2474 (2013) [arXiv:1302.4606 [hep-ph]].

[71] Andreas von Manteuffel and Robert Schabinger, private communication.

[72] W. B. Kilgore and C. Sturm, Phys. Rev. D **85**, 033005 (2012) [arXiv:1107.4798 [hep-ph]].

[73] S. Dittmaier, talk given at RADCOR 2013, www.ippp.dur.ac.uk/Workshops/13/RADCOR2013.

[74] G. Bozzi, J. Rojo and A. Vicini, Phys. Rev. D **83** (2011) 113008 [arXiv:1104.2056 [hep-ph]].

[75] R. D. Ball, V. Bertone, S. Carrazza, C. S. Deans, L. Del Debbio, S. Forte, A. Guffanti and N. P. Hartland *et al.*, Nucl. Phys. B **867** (2013) 244 [arXiv:1207.1303 [hep-ph]].

[76] J. Rojo and A. Vicini, arXiv:1309.1311 [hep-ph].

[77] A. D. Martin, W. J. Stirling, R. S. Thorne, G. Watt, Eur. Phys. J. **C63** (2009) 189-285. [arXiv:0901.0002 [hep-ph]].

[78] H. -L. Lai, M. Guzzi, J. Huston, Z. Li, P. M. Nadolsky, J. Pumplin and C. -P. Yuan, Phys. Rev. D **82**, 074024 (2010) [arXiv:1007.2241 [hep-ph]].

[79] F. Demartin, S. Forte, E. Mariani, J. Rojo and A. Vicini, Phys. Rev. D **82**, 014002 (2010) [arXiv:1004.0962 [hep-ph]].

[80] R. D. Ball, V. Bertone, F. Cerutti, L. Del Debbio, S. Forte, A. Guffanti, J. I. Latorre and J. Rojo *et al.*, Nucl. Phys. B **849**, 296 (2011) [arXiv:1101.1300 [hep-ph]].

[81] A. D. Martin, R. G. Roberts, W. J. Stirling and R. S. Thorne, Eur. Phys. J. C **39**, 155 (2005) [hep-ph/0411040].

[82] R. D. Ball *et al.* [The NNPDF Collaboration], arXiv:1308.0598 [hep-ph].

[83] T. Aaltonen *et al.* [CDF Collaboration], Phys. Rev. Lett. **108**, 151803 (2012) [arXiv:1203.0275 [hep-ex]].

[84] V. M. Abazov *et al.* [D0 Collaboration], Phys. Rev. Lett. **108**, 151804 (2012) [arXiv:1203.0293 [hep-ex]].

[85] T. A. Aaltonen *et al.* [CDF and D0 Collaborations], Phys. Rev. D **88**, 052018 (2013) [arXiv:1307.7627 [hep-ex]].

[86] A. Bodek, Eur.Phys.J.C67:321 (2010), arXiv:0911.2850 [hep-ex]

[87] A. Bodek et. al. , Eur.Phys.J.C72: 2194 (2012), arXiv:1208.3710 [hep-ex]

[88] T. Aaltonen *et al.* [CDF Collaboration], arXiv:1307.0770 [hep-ex].

[89] V. M. Abazov *et al.* [D0 Collaboration], Phys. Rev. D **84**, 012007 (2011) [arXiv:1104.4590 [hep-ex]].

[90] The ATLAS collaboration, ATLAS-CONF-2013-043

[91] A. Denner, S. Dittmaier, M. Roth and D. Wackeroth, Phys. Lett. B **475**, 127 (2000) [hep-ph/9912261]; Nucl. Phys. B **587**, 67 (2000) [hep-ph/0006307].

[92] S. Jadach, W. Placzek, M. Skrzypek, B. F. L. Ward and Z. Was, Phys. Rev. D **65**, 093010 (2002) [hep-ph/0007012].

[93] A. Denner, S. Dittmaier, M. Roth and L. H. Wieders, Phys. Lett. B **612**, 223 (2005) [Erratum-ibid. B **704**, 667 (2011)] [hep-ph/0502063]; Nucl. Phys. B **724**, 247 (2005) [Erratum-ibid. B **854**, 504 (2012)] [hep-ph/0505042].

[94] V. S. Fadin, L. N. Lipatov, A. D. Martin and M. Melles, Phys. Rev. D **61**, 094002 (2000) [hep-ph/9910338]; A. Denner, M. Melles and S. Pozzorini, Nucl. Phys. B **662**, 299 (2003) [hep-ph/0301241]; M. Beccaria, F. M. Renard and C. Verzegnassi, Nucl. Phys. B **663**, 394 (2003) [hep-ph/0304175].

[95] J. H. Kühn, F. Metzler and A. A. Penin, Nucl. Phys. B **795**, 277 (2008) [Erratum-ibid. **818**, 135 (2009)] [arXiv:0709.4055 [hep-ph]].

[96] V. S. Fadin, V. A. Khoze, A. D. Martin and W. J. Stirling, Phys. Lett. **B363**, 112 (1995).

[97] S. Actis, M. Beneke, P. Falgari and C. Schwinn, Nucl. Phys. B **807**, 1 (2009) [arXiv:0807.0102 [hep-ph]].

[98] M. Beneke, P. Falgari, C. Schwinn, A. Signer and G. Zanderighi, Nucl. Phys. B **792**, 89 (2008) [arXiv:0707.0773 [hep-ph]].

[99] M. Skrzypek, Acta Phys. Polon. **B23**, 135 (1992).

[100] "Precision measurement of the W mass with a polarized threshold scan at a linear collider." G. W. Wilson. In *2nd ECFA/DESY Study 1998-2001* 1498-1505 LC-PHSM-2001-09 and in Proceedings of LCWS 1999, Sitges, Spain.

[101] "Investigating In-Situ Center-of-Mass Energy Determination with Di-Muon Events", G. W. Wilson, ECFA LC2013 Workshop, Hamburg, May2013.

[102] S. Schael *et al.* [ALEPH and DELPHI and L3 and OPAL and LEP Electroweak Working Group Collaborations], "Electroweak Measurements in Electron-Positron Collisions at W-Boson-Pair Energies at LEP," arXiv:1302.3415 [hep-ex].

[103] M. Beckmann, B. List and J. List, "Treatment of Photon Radiation in Kinematic Fits at Future e+ e- Colliders," Nucl. Instrum. Meth. A **624**, 184 (2010) [arXiv:1006.0436 [hep-ex]].

[104] H. Abramowicz *et al.* [CLIC Detector and Physics Study Collaboration], arXiv:1307.5288 [hep-ex].

[105] M. Bicer, H. Duran Yildiz, I. Yildiz, G. Coignet, M. Delmastro, T. Alexopoulos, C. Grojean and S. Antusch *et al.*, arXiv:1308.6176 [hep-ex].

[106] R. Hawkings and K. Moenig, Eur. Phys. J. direct C **1**, 8 (1999), hep-ex/9910022.

[107] P. C. Rowson and M. Woods, *Experimental issues for precision electroweak physics at a high-luminosity Z factory*, hep-ex/0012055, Proceedings of the "Linear Collider Workshop 2000", Fermilab Natl. Lab., October 2000.

[108] J. Erler, K. Flottmann, S. Heinemeyer, K. Moenig, G. A. Moortgat-Pick, P. C. Rowson, E. Torrence and G. Weiglein *et al.*, eConf C **010630**, E3004 (2001) [hep-ph/0112070].

[109] SLD Collaboration, K. Abe et al., Phys. Rev. Lett. **84** (2000) 5945.

[110] S. Boogert, M. Hildreth, D. Kafer, J. List, K. Moenig, K. C. Moffeit, G. Moortgat-Pick and S. Riemann *et al.*, JINST **4**, P10015 (2009) [arXiv:0904.0122 [physics.ins-det]].

[111] A. Blondel, Phys. Lett. B **202**, 145 (1988) [Erratum-ibid. **208**, 531 (1988)].

[112] Tevatron Electroweak Working Group [CDF and D0 Collaborations], arXiv:1204.0042 [hep-ex].

[113] R. Assman, A. Blondel, B. Dehning, A. Drees, P. Grosse-Wiesmann, H. Grote, R. Jacobsen and J. P. Koutchouk *et al.*, CERN-SL-95-21.

[114] R. Assmann *et al.* [LEP Energy Working Group Collaboration], Eur. Phys. J. C **39**, 253 (2005) [hep-ex/0410026].

[115] H. Flacher, M. Goebel, J. Haller, A. Hocker, K. Moenig and J. Stelzer, Eur. Phys. J. C **60**, 543 (2009) [Erratum-ibid. C **71**, 1718 (2011)] [arXiv:0811.0009 [hep-ph]].

[116] M. Baak, M. Goebel, J. Haller, A. Hoecker, D. Ludwig, K. Moenig, M. Schott and J. Stelzer, Eur. Phys. J. C **72**, 2003 (2012) [arXiv:1107.0975 [hep-ph]].

[117] M. Baak, M. Goebel, J. Haller, A. Hoecker, D. Kennedy, R. Kogler, K. Moenig and M. Schott *et al.*, Eur. Phys. J. C **72**, 2205 (2012) [arXiv:1209.2716 [hep-ph]].

[118] M. E. Peskin and T. Takeuchi, Phys. Rev. Lett. **65**, 964 (1990).

[119] S. Heinemeyer, W. Hollik, D. Stockinger, A. M. Weber and G. Weiglein, *JHEP* **0608** (2006) 052 [arXiv:hep-ph/0604147].

[120] S. Heinemeyer, G. Weiglein and L. Zeune, DESY 13–015, *in preparation.*

[121] M. Frank, T. Hahn, S. Heinemeyer, W. Hollik, H. Rzehak and G. Weiglein, JHEP **0702** (2007) 047 [hep-ph/0611326].

[122] G. Degrassi, S. Heinemeyer, W. Hollik, P. Slavich and G. Weiglein, Eur. Phys. J. C **28** (2003) 133 [hep-ph/0212020].

[123] S. Heinemeyer, W. Hollik and G. Weiglein, Eur. Phys. J. C **9** (1999) 343 [hep-ph/9812472].

[124] S. Heinemeyer, W. Hollik and G. Weiglein, Comput. Phys. Commun. **124** (2000) 76 [hep-ph/9812320].

[125] T. Hahn, S. Heinemeyer, W. Hollik, H. Rzehak and G. Weiglein, Comput. Phys. Commun. **180** (2009) 1426.

[126] P. Bechtle, O. Brein, S. Heinemeyer, G. Weiglein and K. E. Williams, Comput. Phys. Commun. **181** (2010) 138 [arXiv:0811.4169 [hep-ph]].

[127] P. Bechtle, O. Brein, S. Heinemeyer, G. Weiglein and K. E. Williams, Comput. Phys. Commun. **182** (2011) 2605 [arXiv:1102.1898 [hep-ph]].

[128] S. Heinemeyer, O. Stål and G. Weiglein, Phys. Lett. B **710** (2012) 201 [arXiv:1112.3026 [hep-ph]];

[129] S. Heinemeyer, W. Hollik, A. M. Weber and G. Weiglein, JHEP **0804** (2008) 039 [arXiv:0710.2972 [hep-ph]].

[130] B. C. Allanach, M. Battaglia, G. A. Blair, M. S. Carena, A. De Roeck, A. Dedes, A. Djouadi and D. Gerdes *et al.*, Eur. Phys. J. C **25** (2002) 113 [hep-ph/0202233].

[131] R. Barate *et al.* [LEP Working Group for Higgs boson searches and ALEPH and DELPHI and L3 and OPAL Collaborations], Phys. Lett. B **565** (2003) 61 [hep-ex/0306033].

[132] S. Schael *et al.* [ALEPH and DELPHI and L3 and OPAL and LEP Working Group for Higgs Boson Searches Collaborations], Eur. Phys. J. C **47** (2006) 547 [hep-ex/0602042].

[133] J. Erler, P. Langacker, S. Munir and E. Rojas, JHEP **0908**, 017 (2009) [arXiv:0906.2435 [hep-ph]].

[134] J. Reuter, W. Kilian and M. Sekulla, arXiv:1307.8170 [hep-ph].

[135] C. Degrande, O. Eboli, B. Feigl, B. Jaeger, W. Kilian, O. Mattelaer, M. Rauch and Jr. Reuter *et al.*, arXiv:1309.7890 [hep-ph].

[136] B. Grzadkowski, M. Iskrzynski, M. Misiak and J. Rosiek, JHEP **1010**, 085 (2010) [arXiv:1008.4884 [hep-ph]].

[137] C. Arzt, M. B. Einhorn and J. Wudka, Nucl. Phys. B **433**, 41 (1995) [hep-ph/9405214].

[138] O. J. P. Eboli, M. C. Gonzalez-Garcia and J. K. Mizukoshi, Phys. Rev. D **74**, 073005 (2006) [hep-ph/0606118].

[139] A. S. Belyaev, O. J. P. Eboli, M. C. Gonzalez-Garcia, J. K. Mizukoshi, S. F. Novaes and I. Zacharov, Phys. Rev. D **59**, 015022 (1999) [hep-ph/9805229]; O. J. P. Eboli, M. C. Gonzalez-Garcia and S. M. Lietti, Phys. Rev. D **69**, 095005 (2004) [hep-ph/0310141]; O. J. P. Eboli, M. C. Gonzalez-Garcia, S. M. Lietti and S. F. Novaes, Phys. Rev. D **63**, 075008 (2001) [hep-ph/0009262].

[140] O. J. P. Eboli, M. C. Gonzalez-Garcia, S. M. Lietti and S. F. Novaes, Phys. Rev. D **63**, 075008 (2001) [hep-ph/0009262].

[141] O. J. P. Eboli, M. C. Gonzalez-Garcia and S. M. Lietti, Phys. Rev. D **69**, 095005 (2004) [hep-ph/0310141].

[142] K. Hagiwara, R. D. Peccei, D. Zeppenfeld and K. Hikasa, Nucl. Phys. B **282**, 253 (1987).

[143] K. Hagiwara, S. Ishihara, R. Szalapski and D. Zeppenfeld, Phys. Rev. D **48**, 2182 (1993).

[144] J. Wudka, Int. J. Mod. Phys. A **9**, 2301 (1994) [hep-ph/9406205].

[145] P. S. Wells, Eur. Phys. J. C **33**, S5 (2004); J. Beringer et al. (Particle Data Group), Phys. Rev. D86, 010001 (2012).

[146] W. J. Stirling and A. Werthenbach, Eur. Phys. J. C **14**, 103 (2000) [hep-ph/9903315].

[147] G. Belanger and F. Boudjema, Phys. Lett. B **288**, 201 (1992).

[148] O. J. P. Eboli, M. C. Gonzalez-Garcia and S. F. Novaes, Nucl. Phys. B **411**, 381 (1994) [hep-ph/9306306].

[149] http://feynrules.irmp.ucl.ac.be/wiki/AnomalousGaugeCoupling

[150] A. Alboteanu, W. Kilian and J. Reuter, JHEP **0811** (2008) 010 [arXiv:0806.4145 [hep-ph]].

[151] C. Degrande, N. Greiner, W. Kilian, O. Mattelaer, H. Mebane, T. Stelzer, S. Willenbrock and C. Zhang, arXiv:1205.4231 [hep-ph].

[152] B. Jäger and G. Zanderighi, JHEP **1111** (2011) 055 [arXiv:1108.0864 [hep-ph]].

[153] B. Jäger, C. Oleari, D. Zeppenfeld, JHEP **07** (2006) 015. [arXiv:hep-ph/0603177].

[154] B. Jager, C. Oleari and D. Zeppenfeld, Phys. Rev. D **73**, 113006 (2006) [hep-ph/0604200].

[155] G. Bozzi, B. Jager, C. Oleari and D. Zeppenfeld, Phys. Rev. D **75**, 073004 (2007) [hep-ph/0701105].

[156] B. Jäger, C. Oleari, D. Zeppenfeld, Phys. Rev. **D80** (2009) 034022. [arXiv:0907.0580 [hep-ph]].

[157] A. Denner, L. Hosekova and S. Kallweit, Phys. Rev. D **86** (2012) 114014 [arXiv:1209.2389 [hep-ph]].

[158] P. Nason, JHEP **0411** (2004) 040. [hep-ph/0409146].

[159] S. Frixione, P. Nason, C. Oleari, JHEP **0711** (2007) 070. [arXiv:0709.2092 [hep-ph]].

[160] S. Alioli, P. Nason, C. Oleari, E. Re, JHEP **1006** (2010) 043. [arXiv:1002.2581 [hep-ph]].

[161] T. Figy, C. Oleari and D. Zeppenfeld, Phys. Rev. D **68** (2003) 073005 [hep-ph/0306109].

[162] C. Oleari and D. Zeppenfeld, Phys. Rev. D **69** (2004) 093004 [hep-ph/0310156].

[163] P. Nason and C. Oleari, JHEP **1002** (2010) 037 [arXiv:0911.5299 [hep-ph]].

[164] B. Jäger, S. Schneider and G. Zanderighi, JHEP **1209** (2012) 083 [arXiv:1207.2626 [hep-ph]].

[165] F. Schissler and D. Zeppenfeld, JHEP **04** (2013) 057 [JHEP **1304** (2013) 057] [arXiv:1302.2884 [hep-ph]].

[166] B. Jäger and G. Zanderighi, JHEP **1304** (2013) 024 [arXiv:1301.1695 [hep-ph]].

[167] M. Cacciari, G. P. Salam, Phys. Lett. **B641** (2006) 57. [hep-ph/0512210].

[168] A. Lazopoulos, K. Melnikov and F. Petriello, Phys. Rev. D **76**, 014001 (2007) [hep-ph/0703273].

[169] V. Hankele and D. Zeppenfeld, Phys. Lett. B **661**, 103 (2008) [arXiv:0712.3544 [hep-ph]].

[170] F. Campanario, V. Hankele, C. Oleari, S. Prestel and D. Zeppenfeld, Phys. Rev. D **78**, 094012 (2008) [arXiv:0809.0790 [hep-ph]].

[171] T. Binoth, G. Ossola, C. G. Papadopoulos and R. Pittau, JHEP **0806**, 082 (2008) [arXiv:0804.0350 [hep-ph]].

[172] G. Bozzi, F. Campanario, V. Hankele and D. Zeppenfeld, Phys. Rev. D **81**, 094030 (2010) [arXiv:0911.0438 [hep-ph]].

[173] G. Bozzi, F. Campanario, M. Rauch, H. Rzehak and D. Zeppenfeld, Phys. Lett. B **696**, 380 (2011) [arXiv:1011.2206 [hep-ph]].

[174] U. Baur, D. Wackeroth and M. M. Weber, PoS RADCOR **2009**, 067 (2010) [arXiv:1001.2688 [hep-ph]].

[175] G. Bozzi, F. Campanario, M. Rauch and D. Zeppenfeld, Phys. Rev. D **83**, 114035 (2011) [arXiv:1103.4613 [hep-ph]].

[176] G. Bozzi, F. Campanario, M. Rauch and D. Zeppenfeld, Phys. Rev. D **84**, 074028 (2011) [arXiv:1107.3149 [hep-ph]].

[177] G. Bozzi, F. Campanario, C. NEnglert, M. Rauch, M. Spannoswky and D. Zeppenfeld, arXiv:1205.2506 [hep-ph].

[178] J. M. Campbell, H. B. Hartanto and C. Williams, JHEP **1211**, 162 (2012) [arXiv:1208.0566 [hep-ph]].

[179] R. W. Brown, K. L. Kowalski and S. J. Brodsky, Phys. Rev. D **28**, 624 (1983).

[180] U. Baur, T. Han and J. Ohnemus, Phys. Rev. D **48**, 5140 (1993) [hep-ph/9305314].

[181] U. Baur, T. Han, N. Kauer, R. Sobey and D. Zeppenfeld, Phys. Rev. D **56**, 140 (1997) [hep-ph/9702364].

[182] D. T. Nhung, L. D. Ninh and M. M. Weber, arXiv:1307.7403 [hep-ph].

[183] H. Aihara, T. Barklow, U. Baur, J. Busenitz, S. Errede, T. A. Fuess, T. Han and D. London *et al.*, In *Barklow, T.L. (ed.) et al.: Electroweak symmetry breaking and new physics at the TeV scale* 488-546 [hep-ph/9503425].

[184] V. Lombardo [on behalf of the ATLAS and CMS Collaboration], arXiv:1305.3773 [hep-ex].

[185] G. Aad *et al.* [ATLAS Collaboration], JHEP **1303**, 128 (2013) [arXiv:1211.6096 [hep-ex]].

[186] G. Aad *et al.* [ATLAS Collaboration], Phys. Lett. B **717**, 49 (2012) [arXiv:1205.2531 [hep-ex]].

[187] S. Chatrchyan *et al.* [CMS Collaboration], JHEP **1307**, 116 (2013) [arXiv:1305.5596 [hep-ex]].

[188] ATLAS Collaboration, CERN preprint ATL-PHYS-PUB-2012-005, *http://cds.cern.ch/record/1496527*.

[189] ATLAS Collaboration, CERN Preprint ATL-PHYS-PUB-2013-006, *http://cds.cern.ch/record/1558703*.

[190] T. N. Truong, Phys. Rev. Lett. **61**, 2526 (1988).

[191] A. Ballestrero, D. B. Franzosi, L. Oggero and E. Maina, JHEP **1203**, 031 (2012) [arXiv:1112.1171 [hep-ph]], and references therein.

[192] C. Degrande, J. L. Holzbauer, S. -C. Hsu, A. V. Kotwal, S. Li, M. Marx, O. Mattelaer and J. Metcalfe *et al.*, SNOW13-00189, arXiv:1309.7452 [physics.comp-ph].

[193] G. Aarons *et al.* [ILC Collaboration], arXiv:0709.1893 [hep-ph].

[194] A. Freitas, K. Hagiwara, S. Heinemeyer, P. Langacker, K. Moenig, M. Tanabashi and G. W. Wilson, arXiv:1307.3962 [hep-ph].

[195] E. Accomando *et al.*, Physics at the CLIC multi-TeV linear collider, 2004, hep-ph/0412251.

[196] M. Beyer, W. Kilian, P. Krstonosic, K. Moenig, J. Reuter, E. Schmidt and H. Schroder, Eur. Phys. J. C **48**, 353 (2006) [hep-ph/0604048].

[197] H. Baer, T. Barklow, K. Fujii, Y. Gao, A. Hoang, S. Kanemura, J. List and H. E. Logan *et al.*, arXiv:1306.6352 [hep-ph].

[198] S. Weinberg, Phys. Rev. **166**, 1568 (1968); M. S. Chanowitz and M. K. Gaillard, Nucl. Phys. B **261**, 379 (1985); W. Kilian, Springer Tracts Mod. Phys. **198**, 1 (2003).

[199] W. Kilian, T. Ohl and J. Reuter, Eur. Phys. J. C **71**, 1742 (2011) [arXiv:0708.4233 [hep-ph]].

[200] W. Kilian, J. Reuter, M. Sekulla, *Search for New Physics in Vector boson scattering*, in preparation.

[201] S. Weinberg, Physica A **96**, 327 (1979).

[202] T. Corbett, O. J. P. Eboli, J. Gonzalez-Fraile and M. C. Gonzalez-Garcia, Phys. Rev. D **87**, 015022 (2013) [arXiv:1211.4580 [hep-ph]].

[203] T. Corbett, O. J. P. Eboli, J. Gonzalez-Fraile and M. C. Gonzalez-Garcia, Phys. Rev. D **86**, 075013 (2012) [arXiv:1207.1344 [hep-ph]].

[204] W. Buchmüller and D. Wyler, Phys. Lett. B **177**, 377 (1986).

[205] B. Grzadkowski, M. Iskrzynski, M. Misiak and J. Rosiek, JHEP **1010**, 085 (2010) [arXiv:1008.4884 [hep-ph]].

[206] H. D. Politzer, Nucl. Phys. B **172**, 349 (1980); H. Georgi, Nucl. Phys. B **361**, 339 (1991); C. Arzt, Phys. Lett. B **342**, 189 (1995); H. Simma, Z. Phys. C **61**, 67 (1994).

[207] T. Corbett, O. J. P. Eboli, J. Gonzalez-Fraile and M. C. Gonzalez-Garcia, arXiv:1304.1151 [hep-ph].

[208] ATLAS collaboration, ATL-PHYS-PUB-2012-004.

[209] CMS collaboration, `https://twiki.cern.ch/twiki/bin/view/CMSPublic/HigProjectionEsg2012TWiki`

[210] For an early application of this framework to the Tevatron data see F. de Campos, M. C. Gonzalez-Garcia and S. F. Novaes, Phys. Rev. Lett. **79**, 5210 (1997) [hep-ph/9707511].